**The Dissertation Committee for Aditya D. Joshi certifies that this is the approved version of the following dissertation:**

# STRUCTURAL AND FUNCTIONAL STUDIES OF $Na^+$/DICARBOXYLATE COTRANSPORTERS

**Committee:**

Ana M. Pajor, Ph.D., Supervisor

Steven C. King, Ph.D.

Simon A. Lewis, Ph.D.

Krishna Rajarathnam, Ph.D.

Nancy K. Wills, Ph.D.

Dean, Graduate School

# STRUCTURAL AND FUNCTIONAL STUDIES OF $Na^+$/DICARBOXYLATE COTRANSPORTERS

**By**

**Aditya D. Joshi, M. Sc.**

**Dissertation**

Presented to the Faculty of the Graduate School of Biomedical Sciences

The University of Texas Medical Branch

in Partial Fulfillment

of the Requirements

for the Degree of

**Doctor of Philosophy**

**The University of Texas Medical Branch**

**August 2008**

To my dearest family

# ACKNOWLEDGEMENTS

From bottom of my heart, I would like to convey my sincere appreciation and gratitude to my extremely inspirational and supportive mentor, Dr. Ana M. Pajor for helping me throughout my Ph.D. studies. I am deeply thankful to her for providing me with the invaluable resources in the form of constant encouragement, advice, inspiration, compassion as well as thought provoking ideas, which helped me to complete my doctoral work. I truly believe she has been a wonderful mentor and I am indebted to her for all her support.

I would also like to express my sincere gratitude to Dr. Simon A. Lewis, for providing me insights on understanding physiological aspects of structure-function studies as well as his constant encouragement. I am thankful to Dr. Steven C. King for his advice on Transport Specificity Ratio experiments as well as his constant suggestions during different stages of this dissertation work. I am also grateful to Dr. Nancy K. Wills and Dr. Krishna Rajarathnam for providing me with invaluable advice on experimental design, data interpretation and useful discussions.

I really like to appreciate my colleagues and friends Dr. Jason A. Hall, Dr. Jittima Weerachayaphorn, Dr. Naomi Oshiro, Donovan E. Randolph, Jamie R. Lewis, Dr. Alieen K. Ritchie, Cynthia Cheatham, Aditya Hindupur, Rohit Jangra, Abhisek Mukharjee, and Dr. Lokesh Rao for being helpful and supportive. I would especially like to thank Kathleen M. Randolph not only for her scientific and technical inputs, but also for her joyful and positive encouragement.

I sincerely thank Dr. Werner Braun for giving me an opportunity to work in the Sealy Center for Computational Biology and his constant suggestions regarding the computational modeling aspects of this project. I also thank Dr. Surendra Negi for helping me with NaDC1 computational modeling.

I would like to express my deepest appreciation to my parents, Sunanda and Dilip Joshi, my brother Ojas, sister-in-law, Ketki and my adorable niece, Saniya for inspiring me to put in my best efforts in carrying out this work and their constant encouragement.

I feel that the words are not enough to express my appreciation to my lovely wife, Trupti for being supportive and her efforts to help me make it possible.

# STRUCTURAL AND FUNCTIONAL STUDIES OF $Na^+$/DICARBOXYLATE COTRANSPORTERS

Publication No._____

Aditya D. Joshi, M. Sc., Ph. D.

The University of Texas Medical Branch, June 2008

Supervisor: Ana M. Pajor

The $Na^+$/dicarboxylate cotransporter (NaDC1) is found on the apical membrane of the kidney proximal tubule and the small intestine. It carries various di- and tri- carboxylates such as succinate, α-ketoglutarate and citrate. NaDC1 is involved in regulating the concentration of tricarboxylic acid cycle intermediates in kidney cells and urine. Therefore, NaDC1 influences the homeostasis of citrate, which may be associated with the formation of kidney stones. The studies in this dissertation focus on understanding various structural and functional aspects of NaDC1.

Previous studies indicate importance of TM 7, 10 and 11 for substrate binding. In this study, conserved prolines from TM 7 and 10 were mutated to alanine and glycine to understand structural as well as functional importance of these residues. Alanine is a strong α-helix former and is less flexible whereas glycine, with no side chain, is a strong helix breaker and is more flexible. If prolines in NaDC1 are responsible for kink formation and if kink is necessary for maintaining the stability of the transporter then mutating proline to glycine will have less adverse effect compared with mutating to alanine. This study indicates that Proline 327 in TM 7 when mutated to glycine was not able to reach the plasma membrane, showed no expression as well as succinate transport activity. Proline 351 plays an important role in cell surface regulation and protein trafficking. The prolines found in TM 10 at positions 523 and 524 do not appear to have functional roles but might be important for protein stability.

The current model of NaDC1, based on hydropathy analysis, contains 11 TM but secondary structure prediction algorithms predict at least 13 TM. To differentiate between the 11 and the 13 TM models, individual cysteine residues were substituted

for other amino acids in predicted extracellular and intracellular loops of rbNaDC1. The extracellular accessibility of the cysteines was determined by chemical labeling with MTSEA-biotin [N-biotinylaminoethyl methanethiosulfonate]. Based on the site-directed chemical labeling experiments and computational homology modeling a modified model of NaDC1 was constructed containing 11 TM. Further studies indicate that mutants A39C, K84C, A133C, T252C, G356C, T482C and M493C were accessible in sodium buffer but their reactivity with methanethiosulfonate and their accessibility from outside changes in different buffer conditions in presence and absence of sodium and succinate. This indicates conformational changes in the transporter during the transport cycle. This new model will provide a structural framework towards understanding the structure-function relationship of NaDC1.

To identify conformationally sensitive residues in the $Na^+$/dicarboxylate cotransporter that are accessible from both sides of the membrane, a bacterial homolog of NaDC1, $Na^+$/dicarboxylate symporter (SdcS) from *Staphylococcus aureus* was used. The eukaryotic transporter could not be used due to experimental difficulties in studying accessibility of the transporter from inside the cell. Previous studies indicate that rbNaDC1 contains structurally, functionally and conformationally important residues such as Lys-84, Asp-373, Met-493. When protein sequence of rbNaDC1 was aligned with SdcS these residues correspond to Asn-108, Asp-329 and Leu-436 of SdcS. Cysteines were substituted at these locations in cysteineless SdcS and their accessibility was tested by MTSET reagent in right-side-out vesicles (RSO) and inside-out vesicles (ISO) in different conformational conditions such as in presence and absence of $Na^+$ and substrate. SdcS showed similar succinate affinity in ISO and RSO vesicles but the transport system was asymmetric with $V_{max}$ of SdcS RSO is four times higher than $V_{max}$ of ISO. Residue Asn-108 was accessible from outside and inside in presence of $Na^+$ only. The N108C mutant was not accessible with the conformational state in absence of $Na^+$ and showed substrate protection likely due to steric hindrance by chemical labeling. Therefore, residue Asn-108 is probably located in a transmembrane helix near a water-filled pore or in a re-entrant loop accessible from both sides of the membrane.

In conclusion, this work provides a new insight into structural and functional aspects of $Na^+$/dicarboxylate cotransporters. As limited high-resolution structural information is available about membrane transporters these biochemical and computational studies elucidate fundamental information of structural details of $Na^+$/dicarboxylate cotransporters as well as help us in understanding its role in cellular functions.

# TABLE OF CONTENTS

# LIST OF TABLES

# LIST OF FIGURES

# LIST OF ABBREVIATIONS

| | |
|---|---|
| cDNA | complementary deoxyribonucleic acid |
| 2, 2-DMS | 2, 2-dimethylsuccinate |
| f | Prefix, flounder |
| h | Prefix, human |
| HEPES | N-2-hydroxyethylpiperazine-n-2'-ethanesulfonic acid |
| *Indy* | $Na^+$-independent dicarboxylate transporter from *Drosophila* |
| IgG | Immunoglobin G |
| kDa | kilodalton |
| kb | kilobase |
| m | Prefix, mouse |
| MTSEA | 2-aminoethylmethane thiosulfonate |
| MTSES | 2-sulfonatoethylmethane thiosulfonate |
| MTSET | 2-trimethylammonieothylmethane thiosulfonate |
| NaDC1 | Low-affinity $Na^+$/dicarboxylate cotransporter |
| NaDC3 | High-affinity $Na^+$/dicarboxylate cotransporter |
| NaCT | $Na^+$-coupled citrate transporter |
| NaS | $Na^+$/sulfate cotransporter |
| o | Prefix, opossum |
| OAT | Organic anion transporter |
| PBS | Phosphate-buffered saline |
| PCR | Polymerase chain reaction |

## LIST OF ABBREVIATIONS (CONT.)

| | |
|---|---|
| PMSF | Phenylmethanesulfonyl fluoride |
| r | Prefix, rat |
| rb | Prefix, rabbit |
| RT-PCR | Reverse transcription-polymerase chain reaction |
| SLC | Solute carrier gene family |
| SDS-PAGE | Sodium dodecyl sulfate polyacrylamide gel electrophoresis |
| Sulfo-NHS-LC-Biotin | Sulfosuccinimidyl-6-(biotinamido) hexanoate |
| TM | Transmembrane helix |
| TSR | Transport specificity ratio |
| x | Prefix, *Xenopus laevis* |

# CHAPTER 1: INTRODUCTION

This dissertation focuses on understanding structural and functional aspects of the $Na^+$/dicarboxylate cotransporters, NaDC. The first aim of this dissertation (Chapter 2) was to understand the role of conserved proline residues in $Na^+$/dicarboxylate cotransporter 1 (NaDC1). In the second aim (Chapter 3), the topology of NaDC1 was determined by site-directed chemical labeling. The third aim (Chapter 4) was to identify and characterize conformationally sensitive amino acids in a homolog of NaDC1 from *Staphylococcus aureus*, $Na^+$/dicarboxylate symporter (SdcS). In the final aim (Chapter 5), an attempt was made to identify determinants of citrate binding and transport by using random mutagenesis in SdcS. This introduction begins with general information about membrane transport systems, high-resolution structures of various membrane transporters available, mechanisms of substrate transport, the solute carrier 13 (SLC 13) gene family members and finally NaDC1 as well as SdcS transporters.

## MEMBRANE TRANSPORT PROTEINS

It was only in the 1950s that the first reports began to appear in the literature indicating that the movement of a number of substances, both uncharged and ionic, across cell membranes was catalyzed by specific proteins. The kinetics (and selectivity) of some of these proteins were worked out in great detail, particularly for amino acids in Ehrlich ascites cells (*1*) and for monosaccharides in human erythrocytes (*2*). Later due to increase in the membrane transport protein gene

sequences and structures of the proteins, in 1990s the first draft of a classification system was put forward. Further in 1999 and updated in 2002, a novel classification system of membrane transport proteins was proposed by Milton H. Saier Jr. known as Transport Classification (TC) system (*3-7*) which is based on functional and phylogenic characteristics of transport proteins. This classification system was formally adopted by the International Union of Biochemistry and Molecular Biology (IUBMB) in 2002. According to the TC system, the membrane transport proteins are classified into two major groups, namely channels and carriers (Figure 1.1).

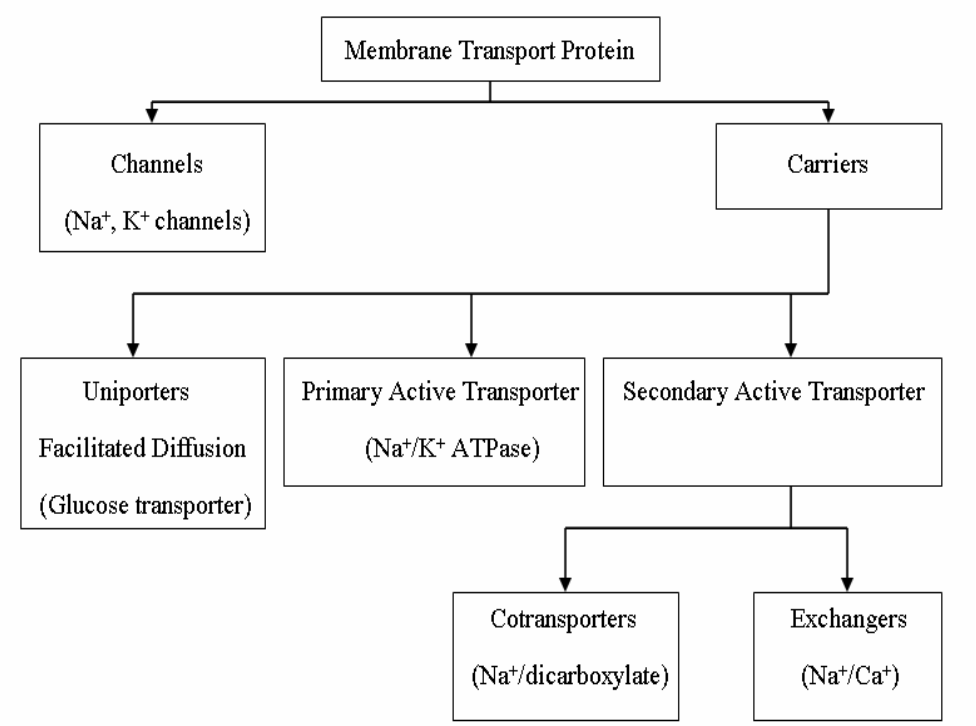


**Figure 1.1** General classification of membrane transport proteins. The transport proteins are classified according to TC system (*3*). Transport proteins are classified into two major types: channel proteins and carrier proteins. Carriers or transporters can be further sub-classified into three types: uniporters, primary active transporters and secondary active transporters.

Ion channels are selective hydrophilic pores that permit the movement of substrates across the membrane down their electrochemical gradients (*8*). On the other hand, membrane transporters are classified into uniporters, primary active transporters and secondary active transporters based on the energy source for transport, nature of the transport and mode of transport (*3*). Uniporters such as glucose transporters (GLUTs) are facilitated diffusion carriers that move substrates down their electrochemical gradient. The primary active transporters (for example, the members of the ATP binding cassette family and P-type ATPases such as $Na^+/K^+$ ATPase) use energy from hydrolysis of adenosine triphosphate (ATP) directly to drive transport of solutes against their electrochemical gradient. The secondary active transporters carry solutes against their electrochemical gradient by coupling to electrochemical gradient generated by the primary active transport process. Major driving forces for secondary active transporters are $Na^+$ and proton gradients. Depending on the direction of the solute transport secondary active transporters are classified into cotransporters (symporters) and exchangers (antiporters). In cotransporters, solutes are transported in same direction (e.g. NaDC1 uses the energy stored in the sodium gradient to transport three sodium ions and one dicarboxylate ion into the cell) whereas in exchangers solutes are transported in opposite directions ($Na^+/Ca^+$ exchanger uses the energy stored in the sodium gradient to transport two sodium ions into the cell and one calcium ion out of the cell). The major focus of this dissertation is on the NaDC transporters which belong to the secondary active cotransporter category.

## STRUCTURAL BIOLOGY OF MEMBRANE TRANSPORTERS

Out of thousands of membrane proteins, high-resolution structures of only about 150 proteins are known, which contributes less than one percent of the total protein structures listed in the Protein Data Bank (PDB). There are several problems involved in crystallization of membrane proteins. Firstly, they are amphipathic in nature as they contain hydrophobic groups in contact with membrane phospholipids and hydrophilic groups in contact with the water. Therefore purifying membrane protein out of the lipid bilayer makes the protein nonfunctional and is challenging. Secondly, for crystallization studies overexpressed proteins are required and are difficult as very few mammalian membrane proteins have been functionally expressed in bacteria, the expression system used to acquire large quantities of proteins. Despite the difficulties in crystallization some high-resolution crystal structures are known.

The first three-dimensional structure of a secondary transporter, the *E. coli* AcrB transporter, was reported in 2002 (*9*). AcrB is a resistance-nodulation cell division transporter (RND) that cooperates with a channel (TolC) to form a proton-driven multidrug exporter system. The structure of ligand bound AcrB was also solved and demonstrated that three ligand molecules can bind to the binding site near a central cavity (*10;11*).

Later the three dimensional structures of *E. coli* lactose permease (LacY) and Glycerol-3-phosphate (GlpT) from the major facilitator superfamily were simultaneously reported in 2003 (*12;13*). Major facilitator superfamily transporters are single-polypeptide secondary carriers capable of transporting small solutes in response to chemiosmotic ion gradients (*14*). LacY is the well-known $H^+$/lactose symporter whereas GlpT catalyses glycerol-3-P/Pi exchange. The transporters are

monomers and contain two homologous domains, each containing six transmembrane helices (TM). Their structures show a large hydrophilic cavity between the two domains that is open to the cytoplasm and closed to the periplasm. The substrate binding site is in the middle of the helices. These structures support the alternating access model for transport in which two domains move relative to each other and open the substrate binding site alternately to two sides of the membrane, that is towards the cytoplasm and periplasm (*12;15*).

In 2004 a structure of *E. coli* ammonia transporter, AmtB, was solved (*16*). The structure is similar to that of major facilitator family proteins (LacY and GlpT) with two structurally homologous domains with five TM in each. The ammonium ion ($NH_4^+$) binds to the AmtB and passage of ammonia ($NH_3$) takes place leaving proton ($H^+$) behind. Later in 2004 the structure of the glutamate transporter ($Glt_{ph}$) homolog from *Pyrococcus horikoshii* was reported (*17*). In vertebrates, the glutamate transporter plays a major role in the uptake of glutamate from the synaptic cleft in the central nervous system. The glutamate transporter forms a trimeric complex with a 'bowl-shape' structure (*17*). The actual substrate binding site is in between two reentrant loops. Translocation is carried out by opening and closing access to the substrate binding site by movement of the reentrant loops (*17;18*).

In 2005, the crystal structure of the leucine transporter ($LeuT_{Aa}$) from *Aquifex aeolicus* was reported at 1.65 Å (*19*). This bacterial structure has made a major contribution in our knowledge of the structure of mammalian membrane proteins as structural details from $LeuT_{Aa}$ have provided a framework to understand the molecular motion within the structure of serotonin transporter (SERT) (*20*). The structure of $LeuT_{Aa}$ is like a shallow 'shot glass', with the opening facing the

extracellular space, the base facing the cytoplasm, and the bottom of the 'glass' located in the membrane bilayer. There are 12 TM domains and the leucine binding site is near the middle of the TM 3 and 8. One of the $Na^+$ binding sites is adjucent to the leucine binding site. Crystal structure shows presence of the extracelluar and cytoplasmic gates that are residues and domains of $LeuT_{Aa,}$ which can alternately allow access to the binding sites from either side of the membrane bilayer.

Little information is known about the molecular mechanism and structural dynamics of membrane transporters because a crystal structure is static at particular conformational state of the transporter and therefore cannot provide image of complete transport cycle. Further no crystal structures for members of Solute Carrier Family 13, of which NaDC1 is a member, are yet available. Therefore, structural information about NaDC transporters is still lacking.

## TRANSLOCATION MECHANISM BY MEMBRANE TRANSPORTERS

Determination of three dimensional structures to atomic resolution has helped to understand various mechanisms of substrate transport across the membrane by membrane transporters (*21*). One mechanism of substrate transport, the 'alternating access mechanism', has been proposed for major facilitator superfamily member transporters such as LacY and GlpT (*12;15*). In this mechanism, substrate and ions bind to specific binding sites in the transporter. A conformational change takes place in the transporter, the cotransporter reorients itself so that the substrate and ion binding sites are now accessible from another side of the membrane and release of substrate takes place. The empty transporter returns to its

original conformational state for the next round of transport. Therefore, the alternating access model not only allows solutes to be transported from one side of the membrane to the other but also provides a mechanism for a transmembrane concentration difference of one solute to be utilized as a driving force to generate a concentration difference for another solute. The serotonin transporter (SERT) also follows an alternating access model which selectively transports 5-hydroxytryptamine (5-HT) into nerve cells together with $Na^+$ and $Cl^-$ and transports $K^+$ ion out of the cell (*20*). For SERT the transport pathway is lined by the cytoplasmic portions of TMs 6, 8, 1, 3 and 5 (*20*).

Membrane proteins such as the ammonium transporter AmtB are controversial in the mechanism of transport of their substrate. Translocation models suggest that the substrate is transported by facilitated diffusion through AmtB but experimental data also shows that the rate of transport of substrate is far below that of open channels but rather typical of transporters that usually undergo larger conformational changes (*22*).

The elevator mechanism has been proposed to explain the transport of multidrug transporters such as AcrB, in which a substrate is transported through the membrane by a funnel formed by protein components that bridge the periplasm. The substrates are delivered at the pore of the outer membrane. Conformational changes taking place in this mechanism are still unknown (*21*).

For glutamate transporters like GLT-1 a sluice-type mechanism of transport involving re-entrant or pore-loop structures has been proposed based on the results of cysteine-scanning mutagenesis and sulfhydryl specific labeling (*18*). In this model, the outer pore-loop opens to allow substrate to come inside the transporter and bind to

the binding site. The outer pore-loop closes thereby occluding the substrate within the transporter. Later an inner pore-loop opens to allow the transport of the substrate to another side of the membrane. The high-resolution structure of glutamate transporter, $Glt_{ph}$, from *Pyrococcus horikoshii* further supports this mechanism. This kind of transport mechanism has also been proposed for other glutamate transporters like GLAST, EAAC1 and excitatory amino acid transporters 4 and 5 (*23;24*). The GABA transporter GAT-1 has been proposed to allow an alternating access to substrate binding site by alternately opening and closing the outer and inner gates (TM 1 and 6 and loops) similar to that seen in the leucine transporter ($LeuT_{Aa}$) from *Aquifex aeolicus*.

## THE SOLUTE CARRIER 13 GENE FAMILY

The $Na^+$/dicarboxylate cotransporters (NaDCs) belong to a distinct gene family, called Solute Carrier Family 13 (SLC13) in the human gene nomenclature (*25;26*). The SLC13 gene family consists of five members in humans, with corresponding orthologs from different vertebrate species. Proteins in the SLC13 gene family are divided into two groups that transport different types of substrates. The $Na^+$/sulfate transporters 1 and 2 (NaS1 and 2) transport substrates such as sulfate and thiosulfate. The other members of the family, the low affinity $Na^+$/dicarboxylate cotransporter 1 (NaDC1), high affinity $Na^+$/dicarboxylate cotransporter 3 (NaDC3) and $Na^+$/citrate cotransporter (NaCT) transport di- and tri- carboxylates such as succinate, citrate, and α-ketoglutarate (Table 1.1). All the members of this family are approximately 40% to 50% identical in protein sequence (*26*). NaDC orthologs have

also been isolated from *C. elegans* (*27*) as well as *Drosophila* (*28*). Recently, a bacterial homolog of $Na^+$/dicarboxylate transporter has been isolated from *Staphylococcus aureus*, called SdcS (*29*).

**Table 1.1** General characteristics of members of the SLC13 family (Modified from (*26*))

| **Human Gene (Protein)** | **Substrate** | **Tissue distribution** | **Orthologs** | **Reference** |
|---|---|---|---|---|
| SLC13A1 (NaS1) | Sulfate $K_m$ 400 μM | Kidney, intestine | Human (h)<br>Rat (r)<br>Mouse (m)<br>*Xenopus laevis* (x) | *(30)*<br>*(31)*<br>*(32)*<br>*(33)* |
| SLC13A2 (NaDC1) | Dicarboxylates: succinate, citrate $K_m$ 800 μM (succinate) | Kidney, intestine | Human<br>Rabbit (rb)<br>Rat<br>Mouse<br>Opossum (o)<br>*Xenopus laevis* | (*34*)<br>(*35*)<br>(*36*)<br>(*37*)<br>(*38*)<br>(*39*) |
| SLC13A3 (NaDC3) | Dicarboxylates: succinate, α-ketoglutarate $K_m$ 20 μM (succinate) | Kidney, brain, liver, placenta | Human<br>Rat<br>Mouse<br>*Xenopus laevis*<br>Flounder (f) | (*40*)<br>(*41*)<br>(*42*)<br>*(43)*<br>*(44*) |
| SLC13A4 (NaS2) | Sulfate $K_m$ 400 μM | Brain, liver, endothelial venules, testis | Human | (*45;46*) |
| SLC13A5 (NaCT) | Citrate, dicarboxylates $K_m$ 600 μM (citrate) | Brain, liver, testis | Human<br>Rat<br>Mouse | (*47*)<br>(*48*)<br>(*49*) |

## THE LOW AFFINITY $Na^+$/DICARBOXYLATE COTRANSPORTER, NaDC1

### Isolation of NaDC1 cDNA

NaDC1 is the best studied $Na^+$/dicarboxylate cotransporter. The first NaDC1 was cloned in 1995 from rabbit kidney using the technique of expression cloning in *Xenopus* oocytes (*35*). NaDC1 cDNA is approximately 2.3 kb in length and codes for a protein of 593 amino acids. The human NaDC1 was cloned from kidney and the gene is found on chromosome 17 p11.1-q11.1 (*47;50*). To date rabbit, human, rat, mouse, opossum and *Xenopus laevis* NaDC1 orthologs have been identified and functional properties of these transporters have been intensively studied (Table 1.1). The amino acid sequences of the orthologs are about 65 to 78 % identical.

### Tissue distribution of NaDC1

Northern blot analysis was used to detect rbNaDC1 mRNA at size of 2.8 kb from both kidney and jejunum (*35*). The expression of hNaDC1 is weak in the kidney compared with that in the small intestine (*34*) whereas *Xenopus* NaDC1 is only detected in intestine (*39*). Immunohistochemistry of rNaDC1 provides more detailed localization of rNaDC1 in kidney. Polyclonal anti-rNaDC1 antibodies were used to stain rat kidney sections revealed a positive staining in the outer strip of the outer medulla and in the cortex. This suggests that the expression of rNaDC1 is exclusively in the renal proximal tubule S2 and S3 segments (*36*).

**Substrate specificity**

NaDC1 has broad substrate specificity. In general the preferred substrates are four carbon dicarboxylates (*37*). Using radiolabelled transport assays substrate specificity for rbNaDC1 and hNaDC1 was studied. Rabbit NaDC1 recognizes and transports divalent dicarboxylates such as succinate, fumarate, malate, α-ketoglutarate and divalent form of citrate but not lactate, pyruvate, aspartate or sulfate (*35*). The hNaDC1 prefers α-ketoglutarate, methylsuccinate, and dimethylsuccinate as its substrate (*34;51*).

**Cation sensitivity**

The transport of dicarboxylates by NaDC1 is coupled specifically to $Na^+$ ions because the replacement of $Na^+$ by other cations, except lithium, inhibits the transport (*52*). Lithium can substitute $Na^+$, but the affinity for succinate in presence of lithium is approximately ten times higher than with $Na^+$ (*53*). Lithium activated dicarboxylate transport takes place in rabbit, mouse, opossum and *Xenopus* NaDC1 whereas human and rat NaDC1 do not support succinate transport in presence of lithium (*37;54*). In presence of $Na^+$, lithium serves as inhibitor in NaDC1 mediated transport. At 2.5 mM lithium in presence of 97.5 mM $Na^+$, succinate uptake is inhibited by ~ 60 % in rbNaDC1 (*55*). It was also seen that high concentration of lithium can substitute $Na^+$ partially in terms of succinate transport in rbNaDC1 whereas low concentration of lithium inhibits succinate transport by competing for the cation binding sites (*37;38;54*).

**Functional characterization of NaDC1**

Functional characterization of NaDC1 was performed mainly by using radiotracer uptake assays and also with two electrode voltage clamp (TEVC) technique (*34;35;39;51;56*). In kinetic experiments, the Michaelis constant ($K_m$) for succinate is between 0.3 to 1 mM depending on the species, therefore NaDC1 is considered as a low affinity cotransporter. For rbNaDC1, $K_{Na}$ is 41 mM whereas for hNaDC1 $K_{Na}$ is 78 mM (*55*). In general, the half saturation coefficient, $K_{Na}$ is between 10 to 80 mM depending on the NaDC1 orthologs (*34;37-39;55*).

**$Na^+$-coupled transport mechanism of NaDC1**

NaDC1 mediates substrate transport with a proposed stoichiometry of three $Na^+$ ions for each dicarboxylate moiety (*51;57*). The transport process is electrogenic with movement of one positive charge from extracellular to cytoplasmic space, first electrophys of NaDC1 (*51*). The initial transport model was proposed for the $Na^+$/dicarboxylate cotransporter in rabbit renal brush-border membrane vesicles (*58*). Later two electrode voltage clamp experiments with hNaDC1 have suggested that $K_m$ of succinate is larger at lower $Na^+$ concentration but the $V_{max}$ is the same regardless of $Na^+$ concentration providing evidence for an ordered binding model in which $Na^+$ binds prior to succinate (*51*).

OUT

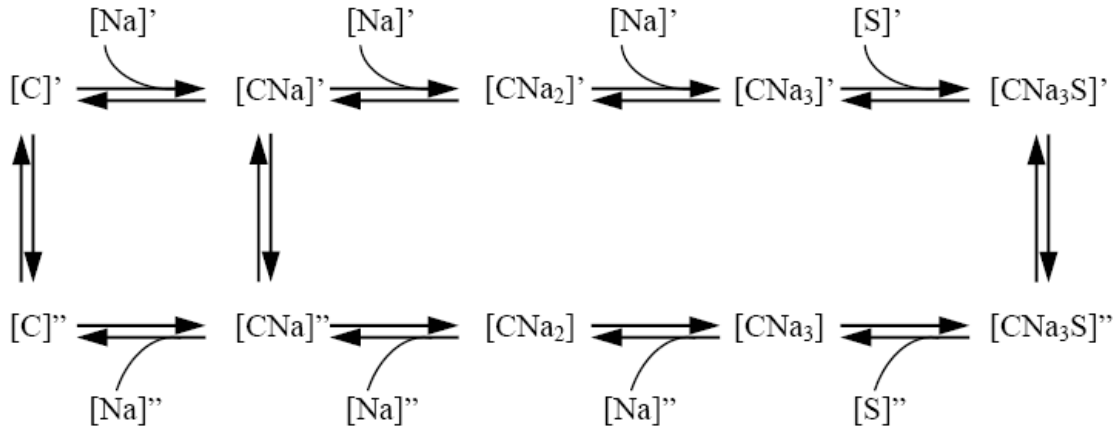


IN

**Figure 1.2** Transport model of $Na^+$/dicarboxylate cotransporter (modified from (*51*)). [C] represents the NaDC1 carrier, S represents dicarboxylate substrate. ‘ refers to an extracellular facing conformation whereas “ represents the intracellular conformation of the NaDC1.

As shown in Figure 1.2 sodium ions bind to the transporter which causes conformational change. This leads to an increased affinity for substrate. After the sodium and substrate are bound, the next step is the translocation of substrate and cations inside of the cell. After the translocation, sodium and substrate are released inside of the cell. There is no information about the order of $Na^+$ and substrate release. Then reorientation of NaDC1 takes place in order to initiate another cycle. The energy for transport is provided by the transmembrane $Na^+$ gradient and the potential difference across the membrane. This model is very similar to the models proposed for SGLT1 (*59*) and NIS (*60*).

**Secondary structure model of NaDC1**

There is currently little structural information known about any member of the SLC13 family. An important step in elucidating structure and function of membrane transporters is to understand their topology. Our current knowledge about NaDC1 topology comes both from hydropathy plots and some experimental data. Hydropathy analysis of the amino acid sequence of rbNaDC1 suggests 8 to 11 putative transmembrane (TM) domains depending on the prediction algorithm and the hydrophobicity scale. Initial model of NaDC1 predicted 8 TM helices for NaDC1 using Kyte and Doolittle hydropathy analysis (*35*). Later a revised secondary structure model based on hydropathy analysis using the Rao and Argos buried helix parameter was used and it predicted 11 TM in rbNaDC1 (*61*) (Figure 1.3). Previous experimental studies using immunofluroscence supported some aspects of this model. The Flag epitope tag (DYKDDDDDK) was fused to the amino terminus of NaDC1 and a monoclonal antibody against the Flag epitope showed that the amino terminus is located intracellularly (*62*). The loop between TM 4 and 5 was identified as being located intracellularly using polyclonal antibodies. These polyclonal antibodies were raised against a fusion protein containing amino acids 164-233 of rbNaDC1 (*62*). Previous studies also identified the N-glycosylation site at Asn–578, which places the carboxy terminus on the extracellular side of the plasma membrane (*61*). This glycosylation site is conserved across all species of NaDC1 and also in NaS1. In rbNaDC1, N-glycosylation appears to be required for protein sorting or targeting as

reflected by decreased protein expression in mutants lacking the N-glycosylation site at position 578 (*61*). Recently membrane topology structure of human high affinity $Na^+$/dicarboxylate cotransporter 3 (NaDC3) has been determined and indicates 11 TM helices with intracellular N terminus and an extracellular C terminus for NaDC3 (*63*). In general, topology of NaDC1 compares well with that of NaDC3.

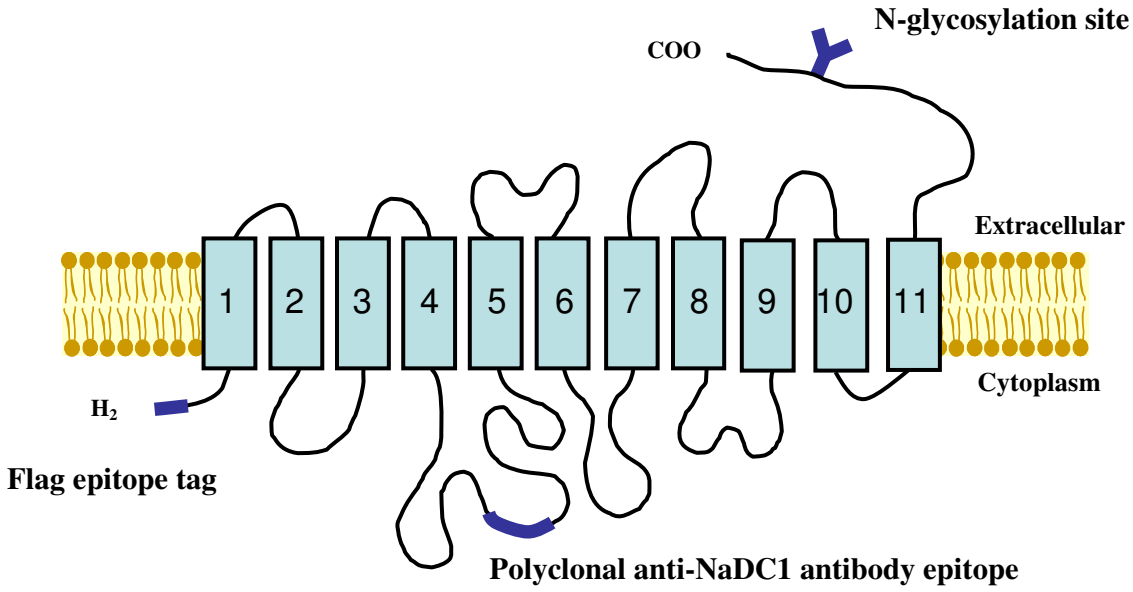


**Figure 1.3** Secondary structure model of NaDC1. The current secondary structure model of NaDC1 contains 11 putative TM helices. This model is based on hydropathy analysis with buried helix parameters by Rao and Argos (*64*). The amino terminus is located intracellularly and the carboxy terminus containing N-glycosylation site (Y) is extracellularly located.

### Structure-function studies of NaDC1

Due to difficulties in purification and crystallization of SLC13 transporters so far our major understanding of structure of NaDC1 comes from chimera studies and

site-directed mutagenesis. Earlier studies involving chimeras between rbNaDC1 and rNaS1 with 43% sequence identity indicates that substrate recognition site for NaDC1 is located near C terminal after Ser-141 (*65*). Chimera studies also indicated that first four helices contain residues that affect cation and substrate affinity (*65*). Further to identify which helices are actually involved in substrate binding, chimeras between rbNaDC1 and hNaDC1 were constructed. Citrate kinetics showed that helices 7, 10 and 11 and connecting loops contains the citrate binding site as well as one of the cation binding sites (*66*). To identify glutarate and adipate binding sites, a chimera between rbNaDC1 and mNaDC1 which share 74% sequence identity was made. Results indicate that TM 3 and 4 are involved in glutarate transport with some role of TM 7, 8 and 10 (*67*). The adipate binding site was found in TM 8, 9 and 10 but not in TM 3 and 4. Experiments also suggested that residue Ala-504 appears to be a determinant of adipate transport (*68*).

The substituted-cysteine scanning method (SCAM) was extensively used to identify functionally important residues in NaDC1. It was found that endogenous cysteine residues are not required for function of NaDC1 since all eleven cysteines can be replaced individually without changes in transport activity, their presence appears to be important for protein stability, trafficking to plasma membrane. Cysteine scanning mutagenesis in putative TM 9 showed that residues Ser-478, Ala-480, Ala-481 and Thr-482 are inhibited by membrane impermeable cysteine specific reagent [2-(trimethylammonium)ethyl] methanethiosulfonate (MTSET) and protected by substrate, succinate (*69*). Further cysteine scanning of TM 10 and extracellular loop 5 indicates that residues Thr-483, Thr-484, Leu-485, Leu-487, Ile-489 and Met-493 were sensitive to chemical labeling by MTSET, depending on conformational

state of the transporter (*70*). Therefore it was concluded that TM 9 and 10 are involved in the conformational changes during transport cycle and might form a part of permeation pathway for substrate and cation (*69;70*).

Site-directed mutagenesis experiments were also conducted to understand the importance of particular amino acids in NaDC1 structure and function. Site-directed mutagenesis studies identified Lys-84 as an important residue for succinate binding (*71;72*). Acidic residues such as Arg-349, Asp-373 and Glu-475 were found to be important for substrate as well as cation binding, which could indicate that the substrate and cation binding sites are located close together (*73*). It was observed that cysteine mutant of Arg-349, R349C, did not show succinate transport activity but the function was restored when labeled with MTSEA, which has similar size and charge as that of arginine; this result indicates the importance of Arg-349 residue for transport function (*74*). The amino acid at position 349 appears to be most accessible to the outside of the cell in the conformational state in presence of $Na^+$. Mutant Asp-373 was sensitive to MTSET and MTSEA but not to MTSES, which adds a negative charge. This study suggested that charge reversal at position 373 by chemical modification with MTSET or MTSEA produces inhibition of transport (*74*). Therefore, both Arg-349 and Asp-373 are involved in conformational changes associated with the transporter.

Mutagenesis of all 11 histidines in NaDC1 showed that His-106 in TM 3 shows a decrease in succinate uptake due to a decrease in $V_{max}$ without a change in $K_m$. The decrease in succinate transport corresponds to a decrease in expression on the plasma membrane. This suggests that His-106 is involved in expression on membrane rather than function of succinate transport (*75*).

Ser-512 or rbNaDC1 or Thr-509 of hNaDC1 when mutated to S512T in rabbit and T509S in human have partial change in $K_m$ for citrate and succinate but larger changes in apparent affinity for substrate and cations. This result suggests that Ser-512 is an important determinant of functional differences in apparent affinity for substrate and cations with substrate and cation binding sites located near one another in NaDC1 (*76*). Taken together the results of site-directed mutagenesis of NaDC1 identify important residues that directly or indirectly interact with the substrate as well as residues important in conformational changes seen during the transport cycle.

**Physiological significance of NaDC1**

NaDC1 is found primarily in the small intestine and kidney. The normal function of intestinal NaDC1 is the absorption of dietary di- and tri- carboxylates from gastrointestinal secretions (*77-79*). The main role of NaDC1 in the kidney is reabsorption of plasma citric acid cycle intermediates such as succinate, citrate and α-ketoglutarate which are filtered through the glomerulus (*26*). Citrate provides 10-15% of the fuel for renal oxidative metabolism (*80*). Recent studies with NaDC1 deficient mice showed an increase in urinary excretion of citric acid cycle intermediates (*81*). Therefore, this study confirms that NaDC1 is a major player in urinary citrate excretion and is responsible for reabsorption of citric acid cycle intermediates

As shown in Figure 1.4 renal proximal epithelial cell NaDC1 functions along with organic anion transporters 1 and 3 which are expressed on the basolateral membrane (*82;83*). NaDCs are involved indirectly in the process of secreting organic

anions, including drugs and xenobiotics out of the cells (*84*). Transported dicarboxylates become a substrate to the organic anion/dicarboxylate exchangers (OAT), which are responsible to take up organic anions from the blood circulation to the cells. Eventually organic anions are eliminated from the cell by OAT 4 (*85-87*), MRP 2 and 4, facilitated diffusion carriers on apical membrane (*82;88*).

In kidney, NaDC1 helps to regulate the urinary citrate concentrations. Low urinary citrate concentrations or hypocitraturia are usually associated with development of urolithiasis (kidney stone) (*89*). The role of citrate in urine is to chelate calcium ions and prevent precipitation of calcium salts (*89*). These calcium ions form insoluble complexes with other anions such as phosphates, oxalates, if urinary citrate concentration is low. Approximately 50% of nephrolithiasis patients have hypocitraturia (*89*). Aruga et al showed that increased expression of NaDC1 has been correlated with a decrease in urinary citrate excretion and thus associating with occurrence of nephrolithiasis (*90*).

A recent study also showed that succinate and α-ketoglutarate serve as natural ligands for orphan G-protein-coupled receptors (GPR91) in the proximal and distal tubules (*91*). This study indicates that succinate can increase blood pressure in mice and the renin-angiotensin system is involved in succinate-induced hypertension. It was also observed that dicarboxylate concentration surrounding proximal tubular cells is an important factor that regulates renovascular hypertension. Thus, one of the hypothesis is that NaDC transporter may affect blood pressure regulation via G-protein-coupled receptors for succinate and α-ketoglutarate in the proximal tubule.

The homolog of NaDC1 from *Drosophila*, *Indy*, is a $Na^+$-independent dicarboxylate transporter (*92*). *Indy* is expressed in midgut (analogous to small

intestine), fat body and oenocyte which are important for metabolism. Mutation in one copy of the *Indy* gene leads to the decrease transport activity and elongation of life span. This suggests that low activity of *Indy* affects metabolism of *Drosophila* leading to increased lifespan (*28*). Similar results were seen in NaDC1 homolog from *C. elegans* (CeNaDC2, $Na^+$/dependent transporter). Knockdown of the function of CeNaDC2 significantly increases lifespan of the worm compared with the control worm by 15% (*27*). It has been well established in *C. elegans* that caloric restriction or suppression of metabolic energy production within the mitochondria is associated with a significant increase in life span (*93*). Thus, the phenomena of caloric restriction or suppression of metabolic energy production in mitochondria is associated with increased life span which may be analogous to involvement of NaDC in aging (*93*). To test this hypothesis further studies were carried out *in vivo* in NaDC1 deficient mice. However these mice did not show any significant difference in metabolic or physiological changes associated due to caloric restriction (*81*). This suggests that NaDC1 may not mediate the effect of caloric restriction.

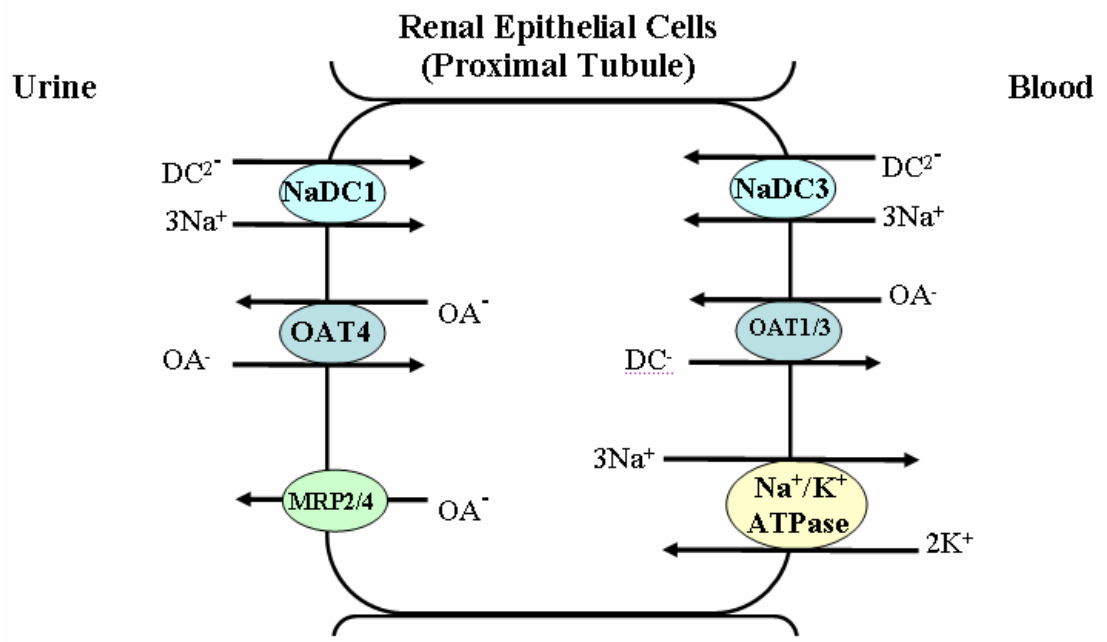


**Figure 1.4** Schematic representation of dicarboxylate transport in renal proximal tubules. The low-affinity $Na^+$/dicarboxylate cotransporter, NaDC1, is expressed on the apical membrane of renal epithelial cells. The high-affinity $Na^+$/dicarboxylate cotransporter, NaDC3, is expressed on the basolateral membrane of renal epithelial cells. The $Na^+/K^+$ ATPase located on the basolateral membrane generates electrochemical gradient of sodium, which is a driving force for NaDC transport. Using electrochemical gradient of sodium, NaDCs transport one divalent dicarboxylate ($DC^{2-}$) inside the cell coupled with three sodium ions. The intracellular dicarboxylates are mostly utilized for metabolism, and also involved in uptake of organic anions ($OA^-$) from the blood circulation or the lumen which is mediated by the dicarboxylate/organic anion exchangers (OAT) on the apical or basolateral membrane. The intracellular $OA^-$ is then secreted out by OAT 4, MRP members (MRP 2 and 4). (Modified from (*25*))

## THE $Na^+$/DICARBOXYLATE SYMPORTER FROM *Staphylococcus aureus*

The $Na^+$/dicarboxylate symporter (SdcS) from *Staphylococcus aureus* was cloned and functionally expressed (*29*). Sequence identity between SdcS and hNaDC1 is 35 %. SdcS has many functional properties similar to that of NaDCs. SdcS is a $Na^+$-coupled transporter. The substrates of SdcS include succinate,

fumarate and malate. SdcS transports these substrates with high affinity ($K_m$ is between 5 to 15 μM). The study of SdcS has several advantages over eukaryotic transporters. SdcS is more easily purified (*94*), potentially crystallized, can be expressed in *E. coli* and one can construct right-side-out and inside-out vesicles and study outside as well as inside of the transporter which is almost impossible in mammalian NaDCs. Therefore, SdcS can be used as a model to further study structural and functional properties of mammalian SLC13 member transporters.

## AIMS OF THE STUDIES IN THIS DISSERTATION

The overall goal of my dissertation research was to understand topological structure of the $Na^+$/dicarboxylate cotransporter as well as to identify and characterize functionally and conformationally sensitive residues, which will provide insight into structural details of the NaDC1 transporter.

### Aim 1: To determine the role of conserved proline residues in the structure and function of $Na^+$/dicarboxylate cotransporter 1

Prolines play important roles in TM of membrane proteins and are particularly involved in helical kink formation. Previous studies indicated the importance of TM 7, 10 and 11 of NaDC1 for substrate binding. Therefore, in this study, conserved prolines from TM 7 and 10 were mutated to alanine and glycine to understand the structural as well as functional importance of these residues. Alanine is a strong α-helix former and is less flexible whereas glycine, with no side chain, is a strong helix breaker and is more flexible. If prolines in NaDC1 are responsible for kink formation

and if kink is necessary for maintaining the stability of the transporter then mutating proline to glycine will have less of an effect compared with mutating to alanine. Therefore, the aim of this study was to understand role of conserved prolines in helical kink formation.

**Aim 2: To determine the topology of $Na^+$/dicarboxylate cotransporter 1 using site-directed chemical labeling.**

The current model of NaDC1, based on hydropathy analysis, contains 11 TM but secondary structure prediction algorithms predict at least 13 TM. Therefore, the aim of this study was to determine the topology of NaDC1 using biochemical as well as computation approaches. To distinguish between 11 and 13 TM topology models, individual cysteines were substituted in putative extracellular and intracellular loops of the rabbit NaDC1 transporter by site-directed mutagenesis. The membrane impermeable reagent, MTSEA-biotin (N-biotinylaminoethyl methanethiosulfonate), was used to covalently label cysteine residues accessible from the outside of the cell.

**Aim 3: Identification of conformationally sensitive amino acids in the $Na^+$/dicarboxylate symporter.**

Biochemical studies indicate similarity between SdcS and mammalian NaDC1. Therefore, SdcS was used as a model to study structural details of NaDC1. The goal of this study was to find conformationally important residues in SdcS that are accessible from both sides of the membrane. Previous studies indicate that

rbNaDC1 contains structurally, functionally and conformationally important residues such as Asp-373, Met-493, Lys-84. When protein sequence of rbNaDC1 was aligned with SdcS these residues corresponds to Asp-329, Leu-436 and Asn-108 of SdcS. Cysteines were substituted at these positions and their accessibility was tested by MTSET reagent in right-side-out and in inside-out vesicles, in different conformational conditions such as in presence and absence of $Na^+$ and substrate.

**Aim 4: Identification of determinants of citrate binding and transport in the bacterial $Na^+$/dicarboxylate symporter using random mutagenesis approach.**

The goal of this study was to identify functionally important residues that are involved in substrate binding in $Na^+$/dicarboxylate symporter (SdcS). A directed evolution approach was used to convert the SdcS, which transports succinate to a citrate transporter. SdcS was subjected to random mutagenesis. Later SdcS mutants were screened for their ability to transport citrate. None of the screened mutants showed citrate transport. Therefore, this study was not continued.

Therefore, these studies provide information about structural details of the transporter as well as are helpful in understanding conformational changes taking place in NaDC1. The structural knowledge of NaDC1 may lead to development of therapeutic agent for treatment or prevention of kidney disease or other disorders mediated by NaDC1.

# CHAPTER 2: ROLE OF CONSERVED PROLINES IN THE STRUCTURE AND FUNCTION OF THE $Na^+$/DICARBOXYLATE COTRANSPORTER 1

(Studies in this chapter have been reproduced from: Joshi A. D. and Pajor A. M (2006). Role of conserved prolines in the structure and function of the $Na^+$/dicarboxylate cotransporter, NaDC1. Biochemistry 45 (13) 4231 – 4239)

## INTRODUCTION

Prolines play important structural as well as functional roles in membrane proteins. Normally, hydrogen bonds between backbone amino acids contribute to the structure and stability of transmembrane α-helices. Proline lacks amide hydrogen that prevents it from forming backbone hydrogen bonds in the helix. This can potentially introduce a kink in the helix, depending on the local environment. Prolines contribute to the structure of membrane proteins by facilitating helix packing (*95*) or by stabilizing the conformation of α-helices and loops (*96*). In bacteriorhodopsin, prolines in transmembrane helices are important in determining the rate of protein folding and assembly (*97*). Prolines also exhibit various functional roles in membrane transporters and ion channels, including acting as ligand binding sites for cations (*98*) and as molecular switches or hinges involved in conformational changes (*99;100*).

NaDC1 contains a number of conserved prolines within or at the boundaries of transmembrane helices (TM) although their functional role is still unknown. In this study focus was given to prolines in TM 7 and 10 as previous experiments by our group suggest that these TM may be part of the substrate binding domain and at least one cation binding site (*66*). The conserved prolines in TM 10 of NaDC1 may be

important in protein structure or targeting since replacement of these prolines with cysteine resulted in little or no protein on the plasma membrane (*70*). To understand the possible role of the conserved proline residues in NaDC1, prolines were replaced with alanine or glycine. Alanine is a strong α-helix former and is less flexible whereas glycine, with no side chain, is a strong helix breaker and is more flexible.

The results of this study show that Pro-327 in TM 7 appears to be critical for protein structure as the glycine mutant at this position had no protein expression and could not be rescued by chemical chaperones or second site mutations. Pro-351 in TM 7 produces misfolded or mistargeted proteins when mutated to alanine or glycine. These mutant transporters were unable to insert into the plasma membrane and were accumulated intracellularly. However, these mutants could be rescued by chemical chaperones or insertion of a proline at a second site. Therefore, this residue may be important in targeting and stability of the transporter protein. Interestingly, the only mutant to exhibit a functional change was the double mutant, P351A-F347P, which had a change in Transport Specificity Ratio and decreased $K_m$ for succinate. The prolines found in TM 10 at positions 523 and 524 do not appear to have functional roles but might be important for protein stability.

## MATERIALS AND METHODS

### Site-directed mutagenesis

Site directed mutagenesis was performed using the QuikChange site-directed mutagenesis kit (Stratagene). In denaturation stage, double stranded cDNA was denatured by increasing the temperature to 95°C. Further, the cDNA was annealed

with sense and antisense oligonucleotide primers containing the desired mutations. The extension was carried out by high fidelity *pfu Turbo* DNA® polymerase. The parental methylated and hemimethylated cDNA was cut with *Dpn*I and the cDNA containing the mutation was transformed into XL1-blue strain of *E. coli*. Rabbit (rb) NaDC1 in pcDNA3.1 vector was used as a template (*35*). I was unable to make the P327A mutant. Double mutants were prepared using single mutants, P351A, P351G and P327G, as templates. Mutants were verified by sequencing at the Protein Chemistry Laboratory at the University of Texas Medical Branch, using an Applied Biosystems Model 3100 automated DNA sequencing unit.

**Expression of rbNaDC1 Mutants in HRPE Cells**

Human retinal pigment epithelial (HRPE) cells transformed with SV40 (AG 06096; Coriell Institute), were cultured in Modified Eagle's Medium (MEM) containing Glutamax, 25 mM HEPES (Invitrogen) along with 10% heat-inactivated fetal calf serum, 100 units/ml penicillin and 100 µg/ml of streptomycin. Cells were incubated at 37 °C in 5% $CO_2$. Since most of the proline mutants showed significantly lower succinate transport activity compared with wild-type, transport assays were performed in 6 well plates. Those mutants with high activity were further characterized by using dual-label competitive uptake experiments in 24 well plates. For 6 well plates, $3 \times 10^5$ cells were plated per well whereas for 24 well plates $1.2 \times 10^5$ cells were plated per well. The next day cells were transiently transfected with 3 µl of FuGENE 6 (Roche Applied Science) and 1 µg of plasmid DNA (ratio of 3:1) for 6 well plates. For 24 well plates, cells were transfected with 1.8 µl of FuGENE 6 and 0.6 µg of plasmid DNA (9:3 ratio). For experiments with chemical

chaperones, the culture medium was replaced with medium supplemented with 0.5 M glycerol or 250 mM dimethyl sulfoxide (DMSO) 6 hours after transfection, and the cells were cultured in this medium a further 42 hours before transport and protein expression were measured. For all experiments, uptakes in vector-transfected cells were subtracted from uptakes in cells transfected with plasmids containing NaDC1 and mutants.

**Transport Assays**

Transport assays were carried out 48 hours after transfections. Sodium buffer containing 120 mM NaCl, 5 mM KCl, 1.2 mM $MgSO_4$, 1.2 mM $CaCl_2$, 5 mM D-glucose, 25 mM HEPES, pH adjusted to 7.4 with 1 M Tris was used for all experiments. Each well was washed twice with sodium buffer and then incubated for 30 min with 1 ml sodium buffer containing 100 μM of $^{3}$H-succinate (ViTrax). Uptakes were stopped and radioactivity was washed away with four washes of 3 ml sodium buffer. Cells were dissolved in 1% SDS, transferred to scintillation vials and counted with a liquid scintillation counter (Packard Tri-Carb 2100 TR). Kinetic parameters for the wild-type and double mutant were calculated by fitting the transport rates to the Michaelis-Menten equation using nonlinear regression analysis (SigmaPlot 8.0).

**Dual-label Competitive Transport Experiments**

For dual-label transport assays sodium buffer containing both 10 μM of $^{3}$H-succinate (ViTrax) and 20 μM of $^{14}$C-citrate (Moravek Biochemicals Inc.) was added to the cells in 24 well plates and competitive transport of these substrates was

measured using a dual-label counting protocol on the scintillation counter. The uptake volume used was 250 µl/well. Transport specificity ratios (TSR) for wild type rbNaDC1 and mutants were calculated using: $TSR = (\nu_{succinate} / \nu_{citrate}) \times ( [citrate] / [succinate] )$ , where $\nu_{succinate}$ and $\nu_{citrate}$ are the initial rates of transport of $^{3}$H-succinate and $^{14}$C-citrate, [citrate] and [succinate] are the concentrations of citrate and succinate used (*101;102*). Statistical analysis was performed using Student's t-test (SigmaStat program).

**Cell Surface Biotinylation and Total Protein Expression**

Cell surface biotinylations of NaDC1 mutants expressed in HRPE cells were performed using the impermeant reagent, Sulfo-NHS-LC-biotin (Pierce), as described previously (*69;70*). HRPE cells were grown in 6 well plates and transfected as described above for transport assays. Forty-eight hours after transfections, each well was washed three times with 3 ml phosphate-buffered saline containing 1 mM of $Ca^{2+}$ and $Mg^{2+}$ (PBS/CM, pH 9). Then 500 µl of 1.5 mg/ml Sulfo-NHS-LC-biotin (Pierce) freshly prepared in PBS/CM was added to each well. Cells were allowed to incubate for 30 min at room temperature. Cells were washed once and then incubated on ice for 20 min with 3 ml of cold quench buffer (PBS/CM with 100 mM glycine). Sulfo-NHS-LC-biotin labeled cells were then lysed with 0.5 ml of lysis buffer (20 mM Tris (pH 7.5), 1% Triton X-100, 150 mM NaCl, 5 mM EDTA, 10 µg/ml pepstatin, 10 µg/ml leupeptin and 0.5 mM phenylmethylsulfonyl fluoride (PMSF)) on ice with gentle rocking for 30 min. The contents of 2 wells were combined in microcentrifuge tube and spun down for 15 min. Supernatants were transferred to new tubes. Samples were then incubated with 50 µl of Immunopure Immobilized Streptavidin (Pierce)

overnight at 4 °C with end-over-end rotation. The next day beads were washed three times with lysis buffer, twice with high salt wash buffer (same as lysis buffer but containing 0.1% Triton X-100 and 500 mM NaCl) and once with no salt wash buffer (50 mM Tris base pH 7.5). Biotinylated proteins were eluted with 50 µl of 3X tricine gel loading buffer (150 mM Tris-HCl pH 7, 30% glycerol, 12% SDS, 6% β-mercaptoethanol, ~ 3% Commassie blue R-250) for 10 min at 85 °C. The procedure used to measure total biotinylated proteins was almost identical to that of the cell-surface biotinylations except that the lysis buffer was added before the Sulfo-NHS-LC-biotin, and this was followed by the streptavidin beads (*62*). Samples were applied to 7.5% Tricine gel and transferred for Western blotting as described (*103*). Blots were incubated with 1:1000 dilutions of anti-NaDC1 antibodies (*75*) or with 1:2000 dilution of anti-calnexin antibodies (Stressgen). Supersignal West Pico chemiluminescent substrate kit (Pierce) was used to detect antibody binding. Images were captured by using Kodak Image Station 440CF. Image 1D analysis software (Eastman Kodak Co.) was used to analyze quantities of protein expressed.

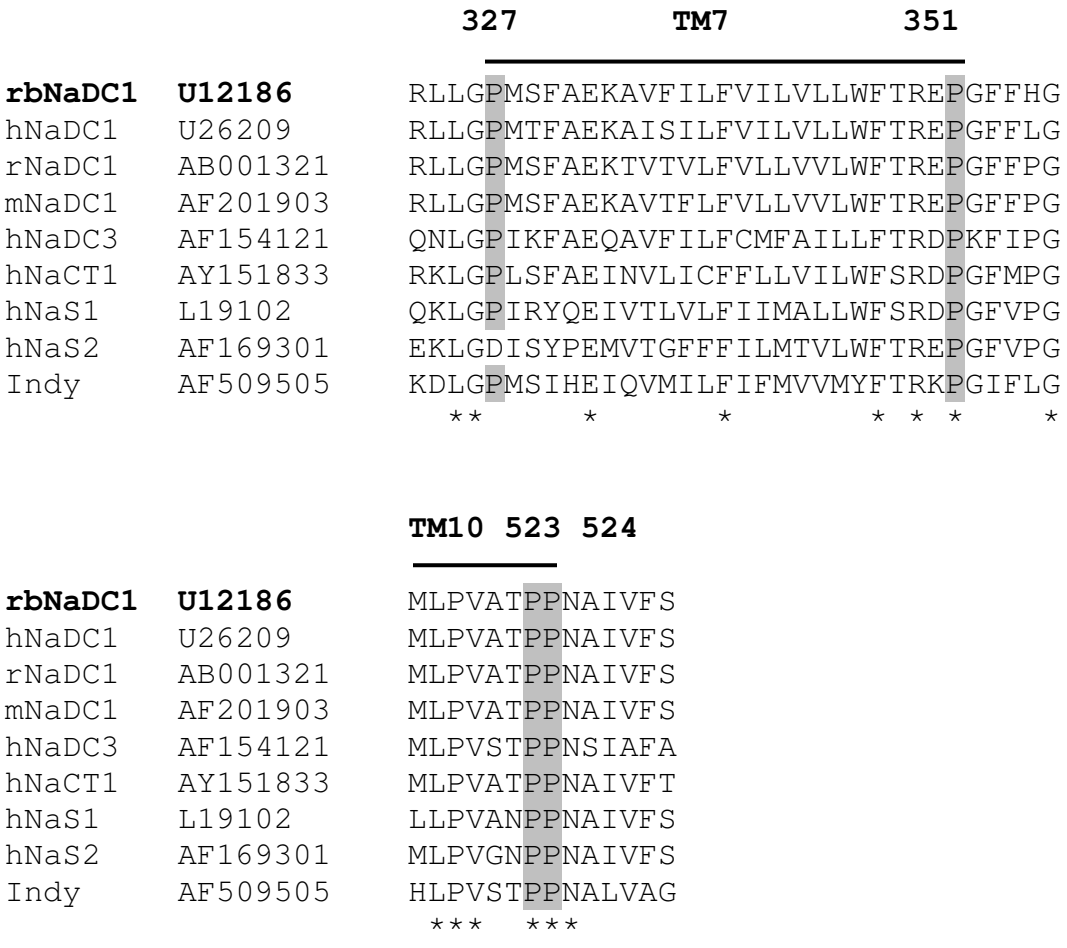


**Figure 2.1** Multiple sequence alignments of transmembrane helices 7 and 10 from rbNaDC1 with some members of SLC13 gene family, including the sodium-independent dicarboxylate transporter from Drosophila, Indy. Positions of conserved prolines mutated in this study are highlighted. The GenBank™ accession numbers are written next to the transporter names. The sequence alignment was performed with ClustalW (1.82) with default parameters using Gonnet matrix. Locations of transmembrane helices 7 and 10, according to the 11 TM helix model based on Rao-Argos buried helix parameter scale (*37;61*) are shown by lines above the sequence. The asterisks indicate conserved amino acid residues in the proteins.

## RESULTS

### Proline to Alanine and Glycine Mutations in rbNaDC1

The sequence alignment of rbNaDC1 with other members of SLC13 gene family shows conserved proline residues in TM 7 and 10, based on the predicted secondary structure model (Figure 2.1) (*61*). The conserved prolines at positions 327, 351, 523 and 524 were mutated to alanine and glycine to determine the involvement of these residues in the conformational stability of the transporter as well as the transport function. Alanine was substituted for proline because it has a methyl group side chain and tends to promote and maintain α-helical structure. Glycine lacks the methyl group side chain, is less hydrophobic than alanine and prefers a flexible conformation. If a proline kink or distortion of the α-helix is necessary for the stability and function of NaDC1, mutating the proline to glycine will have less of an effect compared with alanine.

### Protein Expression and Transport Activity of Proline Mutants

Cell surface expression of mutants was monitored by cell surface biotinylation with the membrane impermeant reagent, Sulfo-NHS-LC-biotin, followed by Western blotting. Total protein expression was measured by lysing the cells before addition of the Sulfo-NHS-LC-biotin. Figure 2.2 shows single representative blots of cell surface and total protein expression for each proline mutant compared with the wild-type control. The two bands represent differently glycosylated forms of the transporter (*61*). The blots were scanned to quantitate the protein expression and each mutant was expressed as a percentage of the wild-type rbNaDC1 from the same blot. The transport activity and protein expression of the single proline mutants are compared in

Figure 2.3A. No cell surface expression was seen for Pro-327 and Pro-351 mutants. However, the Pro-351 mutants appeared to be located intracellularly (Figures 2.2 and 2.3A) indicating possible defects in protein trafficking. In general, the cell surface expression of most of the mutants correlated with the uptake activity, although the P524G mutant had higher cell surface and total protein expression compared with activity (Figure 2.3A). The P524A mutant appeared to have lower protein expression compared with activity.

Double mutants were constructed to determine whether the addition of a proline residue at a second site could reverse the effect of removing a proline. Since an α-helix contains 3.6 residues per turn, we constructed the double mutant P327G-A331P but this mutant was not expressed on the plasma membrane or intracellularly (Figures 2.2 and 2.3B). Five second site mutations were made in transporters lacking Pro-351, three based on P351A and two based on P351G. The double mutants based on P351G introduced proline in place of Gly-352 or Gly-356. In the other double mutants based on P351A, P351A-F347P, P351A-F353P and P351A-W346P, rigidity was introduced and helical conformation was established by introducing alanine at position 351 and then adding proline at various positions in the helical turn to try to restore the activity. Only two of these mutants had increased protein expression and transport activity relative to the single mutants: P351A-F347P, which was restored to almost wild-type levels, and P351A-G352P, which had low transport activity relative to protein expression (Figure 2.3B). The double mutants P351A-F353P, P351A-W346P and P351G-G356P, and the single mutant F347P, had no protein expression, measured from total and cell surface biotinylations (Figure 2.2 and 2.3B). Overall,

the majority of Pro-351 mutants appeared to have problems with misfolding or mistargeting since their cell surface protein expression was reduced.

**Effect of Chemical Chaperones on Inactive TM 7 Mutants**

Chemical chaperones, such as glycerol or dimethyl sulfoxide (DMSO), have proven effective in correcting trafficking defects in mutants of Aquaporin-2 (*104*). Therefore, chemical chaperones were used to test improvement in the expression of the non-expressing NaDC1 mutants. DMSO (250 mM) had less of an effect in improving cell surface expression of NaDC1 mutants compared with glycerol (results not shown). Glycerol concentrations from 0.2 to 4 M were tested but the most effective was 0.5 and 1 M. Figure 2.4 shows cell surface and total protein expression of wild type and various TM 7 single and double mutants. The addition of 0.5 M glycerol to the wild type NaDC1 decreased succinate transport (Figure 2.4 and 2.5A) but the same treatment produced increased activity and cell surface expression of the P351A and P351G mutants (Figure 2.4 and 2.5B). The transport activity for both P351A and P351G was lower than the amount of transporter protein found on the cell surface (Figure 2.5B). Glycerol treatment did not measurably improve the expression of any of the other mutants (Figure 2.4 and 2.5).

**Functional Characteristics of Proline Mutants**

The transport specificity ratio (TSR) is a novel approach to compare the effects of site-directed mutagenesis on function by monitoring relative changes in catalytic specificity ($k_{cat}$ / $K_m$) (*101;102*). Previous studies showed that TSR analysis is independent of protein expression and is valid over a wide range of substrate

concentrations (*101*). The TSR is calculated from the initial rates of transport of two substrates in a dual-label competitive uptake experiment. The time course of uptakes of 10 μM $^{3}$H-succinate and 20 μM $^{14}$C-citrate in HRPE cells expressing the wild-type NaDC1 is shown in Fig. 2.6A. The time course is linear through 30 min and we selected 20 min as the time point for future experiments. TSR values were found to be similar between 5 to 30 minutes (Figure 2.6B). The succinate:citrate transport specificity ratio (TSR) for rbNaDC1 and most of the mutants was found to be approximately 2.5, independent of expression and uptake activity of single substrates. Figure 2.7A shows competitive uptake between radioactive succinate and citrate in each mutant. The only mutant that showed a change in TSR was the P351A-F347P double mutant, which had a mean TSR value of about 8, significantly higher than the wild type (Figure 2.7B). A different combination of substrate concentrations (0.01 μM $^{3}$H-succinate and 10 μM $^{14}$C-citrate) was also tested and the TSR values were similar (results not shown). We did kinetic analysis of the double mutant, P351A-F347P. The apparent $K_m$ for succinate was found to be approximately 14 μM compared with a $K_m$ of about 500 μM in wild type rbNaDC1 (Table 2.1) (*35*). Citrate transport by the P351A-F347P mutant was too low for kinetic analysis.

The succinate:citrate TSR values for P351A and P351G were calculated after treating these mutants with 0.5 M glycerol. Glycerol treatment did not affect the wild-type TSR value, and no significant difference was seen in TSR values between wild-type and the Pro-351 mutants (Figure 2.8). Therefore, although many of the mutants had differences in expression and activity, there was no change in catalytic efficiency of succinate transport relative to citrate in any mutant except P351A-F347P.

**Table 2.1 Succinate kinetics of rbNaDC1 and double mutant P351A-F347P[a]**

| Protein | $K_m$ (μM) | $V_{max}$ (fmol/min-well) | *n* |
|---|---|---|---|
| rbNaDC1 | 590 | 42300 | 1 |
| P51A-F347P | 13.6 ± 0.8 | 1445 ± 48 | 2 |

[a] Wild type rbNaDC1 and the P351A-F347P mutant were transiently expressed in HRPE cells. Succinate uptakes were measured at concentrations up to 2 mM for WT and 0.5 mM for mutant as described in Materials and Methods. The kinetic values for the mutant represent mean ± range of two independent experiments. The rbNaDC1 kinetic parameters compare well with the $K_m$ of 0.5 mM measured in our previous studies (*35*).

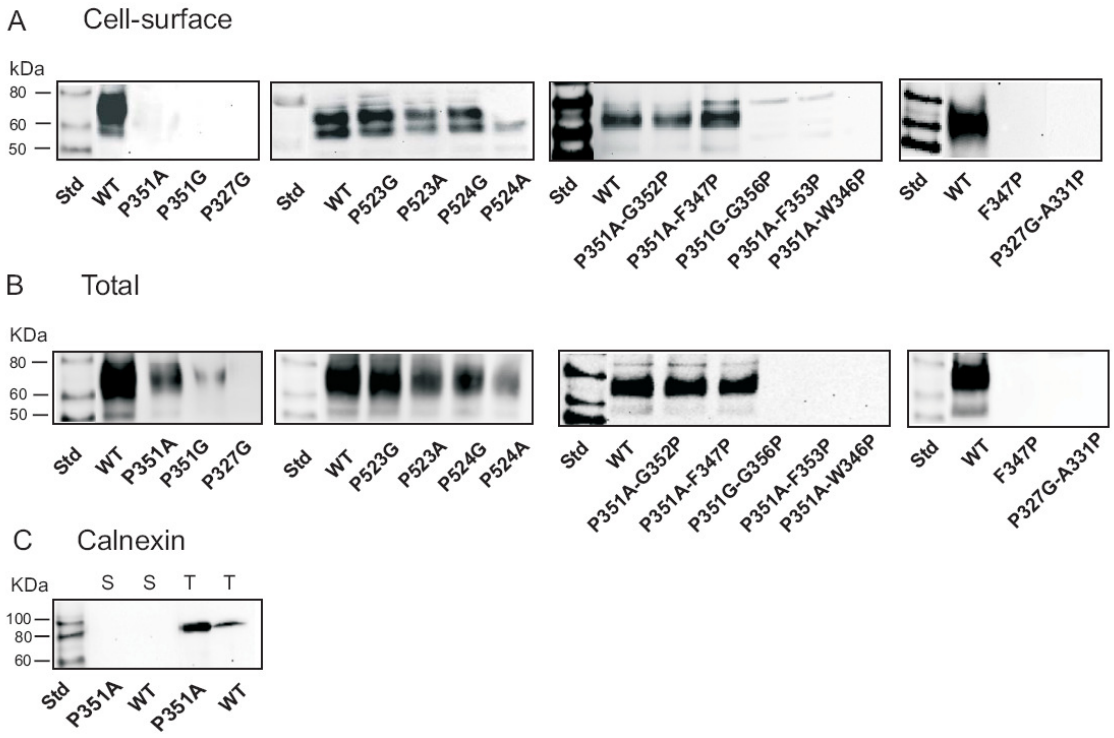


**Figure 2.2** Western blots of (A) cell surface and (B) total biotinylated protein expression. HRPE cells were transiently transfected with wild-type and mutant rbNaDC1 and then treated with Sulfo-NHS-LC-biotin. For total protein expression, cell lysis buffer was added before addition of Sulfo-NHS-LC-biotin. Western blots were probed with 1:1000 dilution of anti-NaDC1 antibodies, followed by 1:5000 dilution of horseradish peroxidase-linked anti-rabbit Ig. The two bands represent differently glycosylated forms of rbNaDC1 (*61;75*). (C) Western blots of cell surface (S) and total (T) biotinylated proteins probed with anti-calnexin antibodies (1:2000 dilution), as a marker of endoplasmic reticulum. Chemiluminescent molecular weight standards (Std) are shown in first lane of each blot.

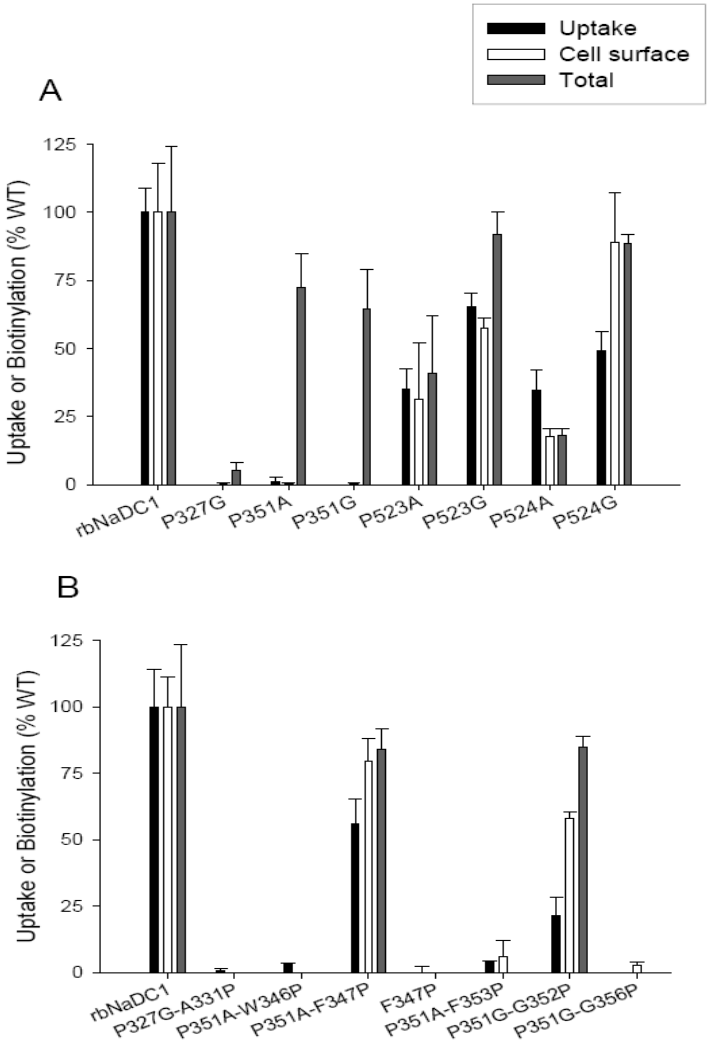


**Figure 2.3** Activity and expression of single (A) and double (B) mutants of rbNaDC1. The activity, cell surface and total protein expression of the mutants are shown as a percentage of wild-type rbNaDC1 (WT) as control. Transport activity of 100 μM $^{3}$H-succinate was measured with 30 minutes incubation in sodium containing buffer. Transport results for the mutants are means ± range or SEM (n = 2 or 3). Protein expression was determined by quantitating the intensities of NaDC1 protein bands from Western blots (such as Figure 2) using Image 1D analysis software. Bars represent mean ± range or SEM (n = 2 to 4 blots). Error bars on the wild-type groups represent the variation between experiments expressed as a percentage of the mean from each panel, n = 11 (activity, Panel A) or 18 (activity, B), n=4-6 (blots, A and B). Background uptakes in vector-transfected cells were: (A) 0.8 ± 0.06 and (B) 1.4 ± 0.07 pmol/min-well. Background-corrected rates in wild type NaDC1 were: (A) 3.2 ± 0.3 or (B) 7.7 ± 1.0 pmol/min-well.

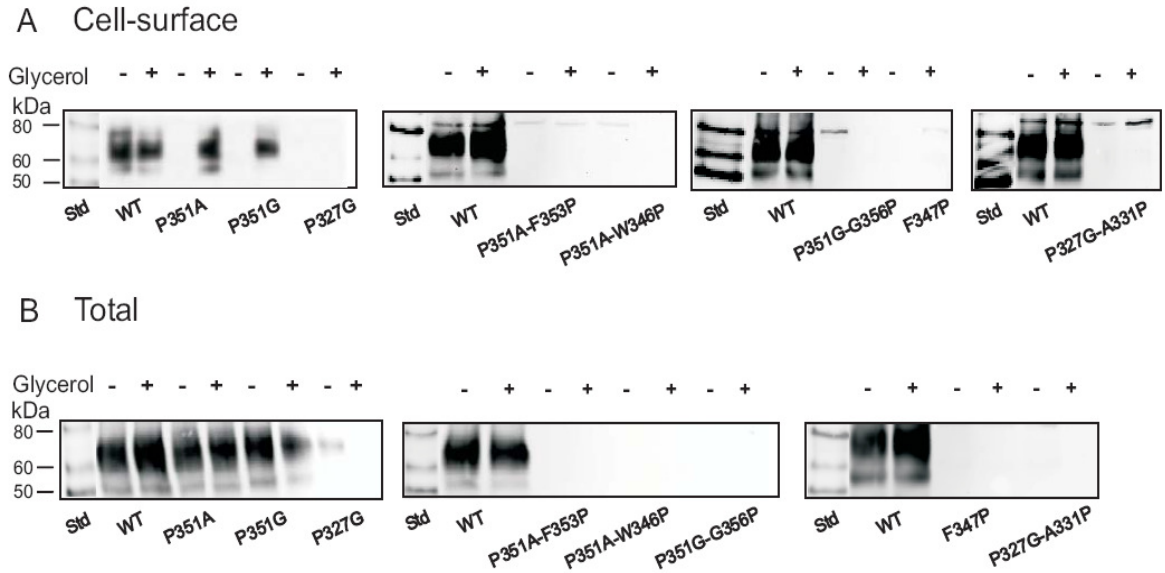


**Figure 2.4** Treatment of non-expressing mutants with glycerol. (A) Representative Western blots of cell-surface biotinylated protein expression and (B) total biotinylated protein expression without (-) and with (+) addition of 0.5 M glycerol to the medium, as described in Experimental Procedures. Blots were probed with 1:1000 dilution of anti-NaDC1 antibodies, followed by 1:5000 dilution of horseradish peroxidase-linked anti-rabbit antibodies. Chemiluminescent molecular weight markers (Std) are shown in the first lane of each blot.

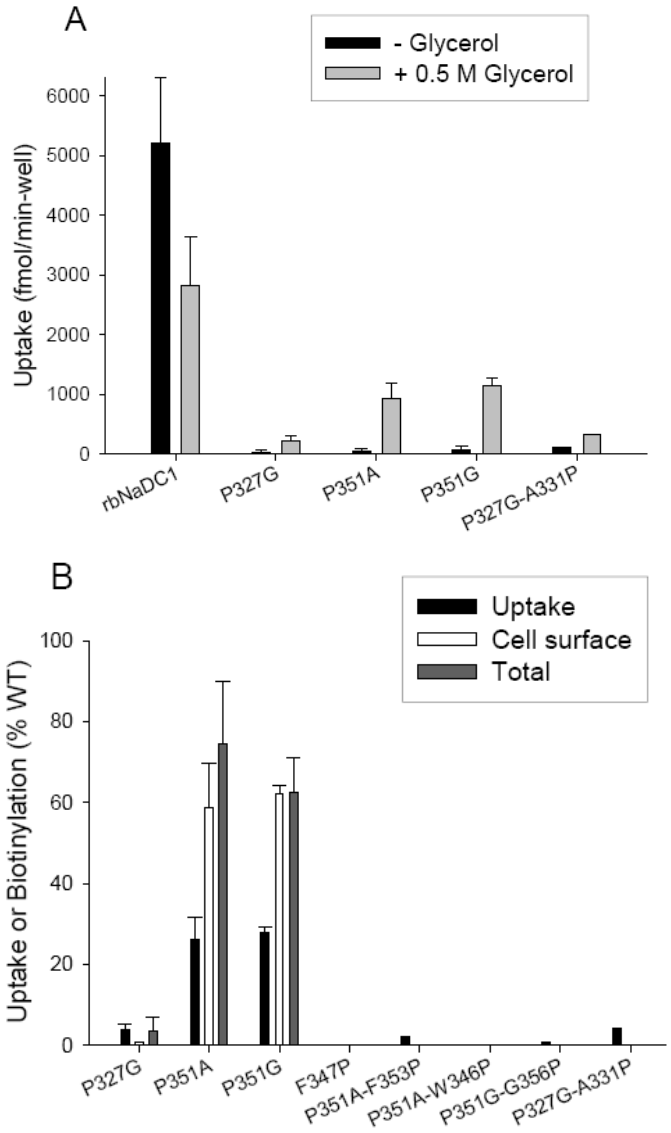


**Figure 2.5** Effect of glycerol on TM 7 mutants (A) Transport of 100 µM $^{3}$H-succinate in wild-type and mutant rbNaDC1 with and without addition of 0.5 M glycerol. Results are means ± range or S.E.M (n = 2 or 3). The P327G-A331P result is from a single experiment. (B) Comparison between transport activity and cell surface expression of TM 7 mutants after addition of glycerol. Transport activity, cell surface and total protein biotinylations were measured. Intensities of the protein bands were quantitated using Image 1D software. The data are expressed as a percentage of wild-type control in each experiment. Results are presented as mean ± range (n = 2) for mutants P327G, P351A and P351G and only mean is indicated for all other mutants (n = 1).

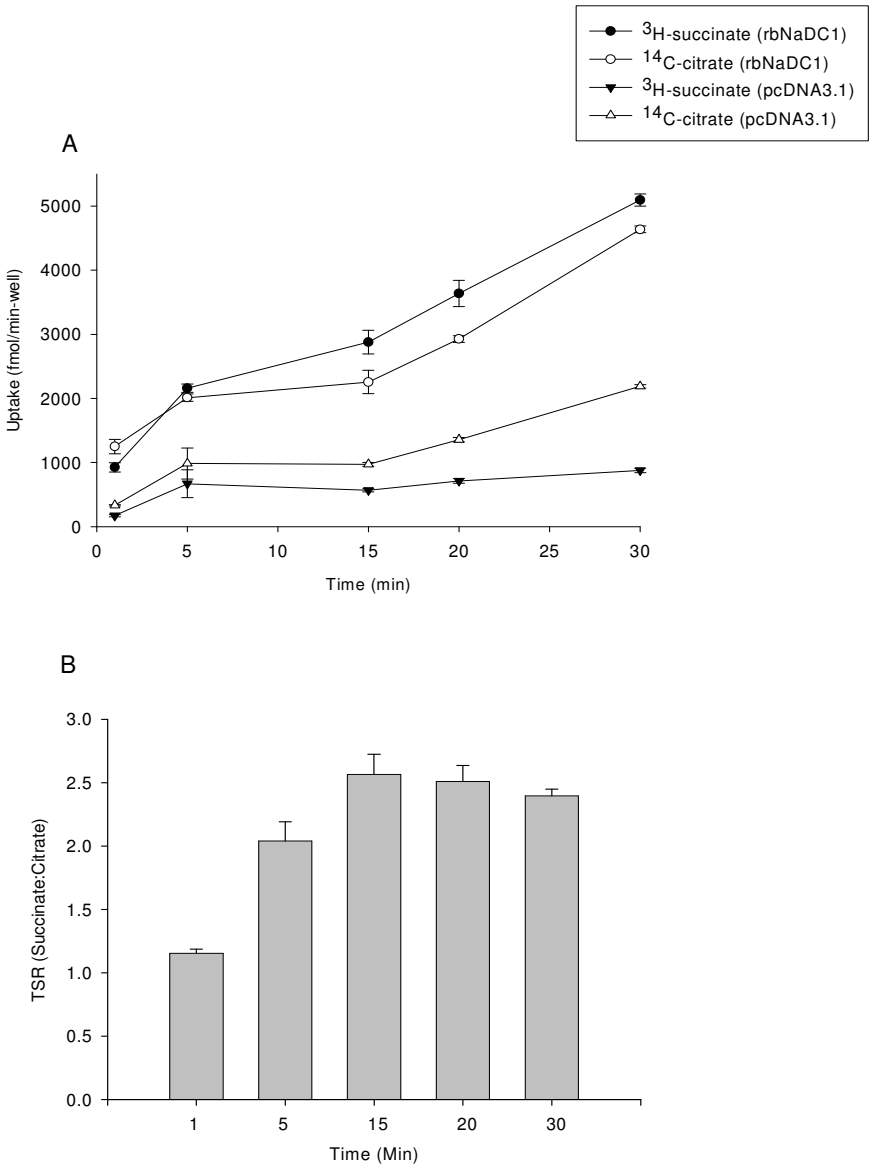


**Figure 2.6** (A) Time course of competitive uptake of succinate and citrate in wild type rbNaDC1. HRPE cells were transiently transfected with the wild type rbNaDC1 or vector only (pcDNA3.1) as described in Experimental Procedures. Dual-label competitive uptake experiment was performed with 10 µM $^{3}$H-succinate and 20 µM $^{14}$C-citrate at time points between 1 and 30 min. Results are mean ± SEM (n = 4 wells from a single transfection). (B) Transport specificity ratios (succinate: citrate) calculated from data in (A) are shown for each time point.

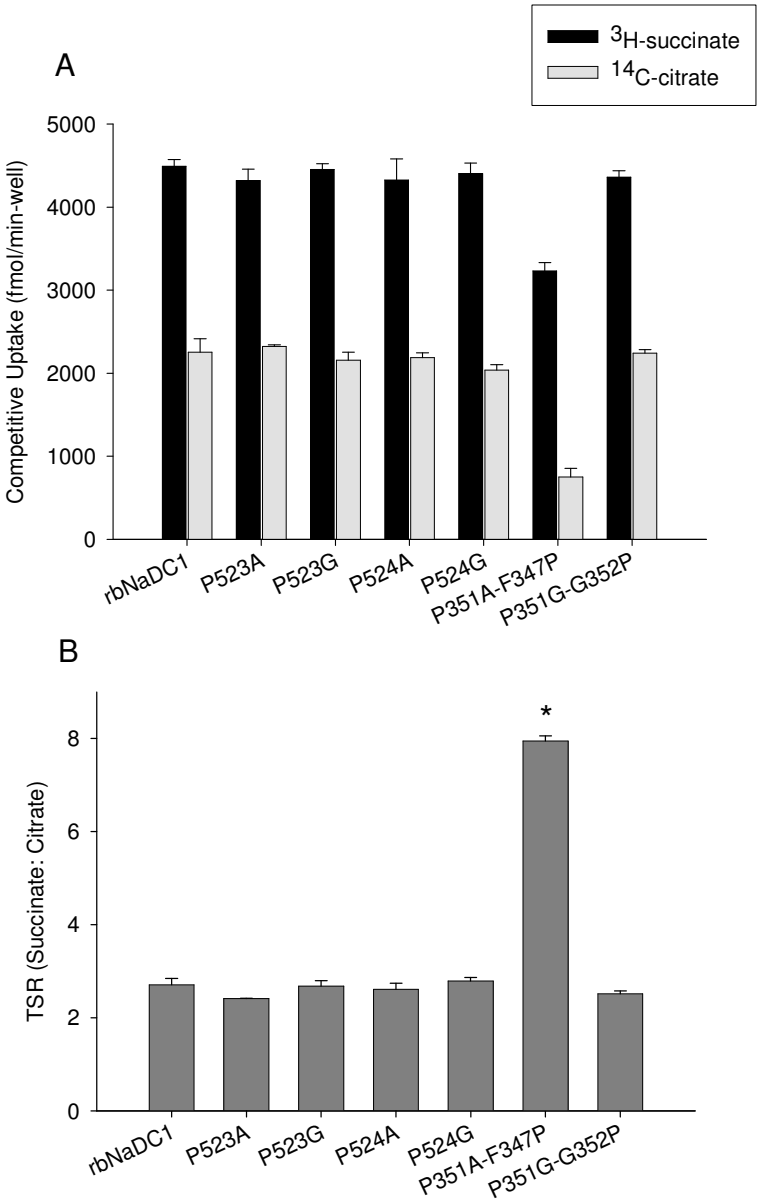


**Figure 2.7** Transport specificity ratio (TSR) of proline mutants compared with wild type rbNaDC1. (A) Competitive transport with 10 μM $^{3}$H-succinate and 20 μM $^{14}$C-citrate was performed for 20 min in 24-well plates. Bars represent mean ± range, n = 2 separate experiments. (B) TSR (succinate:citrate) of wild type and mutants using data from (A). The TSR for F347P-P351 mutant is significantly greater than wild type and other mutants, $P < 0.05$.

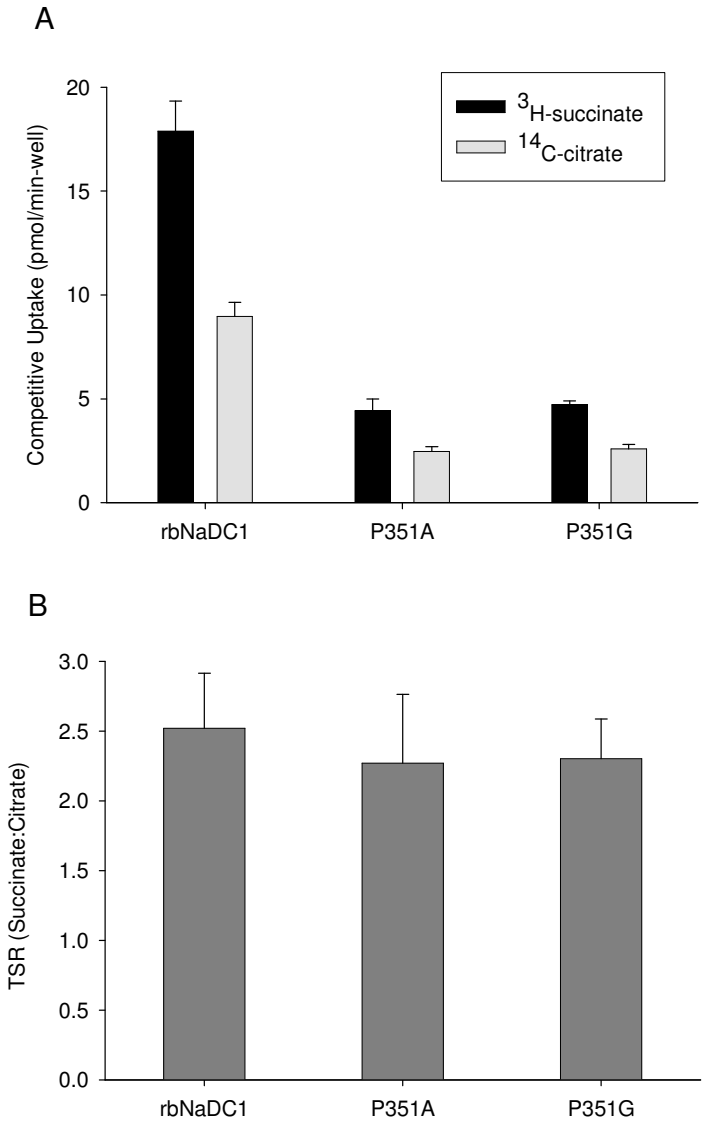


**Figure 2.8** Transport specificity ratio (TSR) of mutants treated with glycerol to improve expression. (A) Competitive dual-label uptake experiment with 10 µM $^{3}$H-succinate and 20 µM $^{14}$C-citrate was performed for 20 min. HRPE cells in 6 well plates were transfected with wild type and mutant cDNAs. Medium containing 0.5 M glycerol was added 6 hr after transfection. (B) TSR of wild type and mutants using data from (A). There were no significant differences between wild type and mutants. Results are shown as mean ± range (n = 2 separate transfection experiments).

## DISCUSSION

In this study the role of four conserved prolines, at positions 327, 351, 523 and 524, associated with transmembrane helices 7 and 10 in the $Na^+$/dicarboxylate cotransporter, NaDC1 was examined. These prolines are conserved in all members of the SLC13 family, including the *Indy* dicarboxylate transporter from *Drosophila*, suggesting that these amino acids may be important for the structure or function of these transporters. TM 7 and 10 of NaDC1 have important functional roles since they contain amino acids that determine substrate and cation specificity (*66*). The results demonstrate that Pro-327 is probably critical for the activity of the transporter and Pro-351, at end of the TM 7, may contribute to protein stability and targeting to the plasma membrane. Although Pro-523 and Pro-524 probably contribute to the stability of TM 10, these prolines do not appear to be involved in the function of the transporter.

Prolines may play important functional roles in transporters and channels because the presence of proline in a transmembrane helix leads to changes in the structure or flexibility of the helix. Since proline is an imino acid it lacks an amino side chain and hence cannot take part in hydrogen bonding, leaving free backbone carbonyls. Proline residues in a transmembrane helix typically introduce a kink in the helix, depending on the local environment, which may allow flexibility of the helix or helix packing (*105-108*). Experiments with the *Shaker* $K^+$ channel from *Drosophila* showed that prolines are necessary for the flexibility of the S6 transmembrane helix, which is important in the gating mechanism (*109*). Recent studies with mammalian dopamine transporters suggested structural as well as functional importance of TM prolines in plasma membrane targeting, assembly, membrane insertion and

contribution to dopamine recognition (*110*). Prolines in the human noradrenaline transporter are involved in assembly of the transporter, inhibitor binding as well as in conformational changes associated with substrate translocation (*111*). Prolines are also required for cell surface expression and targeting in various membrane proteins (*112*). The prolines in transmembrane helices of the lactose permease contribute to helix packing and tight closure of hydrophilic cavity (*12*).

The conserved proline at position 327 in TM 7 appears to be a critical residue in NaDC1. The protein does not tolerate substitutions at this position. Proteins with the P327G mutation were not found either in total or cell surface biotinylated samples, indicating that a protein trafficking problem is not the reason for a lack of expression. Furthermore, we were unable to rescue the P327G mutant by addition of chemical chaperones or with second site mutations.

Pro-351 may be important in determining the structure or stability of NaDC1. Current secondary structure model of NaDC1 places Pro-351 at the extracellular end of TM 7 (Figure 2.9). Alanine and glycine substitutions at position 351 produced proteins that were found in total protein lysates but were not expressed on the cell surface, indicating problems in protein trafficking or an alteration in stability at the plasma membrane. Both these hypothesis were tested by using chemical chaperones and by constructing double mutants. Chemical chaperones such as glycerol, dimethyl sulfoxide, trimethylamine N-oxide, and 4-phenylbutyric acid have been used to prevent mislocalization of CFTRΔF508 (*113*), mutants of the aquaporin-2 channel (*104*) and NaCl cotransporter mutants (*114*). In the present study, the expression and activity of the P351A and P351G mutants could be restored after treatment with 0.5 M glycerol. Since the TSR values of these mutants did not change, the results

indicate that Pro-351 may be involved in protein trafficking and membrane targeting rather than in transport function. To determine whether a proline is absolutely required at position 351 or whether the proline could be substituted at a different location in the helix, five double mutants were constructed around the TM 7 helical turn and in extracellular loop 4. The P351G-G352P mutant exhibited a partial increase in activity and protein expression. The replacement of F347 with proline, four amino acids away from the original P351A mutation, almost completely restored activity. Interestingly, this was the only mutant in our study to exhibit changes in catalytic efficiency. The Transport Specificity Ratio (TSR) was almost fourfold higher in P351A-F347P compared with the wild-type, indicating changes in the transport of succinate or citrate (or both). In kinetic experiments we found that the P351A-F347P mutant had an increased affinity for succinate ($K_m$ 14 μM), although the $V_{max}$ was greatly reduced. The single mutant, F347P, was not expressed and could not be rescued with glycerol. This indicates that the addition of the second proline at Phe-347 to wild-type NaDC1 alters the conformation of the helix and leads to possible misfolding of the protein and alterations in function or stability. Consequently, only one proline may be necessary to maintain a stable conformation of TM 7.

The prolines in TM10 do not appear to have functional roles. Both Pro-523 and Pro-524 could be replaced with alanine or glycine without much change in activity or expression, and the mutants had no change in catalytic efficiency measured by TSR. It is possible that the mutants have equal alterations in the transport of both succinate and citrate, which would not be reflected in the TSR since it is a ratio. Our previous study showed that cysteine substitution of Pro-523 and Pro-524 produced a

much greater decrease in expression and activity than the alanine or glycine substitutions in the present study (*70*). Cysteines do not have any helical preference and provide no flexibility compared with alanine or glycine. Replacement of Pro-524 with alanine appeared to result in lower protein expression than replacement with glycine, which could indicate a preference for flexibility or a kink in TM10. The difference between the alanine and glycine mutants was less pronounced at position 523, but the total protein expression was lower in the P523A mutant. Therefore, it is possible that the prolines in TM10 are involved in the structural stability of the transporter, and may introduce bends in the helix, but they do not contribute to transporter function.

In conclusion, the results of this study suggest various roles played by conserved proline residues in NaDC1. The most important prolines are those associated with TM7. Pro-327 is a critical residue as the glycine mutant at this position had no protein expression and could not be rescued by chemical chaperones or second site mutations. Pro-351 appears to be necessary for cell surface expression and regulation of protein trafficking. In contrast, the two conserved prolines in TM10, Pro-523 and 524, may produce bends in the helix, but these prolines do not have functional effects in NaDC1.

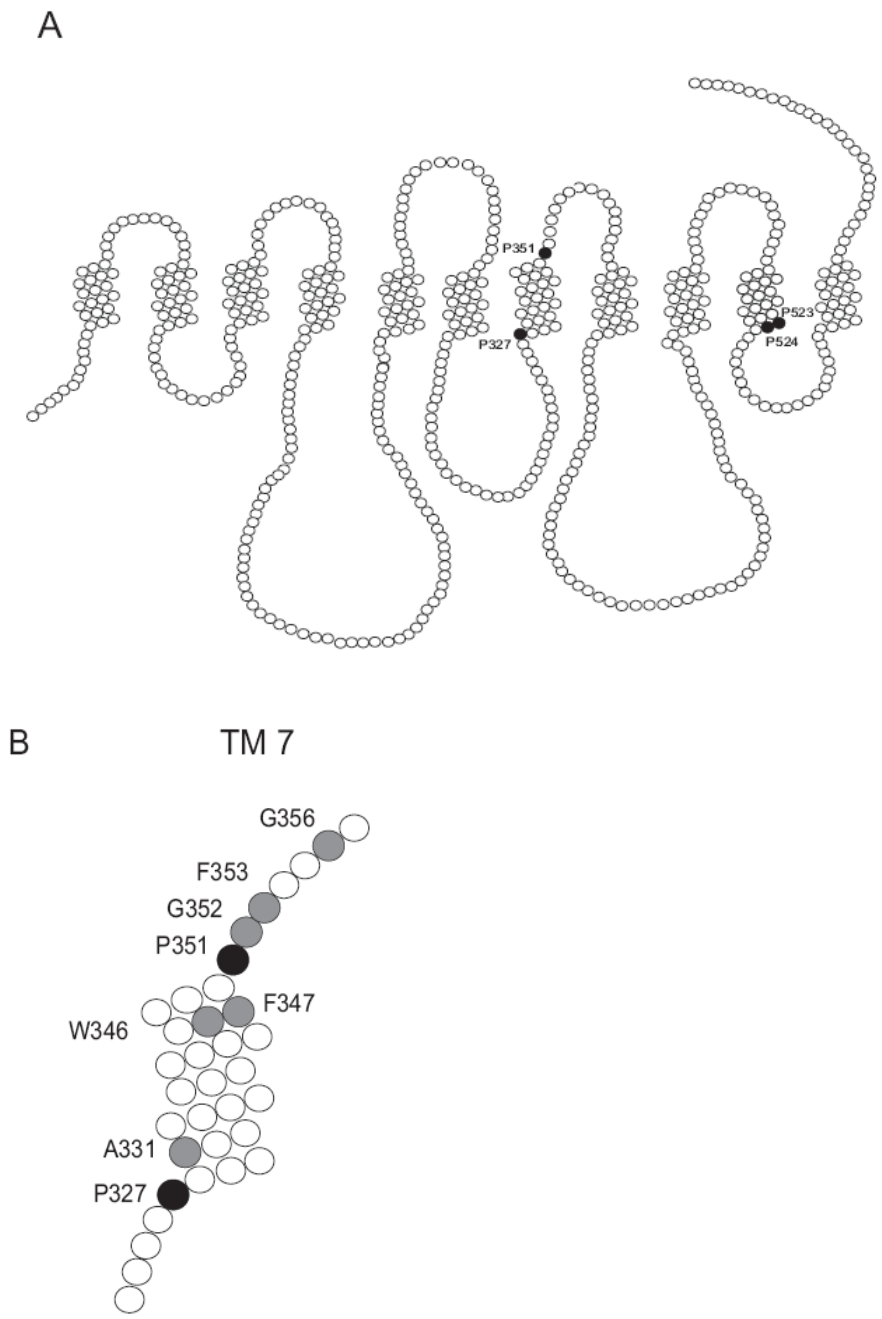


**Figure 2.9** (A) Secondary structure model of NaDC1 showing the location of prolines (filled circles) in TM 7 and 10 that were mutated in this study. The outside of the cell is at the top of the figure. (B) TM 7 showing locations of prolines (black filled circles) and other amino acids (grey filled circles) mutated in this study.

# CHAPTER 3: A MEMBRANE TOPOLOGY MODEL OF $Na^+$/ DICARBOXYLATE COTRANSPORTER 1

## INTRODUCTION

There is currently little structural information known about any member of the SLC13 family. The sequence of NaDC1 contains 593 amino acids and a predicted mass of 65 kDa. Structure-function information has been obtained from various site-directed mutagenesis studies (*69-72;75;115*) as well as from chimera studies (*66;67*). An important step in elucidating structure and function of membrane transporters is to understand their topology. To understand substrate and cation binding sites it is important to know the organization of α-helical domains. Our current knowledge about NaDC1 topology comes both from hydropathy plots and from some experimental data. Hydropathy analysis of the amino acid sequence of rbNaDC1 suggests 8 to 11 putative transmembrane (TM) domains depending on the prediction algorithm and the hydrophobicity scale. A secondary structure model based on hydropathy analysis using the Rao and Argos buried helix parameter predicted 11 TM in rbNaDC1 (*61*). Previous experimental studies supported some aspects of this model. The Flag epitope tag was fused to the amino terminus of NaDC1, and a monoclonal antibody against the Flag epitope showed that the amino terminus is located intracellularly (*62*). The loop between TM 4 and 5 was identified as being located intracellularly using polyclonal antibodies. These polyclonal antibodies were raised against a fusion protein containing amino acids 164-233 of rbNaDC1 (*61*). Previous studies also identified the N-glycosylation site at Asn-578, which places the carboxy terminus on the extracellular side of the plasma membrane (*61*). More recent

analysis of the NaDC1 sequence using secondary structure prediction algorithms suggests that there may be 13 TM.

To differentiate between the 11 and the 13 TM models, individual cysteine residues were substituted for other amino acids in predicted extracellular and intracellular loops of rbNaDC1. The extracellular accessibility of the cysteines was determined by chemical labeling with MTSEA-biotin [N-biotinylaminoethyl methanethiosulfonate]. Some of the results supported the original 11 TM model, whereas others supported part of the 13 TM model. One surprising finding of this study was that some endogenous cysteines in NaDC1 could be exposed by second site mutations. Therefore, a mutant of NaDC1 containing only four endogenous cysteines, called 4N, was used for this study. Based on the results of these experiments we constructed a modified homology model of NaDC1 containing 11 TM. The new model of NaDC1 will be helpful in understanding dicarboxylate transport and in designing future mutagenesis experiments.

## MATERIALS AND METHODS

### Plasmid Constructs and Site-directed Mutagenesis

Single cysteines were substituted for other amino acids in predicted extracellular and intracellular locations into two different mutants of the rabbit NaDC1, called C476S and 4N, using the QuikChange$^{TM}$ site-directed mutagenesis kit (Stratagene) as described in Chapter 2. The C476S mutant contains a serine in place of Cys-476, but no changes to the remaining 10 endogenous cysteines. Cys-476 was found to be sensitive to cysteine selective reagents such as p-

chloromercuribenzesulfonate although it is not sensitive to methanethiosulfonate reagents (*116*). Mutant 4N of rabbit NaDC1 was originally named 4C (Nterm) and contains four cysteines at the N-terminus, at positions 4, 38, 50 and 65. The endogenous cysteines at positions 225, 227, 467, 476, 508 and 583 were mutated to serine and Cys-498 was mutated to alanine (*116*). Unless otherwise specified, the cysteine mutants were constructed in 4N background. Cysteine mutants constructed in C476S are designated as /C476S, for example A39C/C476S (alanine at position 39 replaced with cysteine in C476S parental transporter). Mutants K84C, M493C, T482C were made in C476S backgrounds in previous studies (*69;70*), and were made again in 4N for the current study.

**Expression of Cysteine Mutants in HRPE Cells**

Human retinal pigment epithelial cells (HRPE) transformed with SV40 (AG06096; Coriell Institute) were cultured in Modified Eagle's Medium (MEM) containing Glutamax, 25 mM HEPES (Invitrogen) along with 10% heat-inactivated fetal calf serum, 100 units/ml penicillin and 100 µg/ml of streptomycin. Cells were incubated at 37°C in 5% $CO_2$. Transport assays were performed in 6 or 24 well plates, depending on the succinate transport activity of the mutants. Cell surface biotinylations were carried out in 6 well plates. For 6 well plates, $3 \times 10^5$ cells were plated per well whereas for 24 well plates, $1.2 \times 10^5$ cells were plated per well. Twenty four hours after plating, cells were transiently transfected with 3 µl of FuGENE 6 (Roche Applied Science) and 1 µg of plasmid DNA (3:1 ratio) for 6 well

plates. For 24 well plates, cells were transfected with 1.8 µl of FuGENE 6 and 0.6 µg of plasmid DNA (9:3 ratio) (*69;70*).

**Transport Assays**

Transport assays of NaDC1 and mutants were performed in the same way as described in Chapter 2.

**Chemical Labeling with MTSET**

[2-(trimethylammonium)ethyl]-methanethiosulfonate (MTSET) (Toronto Research Chemicals) was pre-weighed, kept on ice and diluted in either sodium buffer, choline buffer (same as sodium buffer but containing choline chloride in place of NaCl) or sodium buffer with 10 mM succinate, just before use. Depending on the sensitivity of the mutant to MTSET, two concentrations of MTSET were used, 1 mM (diluted with appropriate buffer) or 10 µM (stock solution of 1 mM MTSET freshly prepared in water was further diluted with appropriate buffer just before use). Cells were first washed twice with choline buffer and then incubated without (controls) or with MTSET solutions for 10 min at room temperature. The MTSET solution was removed with three washes of choline buffer. The transport activity remaining after MTSET labeling was measured as described in chapter 2 except that choline buffer was used for washing instead of sodium buffer.

**Cell Surface Biotinylations**

Cell surface protein expression of NaDC1 and mutants was the same as described in Chapter 2.

**Topology Assay: Labeling of Cysteine Mutants with MTSEA-biotin**

NaDC1 mutants expressed in HRPE cells were preincubated with sodium transport buffer with or without 1 mM MTSET for 10 min at room temperature. Cells were washed 3 times with 3 ml of PBS/CM, pH 7.5. A stock solution of 200 mM N-biotinylaminoethyl methanethiosulfonate (MTSEA-biotin) (Toronto Research Chemicals) was prepared in dimethyl sulfoxide (DMSO) and was kept dark on ice until use. The MTSEA-biotin solution was further diluted to 2 mM with PBS/CM, pH 7.5 just before use. MTSEA-biotin (0.5 ml) was added to each well of a 6 well plate and incubated for 30 min at room temperature with gentle rocking. After 30 min incubation wells were washed 3 times with 3 ml of PBS/CM, pH 7.5. Lysis buffer with protease inhibitors was added to the plates which were kept on ice with rocking for cell lysis. The remaining steps were identical to those of the cell surface biotinylation procedure. Biotinylated proteins were identified by Western blotting with anti-NaDC1 antibodies.

To understand the accessibility of the introduced cysteines under different conformational states of the cotransporter during the transport cycle, 1 mM MTSET and 2 mM MTSEA-biotin were dissolved in sodium buffer, choline buffer or in sodium buffer with 10 mM succinate and the labeling was carried out (*69;70*). The remaining steps were the same as described above.

To confirm the extracellular accessibility of some of the cysteine mutants (G429C, G431C, A433C and G437C) labeling with 0.4 mM EZ-link PEO-maleimide-activated biotin (Pierce) was carried out. Unlike MTSEA-biotin which carries a positive charge, EZ-link PEO-maleimide-activated biotin is neutral, soluble in water, contains a comparatively long spacer arm (29.1 Å) and is membrane impermeant

because of the large size of the molecule *(117)*. Transfected HRPE cells were washed with sodium buffer and preincubated without (control) or with 1 mM MTSET diluted with sodium buffer for 10 min. Cells were washed three times with 3 ml of PBS/CM, pH 7.5 and then labeled with 0.4 mM EZ-link PEO-maleimide-activated biotin in PBS/CM, pH 7.5. The remaining procedure was identical to that described for MTSEA-biotin labeling.

**Topology Prediction and Homology Modeling**

The 13 TM model of NaDC1 was determined from a consensus structure prediction method using secondary structure prediction algorithms (*118*). To construct the homology model of rabbit NaDC1, the sequence of rbNaDC1 was submitted to a consensus structure prediction system, 3D-Jury (BioInfobank Meta Server, http://BioInfo.PL/Meta/) (*118*). The 3D-Jury results showed that the crystal structure of lactose permease from Escherichia coli (1PV6) had the best alignment and most similar fold (*12*). The homology model of NaDC1 was made with the modeling package MPACK (*119*) using the crystal structure of 1PV6 as the template. The program EXDIS was used to extract inter-atomic distances and dihedral angle constraints from the structure of the template (http://www.scsb.utmb.edu/FANTOM/fm_home.html). Models were further built with the self-correcting distance geometry program DIAMOD (http://www.scsb.utmb.edu/comp_biol.html/larisa/noah_diamod.html). The program FANTOM was then used to minimize the conformational energy of the protein (*120*).

The geometry of the final model was evaluated using PROCHECK. Graphics were generated with PyMOL, a molecular visualization system (http://www.pymol.org).

## RESULTS

### The 11 versus 13 TM Topology Models for NaDC1

The current secondary structure model of NaDC1 with 11 TM (Figure 3.1) is based on hydropathy analysis using the Rao and Argos buried helix scale parameter (*61*). Experimental evidence supports an odd number of TM for NaDC1 because the N-terminus is on the inside and the C-terminus on the outside (*61*), although a definitive topology model of NaDC1 is lacking. More recent topology analysis using a consensus secondary structure prediction algorithm (*118*), predicted 13 TM for NaDC1 (Figure 3.1). In order to test the 11 TM and 13 TM models, we used the substituted cysteine accessibility method. Cysteine residues were substituted one at a time for amino acids in predicted intracellular and extracellular loops. The accessibility of the introduced cysteines to membrane impermeant methanethiosulfonate reagents was then examined. Figure 1 compares the expected locations of substituted cysteines in the 11 TM and 13 TM models.

Our previous study showed that the protein expression of NaDC1 is related to the number of cysteines present. The cysteine-less mutant of NaDC1 is not expressed on the plasma membrane and at least four cysteines are required for measurable activity (*116*). The C476S mutant of NaDC1 contains 10 of the 11 endogenous cysteines, and it is insensitive to membrane impermeant methanethiosulfonate reagents (*70*). C476S has transport activity and protein expression similar to those of

the wild-type NaDC1 (*70*). Therefore, the initial cysteine mutations were made using the C476S mutant as the parental transporter.

**Protein Expression and Transport Activity of Cysteine Mutants: C476S background**

The cell surface protein abundance of cysteine mutants made in the C476S/NaDC1 background was measured with the membrane impermeant reagent Sulfo-NHS-LC-biotin, which labels extracellularly-accessible lysine residues. Single representative Western blots are shown in Figure 3.2A. The two protein bands represent differently glycosylated forms of the protein (*61;75*). The quantitative results from multiple blots are compared with the transport activity of the mutants expressed in HRPE cells (Figure 3.2B). Cell-surface protein expression and succinate transport activity was expressed as a percentage of the C476S parental transporter measured in the same transfection experiment. The cysteine substitutions at positions 112, 367, 486 and 493 were well tolerated and the mutants had similar succinate transport activity as the parental C476S. Mutants at positions 104, 429 and 431 had very low transport activity. Interestingly, the G431C/C476S mutant was as abundant on the plasma membrane as the C476S transporter, but had < 10 % of the activity. Most of the mutants had less than 50% of the protein expression and activity of the parental transporter. The A39C/C476S and I109C/C476S mutants were well

expressed on the plasma membrane but had low transport activity, suggesting that these residues might be functionally important.

**Sensitivity to MTSET: C476S background**

The cysteine-substituted mutants were screened for their sensitivity to membrane impermeable thiol specific reagent MTSET. Mutants G356C, G429C, L486C and M493C showed high sensitivity to MTSET (Figure 3.3). None of the other cysteine-substituted mutants were sensitive to inhibition by 1 mM MTSET.

**Cysteine Accessibility to Methanethiosulfonate Reagents: C476S background**

The cysteine mutants were next tested for their accessibility to cysteine-specific reagents applied to the outside of the cells. The biotinylated reagent, MTSEA-biotin, reacts with extracellularly accessible cysteines and the biotin group allows the biotinylated proteins to be precipitated with streptavidin beads. However, because the MTSEA-biotin has been shown to be somewhat membrane permeant, specific extracellular labeling of cysteines was determined by preincubating the cells with the membrane-impermeant reagent, MTSET (*121*). Specific labeling of extracellular cysteines is defined as the MTSET-dependent component of MTSEA-biotin labeling. The parental C476S mutant showed some non-specific background labeling by MTSEA-biotin that was not decreased by preincubation with MTSET (Figure 3.3A and B). This indicates that one or more intracellularly accessible cysteines are labeled by the MTSEA-biotin but these residues are not accessible to the MTSET. The substituted cysteines at positions 39, 112, 252, 356 and 493 showed specific labeling by MTSEA-biotin, indicating that these cysteines are accessible to

the outside of the cell. The remaining substituted cysteines at positions 29, 104, 109, 133, 429, 431, 433, and 486 were not accessible to MTSEA-biotin or did not show MTSET-blockable binding of MTSEA-binding. Therefore, these mutants were either inaccessible from the outside (located intracellularly or in a transmembrane helix) or their protein expression was too low for labeling by MTSEA-biotin.

Surprisingly, mutant G367C/C476S exhibited increased MTSEA-biotin labeling after preincubation with MTSET, instead of the decrease seen in the other mutants (Figure 3.4). One possible explanation is that MTSET binding to the cysteine at position 367 may produce a conformational change in the transporter that exposes previously inaccessible cysteines. To test this hypothesis we repeated the experiment by making the G367C mutant in a parental transporter containing fewer endogenous cysteines, called 4N. The 4N transporter, previously named 4C (Nterm), is a mutant of rabbit NaDC1 containing only four endogenous cysteines at the N terminus with the remaining seven cysteines mutated to serine or alanine (*116*). These four endogenous cysteines at positions 4, 38, 50 and 65 were shown in our previous study to be less reactive to cysteine-specific reagents (*116*). The 4N transporter had approximately 25% of the succinate transport activity of the wild-type NaDC1 and was not inhibited by MTSET or MTSES. The protein abundance of 4N was approximately 35% of wild type (Figure 3.5A). 4N was not labeled by MTSEA-biotin, indicating that none of the four cysteines was accessible to the reagent (Figure 3.4A). We then constructed mutant G367C/4N which did not show any increased MTSEA-biotin labeling in presence of MTSET (Figure 4). Therefore, the cysteine at position 367 is likely to be located intracellularly or in the transmembrane helix.

**Protein Expression and Transport Activity of Cysteine Mutants: 4N background**

A total of 20 cysteine mutants were constructed in the 4N background (Figure 3.1). Most of the mutants were found on the plasma membrane with similar or greater abundance than the 4N construct of rbNaDC1 (Figure 3.5). Mutants A39C, K84C and G429C had < 35% cell-surface expression compared with 4N (Figure 3.5B). The succinate transport activity of the cysteine mutants was compared with the 4N parental transporter (Figure 3.5B). Mutants T482C and M493C had very high activity and protein abundance compared with that of 4N (Figure 3.5B). Many of the mutants had very low transport activity, much lower than expected based on protein expression: A39C, A133C, I139C, T252C, G300C, G356C, G431C, A433C, and G437C. I29C, A75C, K84C, R112C, and S187C had about 30 to 60 % succinate transport activity compared with the parental 4N, and the transport activity was similar to the protein expression. (Figure 3.5B).

**Sensitivity to MTSET: 4N background**

The functional effects of chemical labeling of cysteine mutants were tested by incubation with MTSET followed by measurement of succinate transport activity. Only three of the mutants, G356C, T482C and M493C, had significant decreases in succinate transport activity after treatment with 1 mM MTSET (Figure 3.6). None of the other cysteine mutants were sensitive to inhibition by MTSET. These results agree well with our previous data showing that T482C and M493C in the C476S background are inhibited after chemical labeling with MTSET (*69;70*). Mutant M493C/4N was very sensitive to inhibition by MTSET, with an $IC_{50}$ value of ~ 2 µM. Therefore, a concentration of 10 µM MTSET was used in subsequent experiments.

**MTSET Sensitivity of 4N Cysteine Mutants with Different Cations and Substrate**

Experiments were carried out to determine whether substituted cysteines would be accessible to MTSET under different conformational conditions. NaDC1 follows an ordered binding mechanism in which three sodium ions bind first followed by binding of the substrate (*51*). Previous studies have shown that the accessibility of substituted cysteines can change depending on the presence or absence of sodium and substrate in the incubation solution. Cysteine-substituted mutants in the 4N background were treated with MTSET in either sodium buffer, choline buffer or sodium buffer containing 10 mM succinate followed by measurement of succinate transport activity. Similar to our previous results with mutants made in the C476S background (*70*), T482C and M493C were most sensitive to MTSET when the preincubation was done in sodium buffer suggesting that these mutants are most accessible in the conformational state produced by sodium (Figure 3.7). Both mutants showed substrate protection, because the decrease in succinate transport activity with MTSET could be prevented by the presence of 10 mM succinate. Mutant G356C was inhibited by MTSET under all conditions, and there was no evidence of substrate protection. The inhibition was significantly greater in choline compared with sodium. There was no effect of MTSET on succinate transport by mutants A39C, K84C, A133C, T252C and the parental transporter 4N under any condition (Figure 3.7).

**Cysteine Labeling by MTSEA-biotin: 4N background**

MTSEA-biotin labeling experiments of cysteine-substituted mutants in the 4N background were performed in the same way as described for Figure 3.3. No background labeling with MTSEA-biotin was seen in the parental 4N mutant (Figure 3.8). Mutants A39C, K84C, A133C, T252C, G356C, T482C and M493C had specific MTSEA-biotin labeling that could be inhibited by MTSET, indicating that these residues are accessible from the outside. Other residues, such as A75C, were labeled by MTSEA-biotin, but this was not inhibited by MTSET, suggesting that these amino acids are accessible to a membrane permeable reagent, but not to an impermeant reagent. We attempted to test this further by examining MTSEA-biotin labeling in digitonin-permeabilized cells, but the digitonin treatment (20µg/ml) interfered with the MTSEA-biotin labeling of extracellular cysteines in the M493C control mutants. Some residues were not labeled with MTSEA-biotin although the proteins were found on the plasma membrane (I29C, N104C, R112C, I139C, S187C, G300C, G533C), indicating that these residues are either located intracellularly or in a transmembrane helix (Figure 3.8).

In the 11 TM model, residues G429C, G431C, A433C and G437C are located intracellularly whereas these residues are located extracellularly in 13 TM model. Mutants G429C, G431C and G437C showed some labeling with MTSEA-biotin, although it was not prevented by MTSET pretreatment. No labeling was observed for mutant A433C. In one experiment, G431C was decreased by MTSET but in another it was not, possibly a result of the low signal. The results indicate that these mutants are likely to be located intracellularly or in a transmembrane helix. To verify the accessibility of these residues, the mutants were tested with a less membrane

permeant thiol specific labeling reagent, PEO-maleimide-activated biotin. The experimental design was the same as for Figure 3.8 except that PEO-maleimide-activated biotin was used instead of MTSEA-biotin. The only mutant labeled was the positive control, M493C (Figure 3.9). No labeling was seen for the 4N parental mutant as well as for the G429C, G431C, A433C and G437C mutants confirming that their location is either intracellular or in a transmembrane helix (Figure 3.9). We also tried labeling by permeabilizing cells with digitonin, but this decreased labeling of positive controls.

**Effect of Cations and Substrate on Labeling of Cysteine-Substituted Mutants by MTSEA-biotin**

Cysteine-substituted mutants that were accessible to MTSET in sodium buffer were further tested for their accessibility in various conformational states of the transporter. The biotinylation reaction was carried out in sodium buffer, choline buffer or in sodium buffer containing 10 mM succinate. Mutant 4N was not accessible in any of the conditions, indicating that changes in conformation do not expose any of the cysteines (Figure 3.10A). Mutant A39C was accessible in all conformational states, and there was a large increase in MTSEA-biotin labeling in the presence of substrate. Mutant K84C had similar MTSEA-biotin labeling in all three conditions. G356C was accessible in all three conditions, but it was difficult to determine differences because of the low signal. Mutant M493C was accessible in all the conformational states, and the signal appeared to increase in choline and decrease in succinate. Mutants A133C, T252C and T482C (Figure 3.10B) exhibited substrate

protection of MTS reagent binding. In these three mutants, the addition of succinate resulted in less inhibition of MTSEA-biotin binding by MTSET.

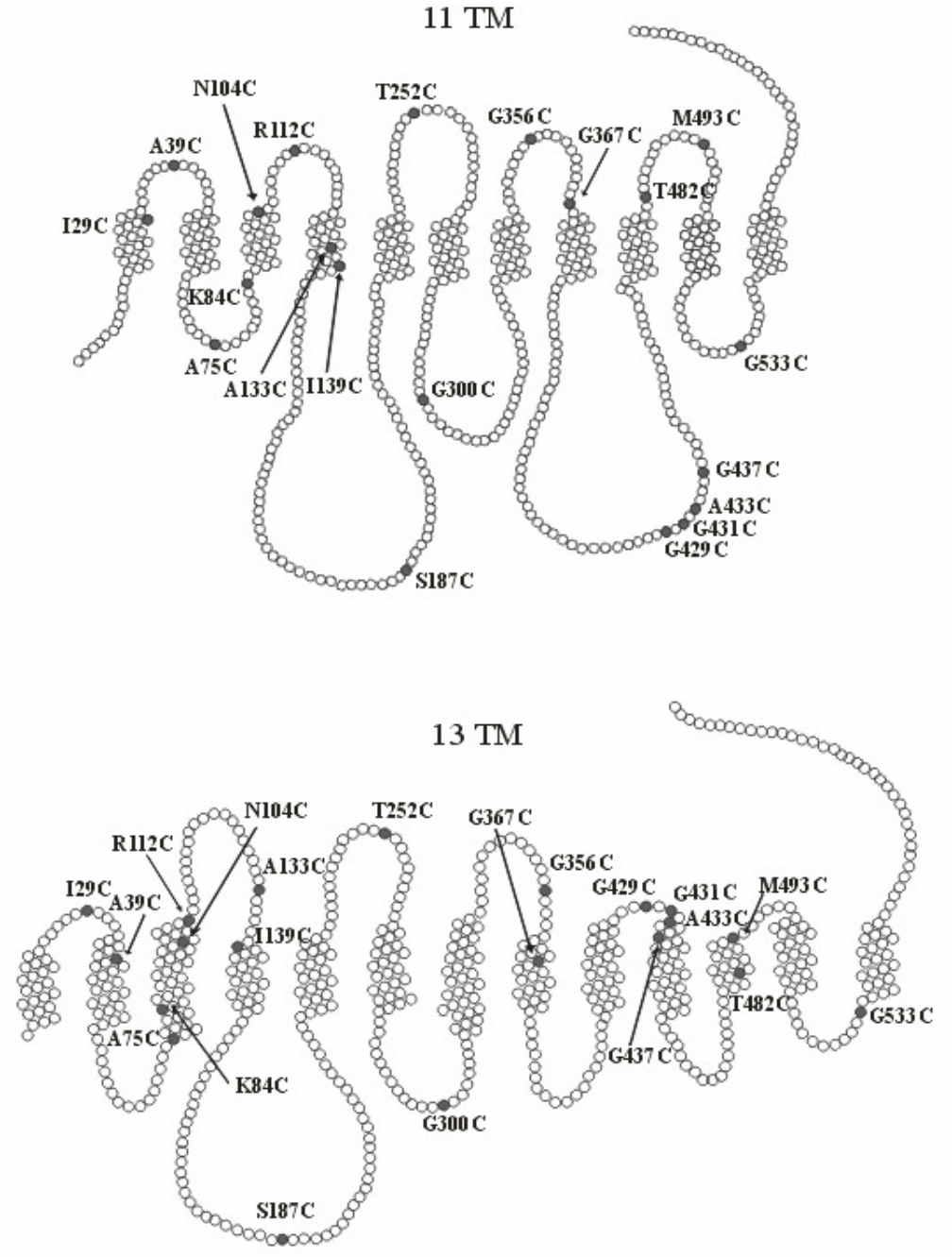


**Figure 3.1** Comparison of the 11 TM versus 13 TM topology models for rbNaDC1. The 11 TM model was made using hydropathy analysis with the buried helix scale of Rao and Argos (*61*). The 13 TM model was made using secondary structure prediction algorithms. Filled circles indicate sites of cysteine substitutions.

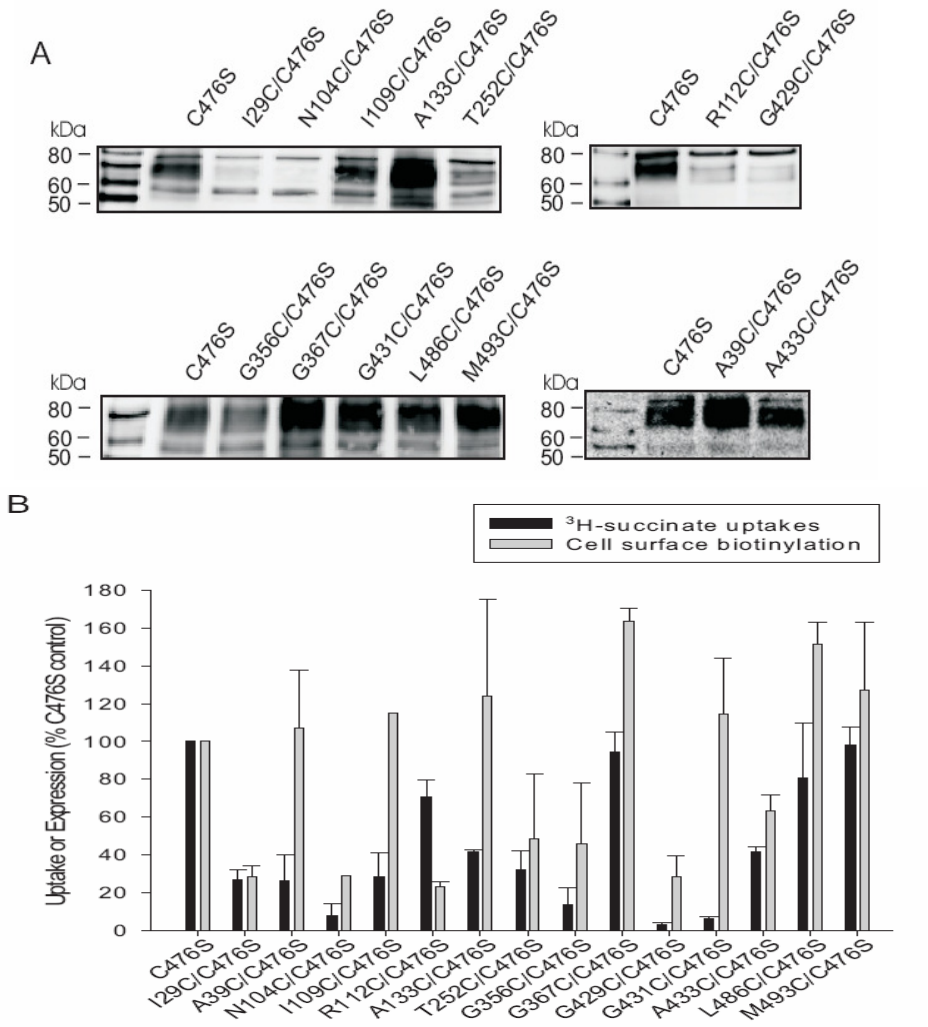


**Figure 3.2** (A) Western blots of cell surface protein expression of cysteine mutants substituted in the NaDC1/C476S parental transporter. HRPE cells expressing cysteine mutants were treated with Sulfo-NHS-LC-biotin as described under "Materials and Methods". Western blots were probed with anti-NaDC1 antibodies (1:1000 dilution) followed by 1:5000 dilution of horseradish-peroxidase-linked anti-rabbit Ig. Each blot includes the control parental transporter C476S. The Magic Mark Western standards (Invitrogen) are shown in lane 1 and the mass (in kDa) is indicated on the left. (B) Succinate transport activity and protein expression of cysteine-substituted mutants made in C476S background expressed in HRPE cells. The activity and cell surface expression of mutants are shown as a percentage of the parental transporter C476S. Transport activity of 100 µM $^{3}$H-succinate was measured with 30 minutes incubation in sodium containing buffer. Transport results are shown as mean ± range (n = 2). Protein expression was determined by quantitating the intensities of NaDC1 protein bands from Western blots (such as in A) using Image 1D analysis software. Bars represent mean ± range or SEM (n = 2 or 3 separate transfections).

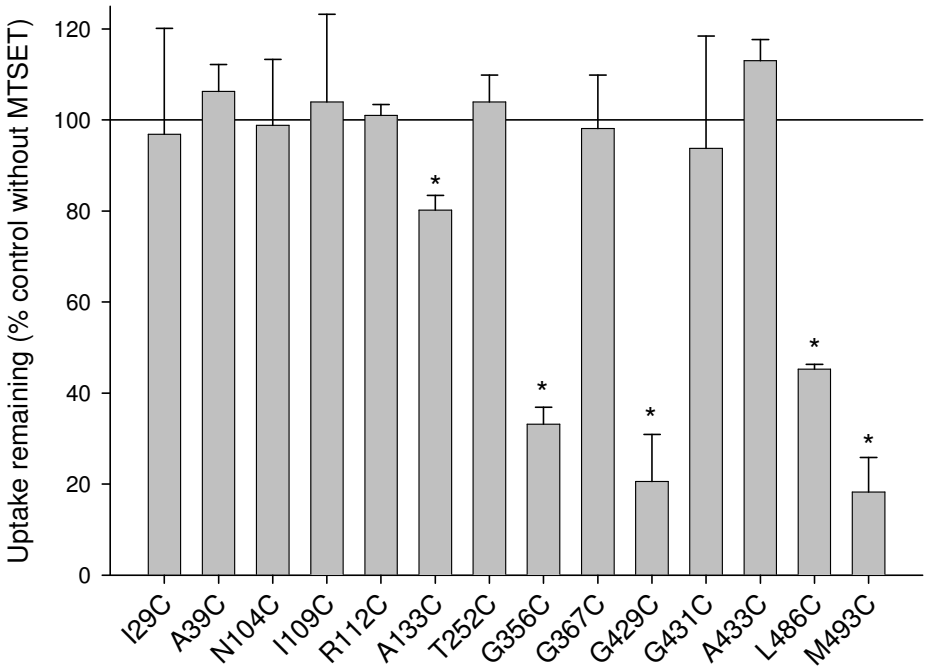


**Figure 3.3** Effect of 1 mM MTSET on succinate transport by cysteine-substituted mutants. HRPE cells expressing cysteine-substituted mutants in C476S background were preincubated for 10 min in sodium buffer containing 1 mM MTSET or sodium buffer alone (as control). The preincubation solution was washed away with sodium buffer and 100 μM $^{3}$H-succinate uptake was measured. Uptake activities in cells pretreated with MTSET are expressed as a percentage of the uptakes in control cells pretreated with sodium buffer alone. The bars represent mean ± range or SEM (n = 3, separate transfections). *, significantly different from control group ($p < 0.05$).

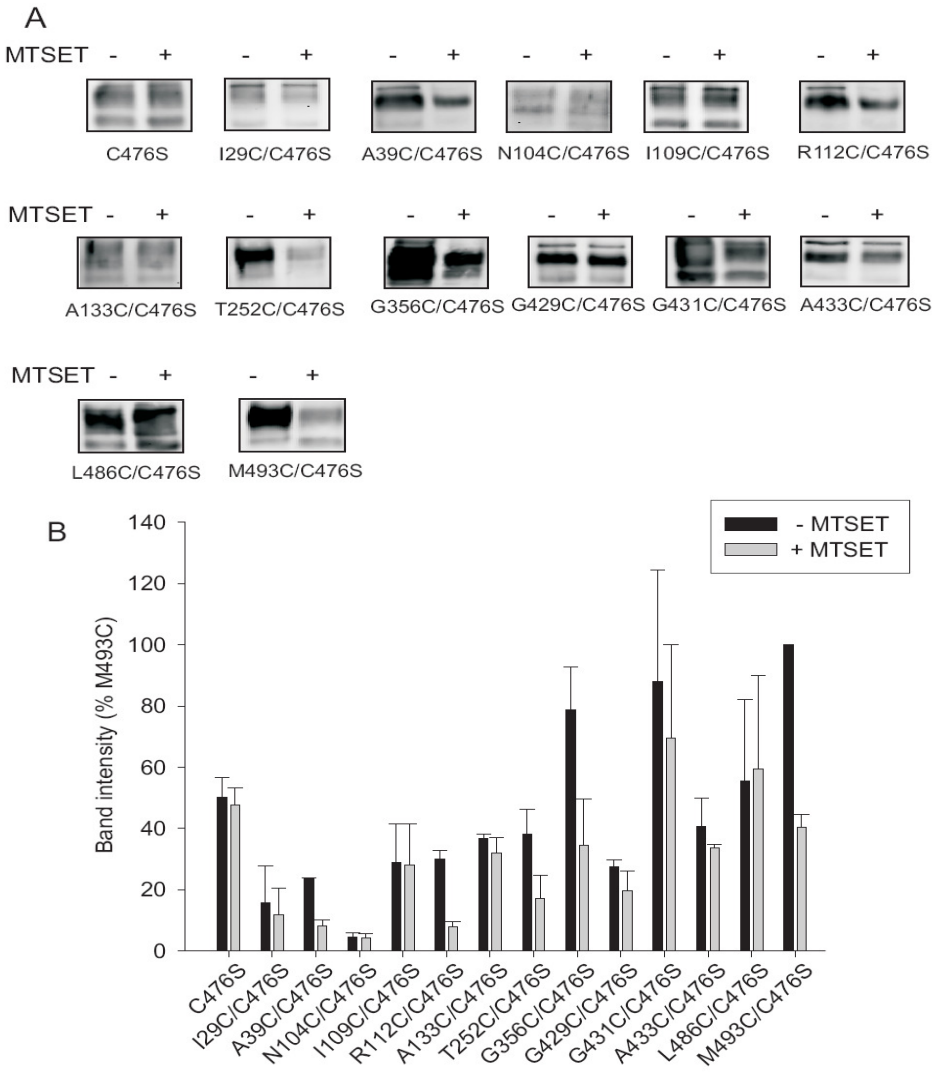


**Figure 3.4** (A) Labeling of cysteine-substituted mutants with MTSEA-biotin. HRPE cells expressing the C476S parental transporter or cysteine-substituted mutants were preincubated with sodium buffer, without (-) or with (+) 1 mM MTSET in order to label the extracellularly accessible cysteine residues. Cells were then labeled with 2 mM MTSEA-biotin. NaDC1/C476S cysteine mutants were identified by Western blotting as described under "Experimental Procedures". The blots were treated with anti-NaDC1 antibodies (1:1000 dilution). The parental transporter C476S was used as a negative control whereas mutant M493C in C476S was used as a positive control and both were included in all biotinylation experiments. (B) Comparison of the band intensities of MTSEA-biotinylated mutants. Western blots such as those shown in (A), were quantitated and expressed as a percentage of the M493C intensity (without MTSET) from the same blot. The bars represent mean ± range (n = 2 blots, separate transfections).

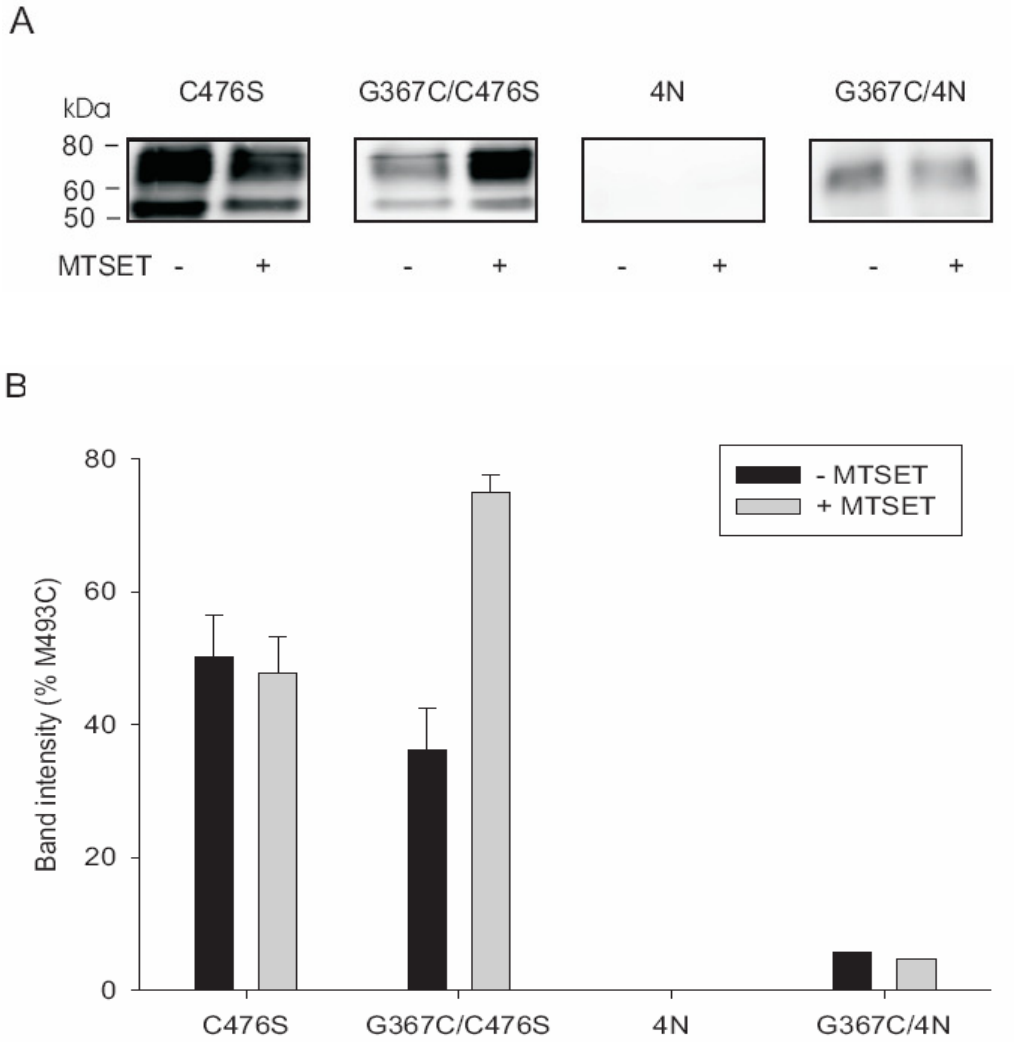


**Figure 3.5** (A) MTSEA-biotin labeling of G367C mutant made in C476S and 4N parental transporters. Preincubation was done without (-) or with (+) 1 mM MTSET (as in Fig. 3.4) followed by 2 mM MTSEA-biotin labeling. Western blots were treated with anti-NaDC1 antibodies (1:1000 dilution). (B) Western blots as shown in (A) were quantitated and band intensity is shown as a percentage of M493C without MTSET from the same blot. The bars represent mean ± range (n = 2 blots, separate transfections).

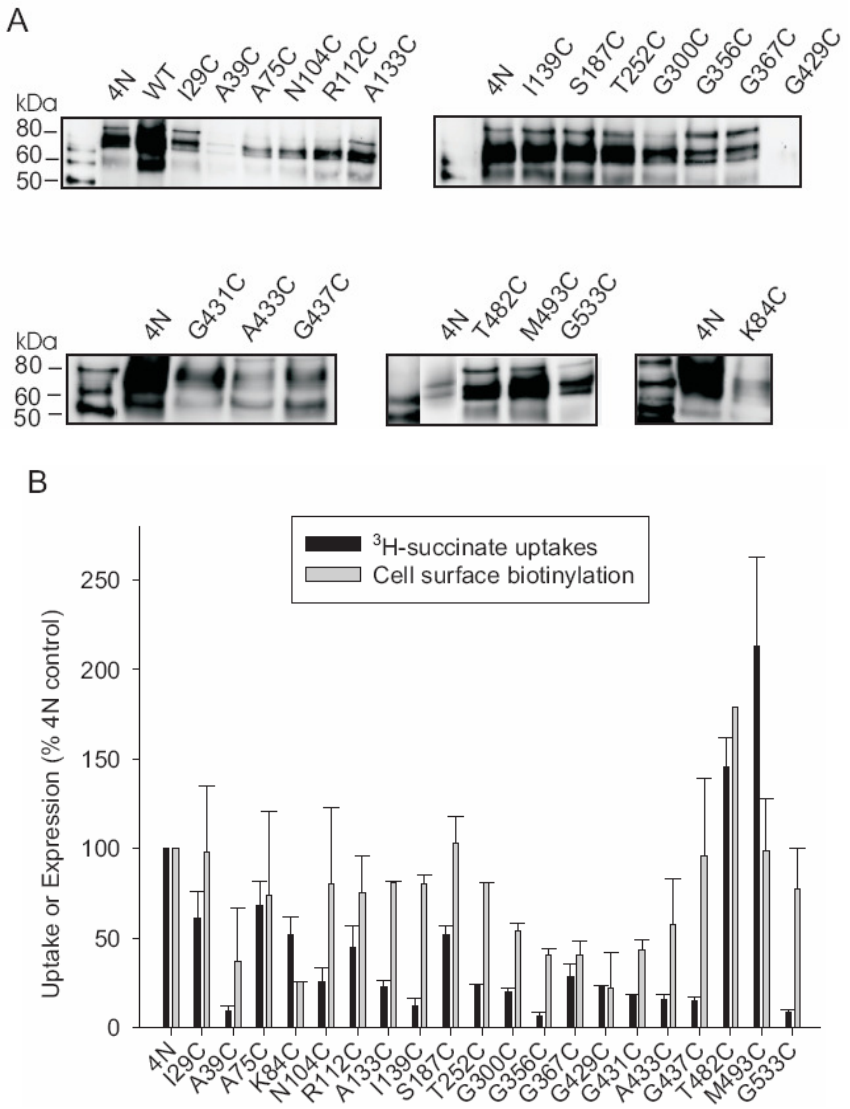


**Figure 3.6** (A) Western blots of cell surface protein expression of cysteine mutants substituted in the NaDC1/4N parental transporter. HRPE cells expressing cysteine mutants were treated with Sulfo-NHS-LC-biotin as described under "Materials and Methods" and in Fig. 3.2. Each blot includes the parental transporter 4N as a control. (B) Transport activity and cell surface protein abundance of cysteine-substituted mutants in the 4N parental transporter. The activity and the cell surface expression are shown as percentage of 4N. The 4N parental mutant had about 50% cell surface abundance compared with the wild-type (WT) rbNaDC1. Transport activity of 100 μM $^{3}$H-succinate was measured with 30 minutes incubation in sodium containing buffer. Transport results are shown as mean ± SEM (n = 3). Cell surface protein was quantitated and expressed as a percentage of 4N. The bars represent mean ± range (n = 2 separate transfections).

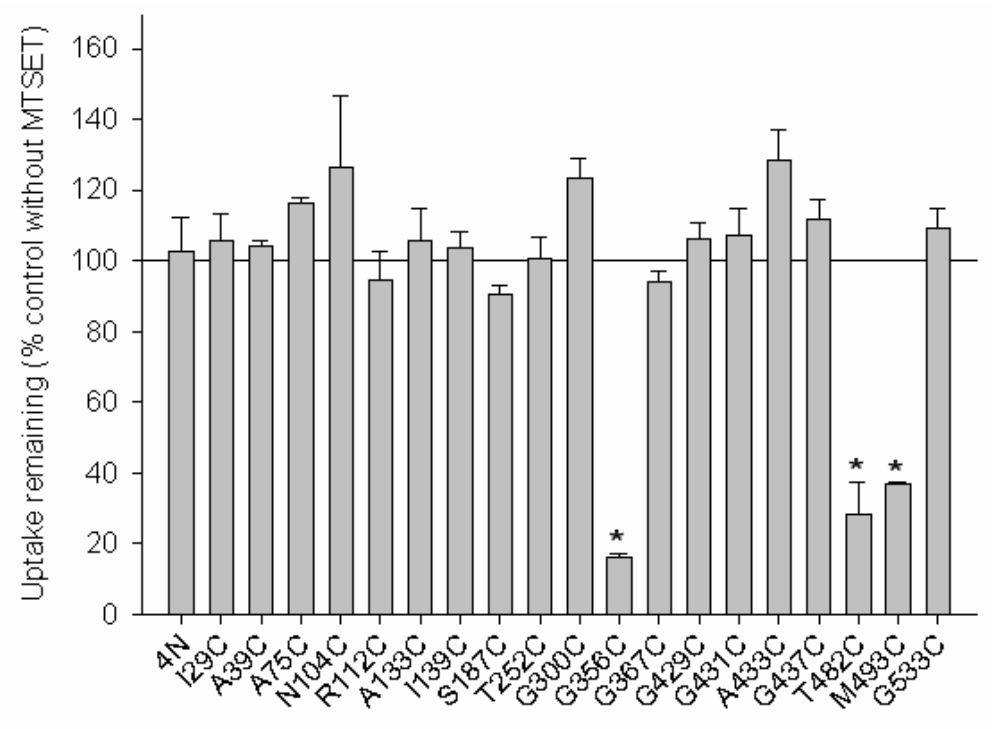


**Figure 3.7** Effect of 1 mM MTSET on succinate transport by cysteine-substituted mutants. HRPE cells expressing cysteine-substituted mutants in 4N background were preincubated for 10 min in sodium buffer containing 1 mM MTSET or sodium buffer alone (as control). The preincubation solution was washed away with sodium buffer and 100 µM $^{3}$H-succinate uptake was measured. Uptake activities in cells pretreated with MTSET are expressed as a percentage of the uptakes in control cells pretreated with sodium buffer alone. The bars represent mean ± range or SEM (n = 2 to 3, separate transfections). The * denotes significant difference from control group without MTSET ($p < 0.05$).

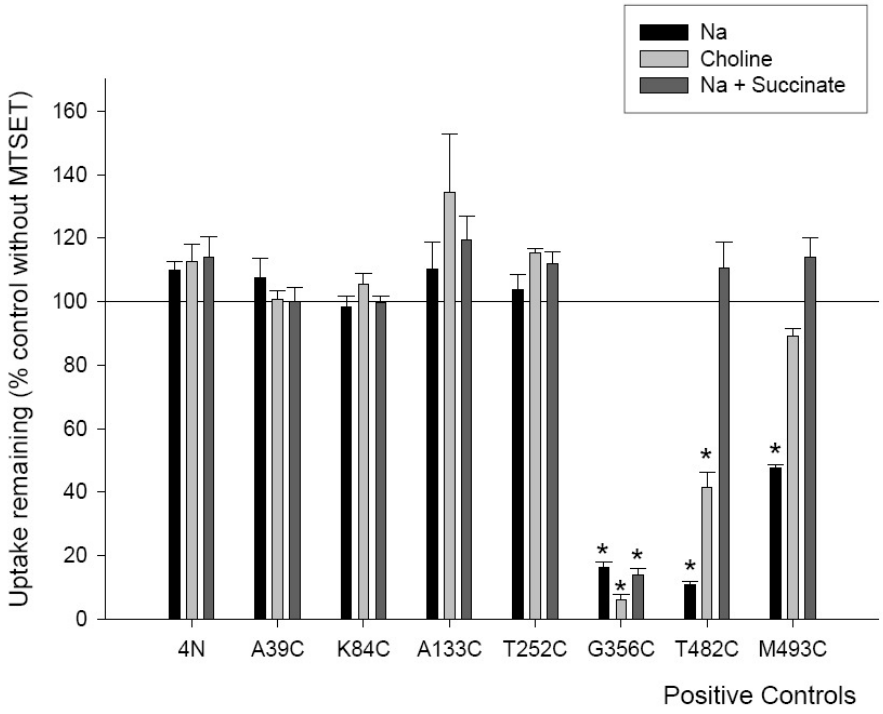


**Figure 3.8** Effect of substrate and cation on sensitivity of cysteine-substituted mutants to MTSET labeling. HRPE cells expressing cysteine-substituted mutants in 4N background were preincubated for 10 min in sodium or choline buffer or sodium buffer + 10 mM succinate, with or without MTSET. For mutants A39C, K84C, A133C, T252C and G356C, 1 mM MTSET was used whereas for mutants T482C and M493C the concentration was 10 µM. Concentrations of MTSET were chosen depending on the sensitivity of each mutant. The preincubation solution was washed away and uptake activity of 100 µM $^{3}$H-succinate was measured. For mutants A39C, K84C, A133C, T252C and G356C, uptakes were carried out in 6 well plates due to low succinate transport activity of these mutants. Mutant G356C showed low succinate transport activity over background when transfected into HRPE cells and hence was transfected into COS7 cells. For mutants T482C and M493C uptakes were performed in 24 well plates. Uptake activities of cells pretreated with MTSET are shown as a percentage of the uptakes in the control cells pretreated with the same buffers without MTSET. Bars represent mean ± range or SEM (n = 2 for A39C, K84C, T252C or 3 for 4N, A133C, G356C, T482C and M493C). *, significantly different from control group ($p < 0.05$).

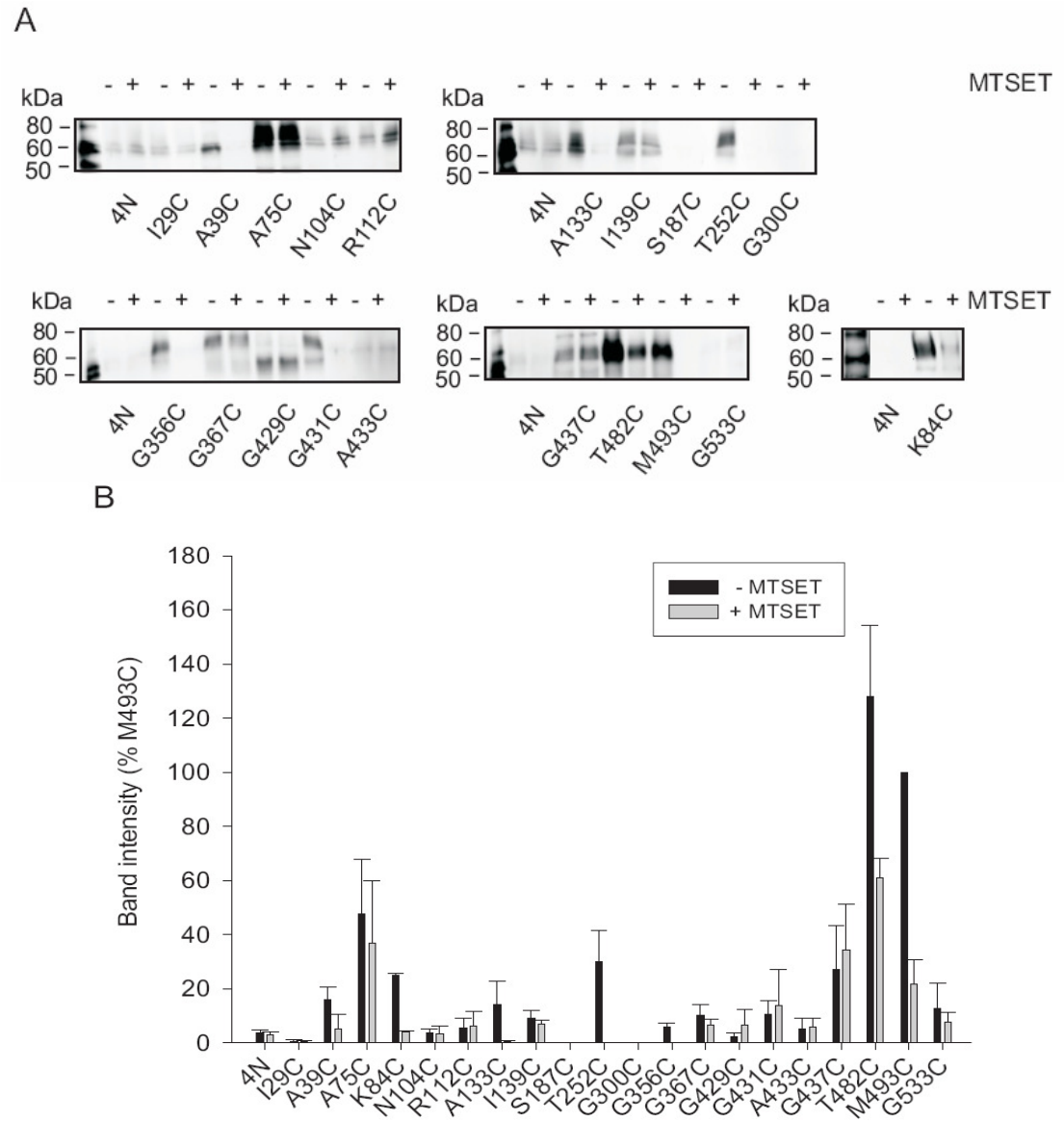


**Figure 3.9** Labeling of substituted cysteine residues with MTSEA-biotin. (A) Western blots showing MTSEA-biotin labeling of cysteine-substituted mutants in 4N parental background. HRPE cells expressing cysteine mutants were preincubated without (-) or with (+) 1 mM MTSET followed by labeling with 2 mM MTSEA-biotin. Blots were treated with anti-NaDC1 antibodies (1:1000 dilution). The parental transporter 4N and positive control M493C in 4N, were included in each biotinylation experiment. (B) Summary of MTSEA-biotinylation results. Western blots such as those shown in (A) were quantitated and expressed as a percentage of positive control M493C without MTSET treatment from the same blot. Bars represents mean ± range (n = 2, separate transfections).

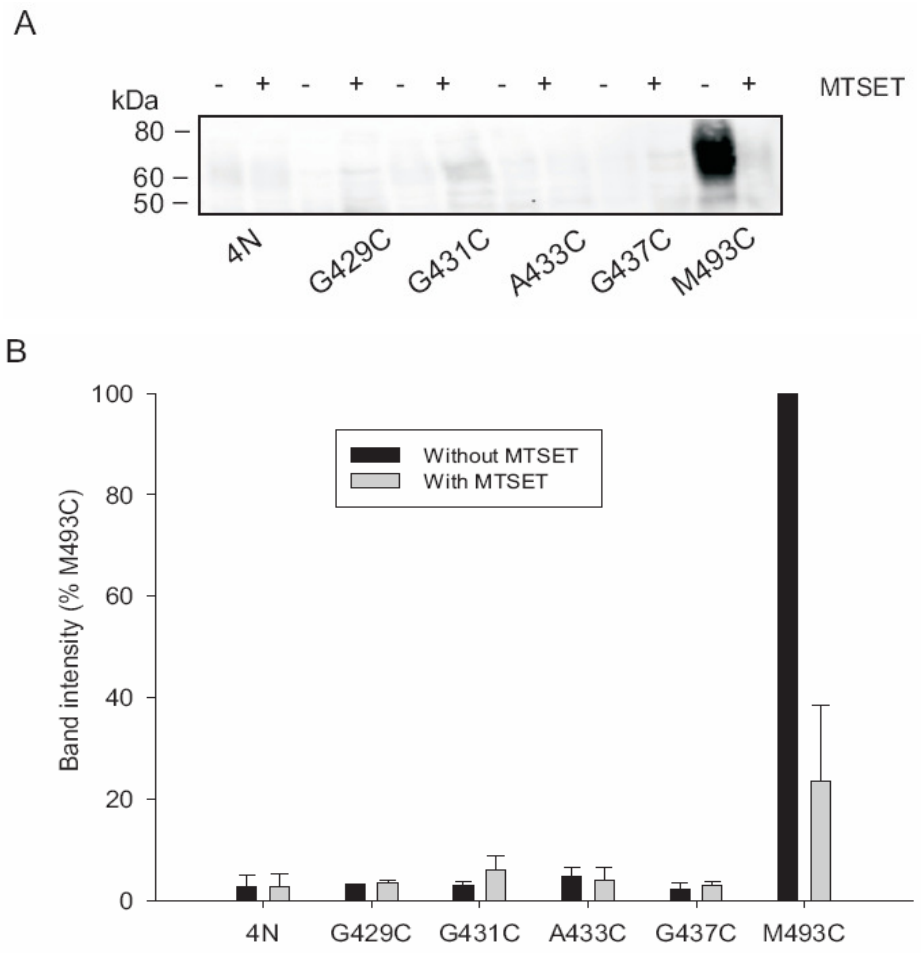


**Figure 3.10** Labeling of substituted cysteine residues with EZ-Link™ PEO-Maleimide Activated Biotin. (A) HRPE cells expressing parental mutant 4N or cysteine-substituted mutants, G429C, G431C, A433C, G437C, M493C in 4N were treated without (-) or with (+) 1 mM MTSET in sodium buffer. Labeling was done using 0.4 mM EZ-Link™ PEO-Maleimide Activated Biotin (Pierce). Western blots were probed with anti-NaDC1 antibodies (1: 1000 dilution). Blot includes an internal control of the parental transporter 4N and an M493C mutant in 4N background as a positive control. (B) Summary of EZ-Link™ PEO-Maleimide Activated Biotin labeling results. Western blots such as those shown in (A) were quantitated and expressed as a percentage of positive control M493C without MTSET treatment from the same blot. Bars represents mean ± range (n = 2, separate transfections).

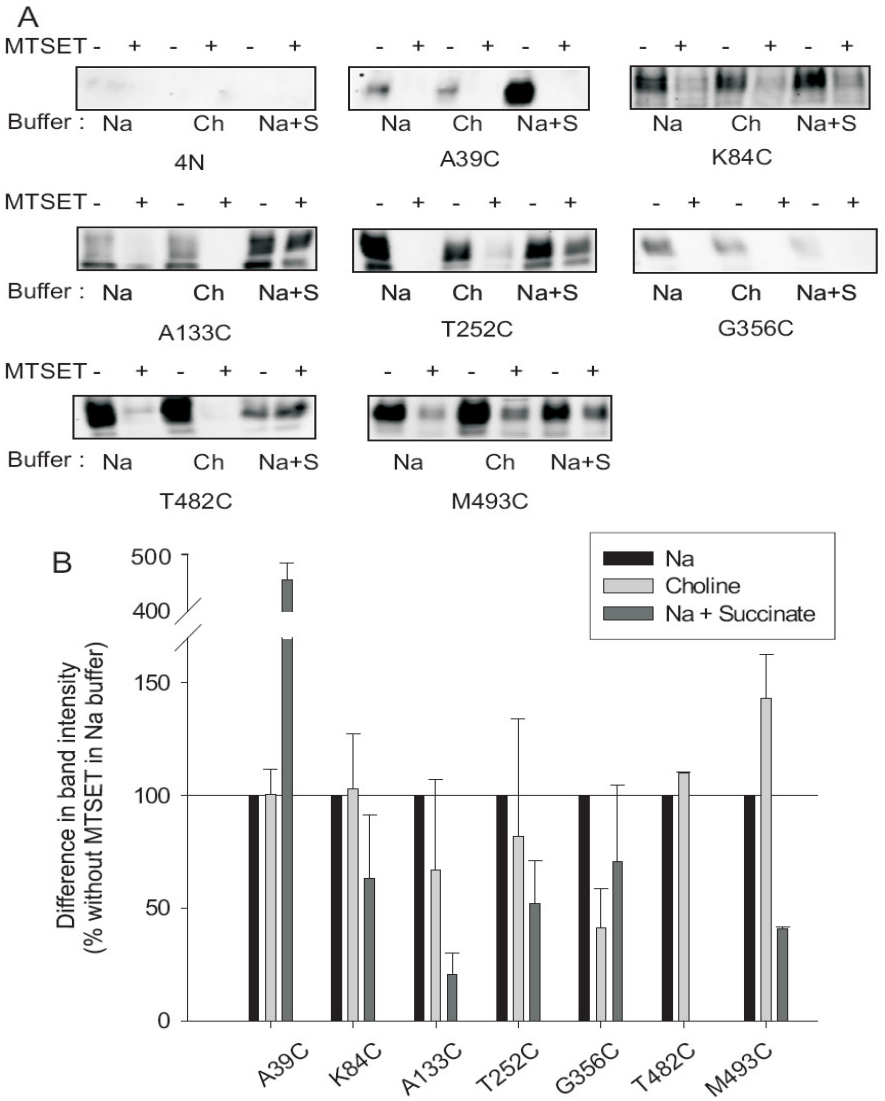


**Figure 3.11** MTSEA-biotin labeling of cysteine-substituted 4N mutants under different buffer conditions. (A) Mutants that were labeled with MTSEA-biotin (from Fig. 8) and hence were accessible in sodium buffer were chosen for further study. HRPE cells expressing cysteine substituted mutants were pretreated without (-) or with (+) 1 mM MTSET in sodium buffer or choline buffer or in sodium buffer + 10 mM succinate. Labeling was done with 2 mM MTSEA-biotin in sodium buffer or choline buffer or sodium buffer with 10 mM succinate. Anti-NaDC1 antibodies (1:1000 dilution) were used to identify biotinylated NaDC1. (B) Blots were quantitated and expressed as a percentage of the same mutant without MTSET in sodium buffer alone (control). Bars represent specific differences in MTSEA-biotin labeling in the presence and absence of MTSET. Difference between the signal in the presence and absence of MTSET represents specific binding of MTSEA-biotin. Bars represent mean ± range (n = 2 separate transfections).

## DISCUSSION

This study was conducted to determine the membrane topology of NaDC1. Hydropathy analysis suggested that NaDC1 has 11 TM whereas more recent modeling based on secondary structure prediction algorithms predicted 13 TM. Although other topology prediction tools have suggested anywhere from 8 to 14 TM, previous experimental results have shown that the N-terminus is located intracellularly whereas the C-terminus containing the N-glycosylation site is located extracellularly (*61*). This essentially limits the possible topologies of NaDC1 to 11 or 13 TM. The primary difference between the two topology models is between residues 385 and 465 which might pass through the membrane and form two transmembrane α helices (in the 13 TM model) or remain as an intracellular loop (in the 11 TM structure). Although bioinformatics tools can provide valuable insight into potential topologies, experimental data are essential to test the models. The main finding of the present study is that NaDC1 has 11 TM; however, the new model contains some features of the 13 TM model.

The accessibility of introduced cysteines toward methanethiosulfonate reagents was used to test the topology models. The first part of the project was done using the C476S mutant of rbNaDC1 as the parental transporter (*70*). The advantage of C476S is that its functional properties and cell-surface expression are very similar to those of wild-type NaDC1. Our previous studies showed that NaDC1 protein expression depends on endogenous cysteines and at least four cysteines are required for measurable activity (*116*). The C476S mutant contains ten of the eleven endogenous cysteines but it is insensitive to membrane impermeant methanethiosulfonate reagents. However, the assumption that the endogenous

cysteines are always inaccessible to the outside may not be correct. The G367C mutant made in the C476S background exhibited increased labeling with MTSEA-biotin after preincubation with MTSET. The MTSET should block MTSEA-biotin labeling by binding to the cysteine at position 367. This result suggests that the mutation at position 367 produced a conformational change in the C476S/NaDC1 parental protein that exposed endogenous cysteines. Therefore, it is possible that other mutants made in the C476S background might also have changed the conformation of the transporter. Therefore, most of the study was done using the 4N mutant of NaDC1, containing only four endogenous cysteines (*116*). We found that the membrane impermeant reagent, MTSEA-biotin, did not label the 4N parental mutant. More importantly, the G367C/4N mutant was no longer labeled by MTSEA-biotin and none of the mutants exhibited increased MTSEA-biotin labeling after pretreatment with MTSET.

Single cysteine residues were introduced into the 4N mutant of rbNaDC1 in putative extracellular and intracellular loops (Figure 3.1). We observed specific MTSEA-biotin labeling that was blockable by MTSET in mutants A39C, K84C, A133C, T252C, G356C, T482C and M493C. Therefore, these residues are located on the outside of the cell or in a water-filled pore. Based on these results, we propose the modified 11 TM model shown in Figure 11. The model is similar to the original 11 TM model for rbNaDC1 with a change in the positions of TM 3 and 4 to account for MTS labeling of K84C, originally proposed to be in an intracellular loop. The revised model for TM3, containing Ala-75 and Lys-84, is likely to contain a water-facing region that is accessible to the outside of the cell. Our previous study, with mutants made in the C476S background, suggested that Lys-84 could be in a water-

filled pore or reentrant loop (*72*). The K84C/C476S mutant was inhibited by MTSES, not MTSET, and showed cation-dependent and substrate-protectable labeling (*72*). The results of the present study with K84C/4N verified those results. Interestingly, although MTSET did not affect the transport activity of K84C, this reagent does prevent binding of MTSEA-biotin. The A75C mutant was not labeled by MTSET, indicating that the open pore formed by TM3 does not extend as far as this residue.

The NaDC1 transport cycle involves the ordered binding of three sodium ions followed by substrate. Sodium binding triggers conformational changes in the transporter that increase the affinity for substrate, which then allows the substrate to bind (*51*). Therefore, different conformational states should predominate in the presence or absence of sodium or substrate. Only three NaDC1 mutants in the present study exhibited functional effects of MTSET on transport activity: G356C, T482C and M493C. G356C was inhibited by MTSET in all incubation conditions whereas T482C and M493C were more accessible in the conformational state seen in the presence of sodium. Mutants T482C and M493C also showed substrate protection from MTSET labeling, both for transport and for MTSEA-biotin labeling. The results are consistent with previous findings using T482C and M493C in the C476S background (*69;70*). One of the NaDC1 mutants directly labeled by MTSEA-biotin, mutant A39C, had increased labeling in the presence of succinate, indicating that this residue may be exposed in the conformational state produced by substrate binding. This may be similar to the A116C mutant of the serotonin transporter (SERT) which exhibits increased reactivity towards MTSEA in the presence of

substrate and sodium (*122*). The interpretation is that A116C-SERT may be partially buried in the protein, but is exposed after substrate binding.

There is low sequence similarity between NaDC1 and other membrane proteins of known structure. Therefore, to construct a structural model of NaDC1 an alternate approach was used based on comparison of the predicted fold of NaDC1 with already known fold structures (*123;124*). Proteins can adopt similar folds even without significant sequence similarly. The approach of fold recognition and comparative modeling has been applied successfully for structural modeling and functional prediction of several proteins including the V8 protease from S*taphylococcus aureus* and sialyltransferases (*125;126*). To identify a possible template for rbNaDC1, the sequence was submitted to the BioInfobank Meta Server (*118*). The analysis showed that the lactose permease from *E. coli* (LacY) would be a suitable modeling template because of similarities between its folding pattern and the predicted NaDC1 fold. The highest similarity was with the substrate-free structure of LacY (*127*). LacY is a $H^+$/lactose cotransporter which belongs to the major facilitator superfamily. The structure of the LacY protein is organized into two six-helix bundles separated by a large water-filled cavity containing the substrate and proton binding sites (*12*). The transport mechanism of LacY involves a general change in protein structure as a result of substrate binding, involving the formation of a water accessible cavity on one side of the substrate binding site, and closing of the other side (*128*). Using the structure of LacY as a template we built a homology model for rbNaDC1. Figure 3.12A shows a ribbon representation of the NaDC1 model and Figure 3.12B shows the model when viewed from the outer surface of the membrane. The 11 α-

helices in NaDC1 are approximately parallel to each other surrounding a central pore which could form the substrate and cation transport pathway.

The NaDC1 model is consistent with experimental data examining functional effects of MTS reagents. The MTSET-sensitive residues T482C, T484C, L485C, L487C and M493C are located in the extracellular loop between TM 9 and 10 (*70*). Residue Ala-504 is a determinant of a substrate affinity and is predicted to be in the TM 10 facing the water filled pore. Residues Thr-461, Phe-473, Thr-474, Glu-475 and Asn-479 were found to be important for succinate transport whereas Ser-478, Ala-480, Ala-481 were inhibited by MTSET (*69*). All of these residues are located in TM 9 in the model. Mutations of Asp-373 and Glu-475 affect succinate as well as cation affinity in rbNaDC1 (*69;74*). D373C is accessible to MTSET from the outside of the cell in both sodium and choline buffers and also shows substrate protection (*74*). In the model Asp-373 is in the TM 8 which faces the water-filled pore and therefore Asp-373 might be accessible by MTS reagents. Finally, residue Arg-349 is accessible to MTSEA in the presence of sodium (*74*) and in the model Arg-349 is in the extracellular loop between TM 7 and 8, accessible from the outside (Figure 3.11).

A recent study has addressed the membrane topology of the human high affinity $Na^+$/dicarboxylate cotransporter (NaDC3) using accessibility of substituted cysteines as well as immunofluorescence microscopy to localize epitope tags on the N and C terminus (*63*). Similar to NaDC1, NaDC3 is predicted to contain 11 TM helices with an intracellular N terminus and an extracellular C terminus. The main difference between the models is that the NaDC3 model predicts a re-entrant loop or helix between TM 8 and 9 whereas the NaDC1 model predicts an intracellular loop at that site. There is no information on the accessibility of Leu-87 (corresponding to

Lys-84 in NaDC1), although Val-81 in NaDC3 (Val-78 in NaDC1) is found to be inside (*63*), similar to our findings with Ala-75.

In conclusion the cysteine substituted mutants A39C, K84C, A133C, T252C, G356C, T482C and M493C were accessible to membrane-impermeant methanethiosulfonate reagents applied from the outside of the cell. The reactivity of the substituted cysteines to methanethiosulfonate reagents changed in different buffer conditions, which indicates different exposure of protein domains during the conformational changes of the transport cycle. The results of substituted cysteine accessibility experiments support a modified 11 TM model with the N-terminus located intracellularly and the C-terminus located extracellularly. The positions of TM 3 and 4 in the new model are oriented according to the 13 TM model. The experimental results were combined with a comparison of predicted folding similarities with the lactose permease to construct a modified homology model of NaDC1 containing 11 TM. This new model will provide a structural framework towards understanding the transport mechanism of NaDC1.

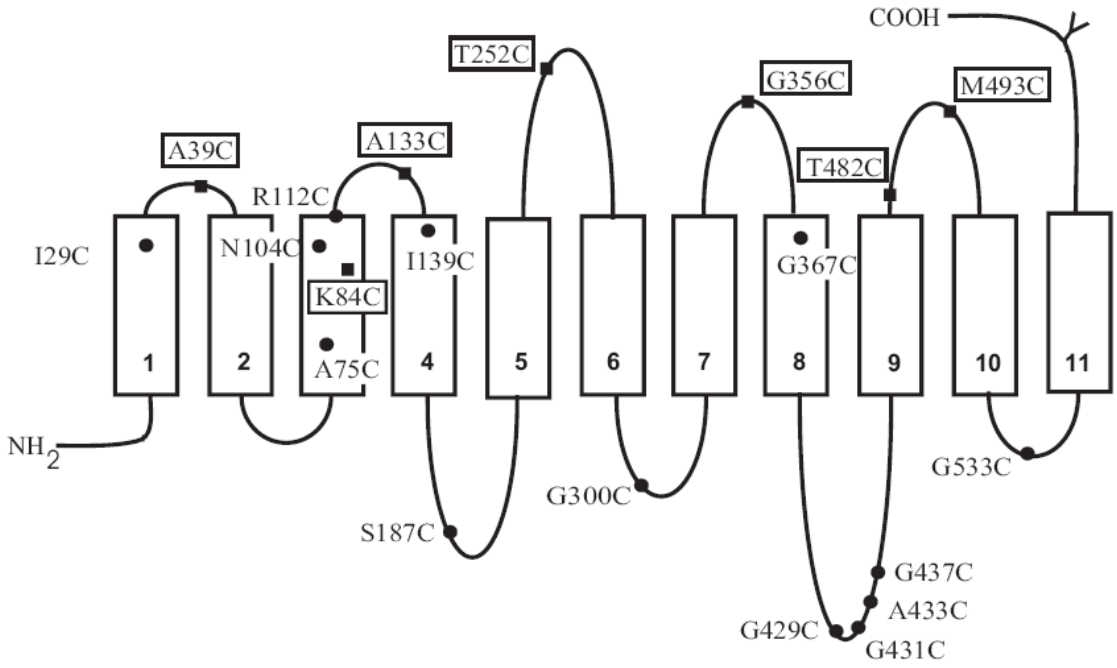


**Figure 3.12** Revised topology model of rbNaDC1. The results of the present study support a model with 11 TM. The black squares with mutant names in boxes represent the residues that are accessible by MTSEA-biotin specific labeling. Circles represent residues that are not accessible by MTSEA-biotin. Y represents position of N-glycosylation site at the C terminus.

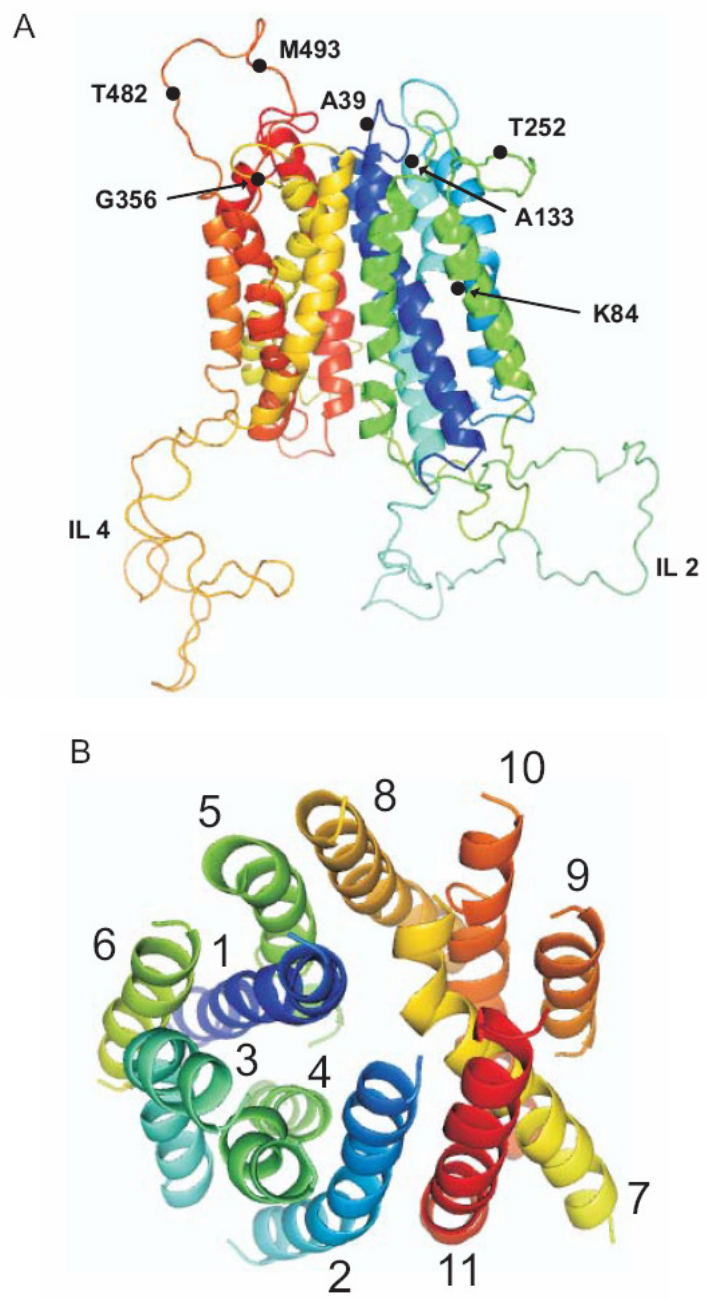


**Figure 3.13** Model of three dimensional structure of rbNaDC1 containing 11 TM. (A) Ribbon representation of rbNaDC1 model. The 11 TM are colored from N terminus in blue to the C terminus in red. The C terminus is outside (top) of the cell whereas the N terminus is intracellular (bottom). Residues accessible by specific labeling by MTSEA-biotin reagent are shown. (B) Ribbon representation of rbNaDC1 viewed along the membrane. Graphics were generated by PyMol.

# CHAPTER 4: IDENTIFICATION OF CONFORMATIONALLY SENSITIVE AMINO ACIDS IN THE $Na^+$/DICARBOXYLATE SYMPORTER

## INTRODUCTION

Understanding structural details including substrate and cation binding sites, conformational changes in the helices of the transporter and residues involved in the permeation pathway of the transporter is a focus of membrane transporter studies. The primary goal of this study was the identification of conformationally sensitive amino acids in $Na^+$/dicarboxylate cotransporters. Conformationally sensitive amino acids are accessible from outside and/or inside in a particular conformation of the transporter and are inaccessible in other conformational states of the transporter. Therefore, the accessibility of these residues depends on the conformational state of the transporter. To identify conformationally sensitive residues a $Na^+$-coupled dicarboxylate transporter from *Staphylococcus aureus*, $Na^+$/dicarboxylate symporter (SdcS) was used. SdcS is ~ 35 % identical to human NaDC1, has similar transport properties, and was functionally expressed in *E. coli* (*29*). SdcS contains a single cysteine and the cysteineless mutant, C457S shows similar transport properties as the wild-type SdcS. Therefore, cysteines were substituted in cysteineless SdcS, at sites that have been shown to be conformationally sensitive in rbNaDC1. The accessibility of the substituted cysteines was examined in rightside out and inside out membrane vesicles to determine accessibility from both sides of the membrane. In mammalian NaDC cotransporters these studies could not be carried out due to experimental difficulties in studying accessibility of the transporter from inside the cell.

In this study, functional properties of SdcS expressed in right-side-out (RSO) and inside-out (ISO) *E. coli* membrane vesicles were determined. The succinate affinity was similar for RSO and ISO vesicles whereas the maximum velocity of succinate transport was four times higher in RSO than ISO. The experimental design was useful in testing accessibility of cysteine-substituted mutants from outside as well as inside. Mutant D329C was accessible in presence of $Na^+$ from outside only whereas L436C mutant did not show any change in the succinate uptake after MTSET labeling. Mutation in Leu-436 might cause overall conformational change in the transporter which leads to less affinity towards succinate as shown by increased $K_m$. Mutant N108C was accessible from outside and inside in presence of $Na^+$ only. It was not accessible with the conformational state in absence of $Na^+$ or presence of choline. N108C also showed substrate protection likely due to steric hindrance due to chemical labeling and not because of conformational change after substrate binding. In conclusion, this study indicates residue Asn-108 is located in the transmembrane helix near the water-filled pore or probably in a dynamic reentrant loop accessible from both sides of the membrane.

## MATERIALS AND METHODS

### Site-directed Mutagenesis

Site directed mutagenesis was performed using the QuikChange site-directed mutagenesis kit (Stratagene) as described in Chapter 2. Plasmid pQE-80L encoding SdcS with N-terminal MRGS$(H)_6$GS amino acid extension (*29*) was used as a template to construct cysteineless mutant, C457S. The cysteineless mutant, C457S

was then used as the template for constructing the single cysteine mutants: N108C, D329C and L436C.

**Preparation of Membrane Vesicles**

Recombinant SdcS was expressed in *E. coli* BL21 strain [$F^-$ ompT $hsdS_B(r_B^- m_B^-)$ gal dcm] as described (*29*). Briefly, overnight cultures of bacteria containing SdcS, pQE-80L, cysteineless mutant C457S and D329C, L436C, N108C mutant plasmids were used to inoculate 500 ml of LB broth (1: 10 dilutions) containing 50 µg/ml of carbenecillin. Cells were grown at 37°C to an optical density at 660 nm of 0.4 to 0.6. To induce SdcS and cysteine mutants expression, 150 µM isopropyl-β-D-galactopyranoside (IPTG) was added and cells were harvested in mid-exponential phase by centrifugation.

Right-side-out vesicles (RSO) were prepared by a modification of Kaback's method (*129*). Briefly, centrifuged pellets were resuspended in 30% sucrose, 30 mM Tris-HCl, pH 8. RNAse solution (1 µg/ml) and 10 mM $K_2$-EDTA, pH 7 were added and incubated at room temperature for 2–3 min. Lysozyme (6.4 mg to 300 ml resuspended pellets) was added and flasks were kept on rotary platform shaker for 15 min. at room temperature. Centrifugation was carried out for 30 min at 17,000 x g and pellets were resuspended in 30% sucrose, 20 mM $MgSO_4$, 100 mM potassium phosphate pH 6.6 using glass–teflon homogenizer (Setting 60, 5 passes). RNAse and DNAse (1.7 mg) were added and homogenates were poured into 1 L flasks containing 50 mM potassium phosphate buffer, pH 6.6. Flasks were kept at 30°C incubator shaking at 75 rpm for 10 min. 1 M $K_2$-EDTA was added and incubated for 15 min.

Later 1 M $MgSO_4$ was added and further 15 min. incubation was carried out. Centrifugation was performed at 27,500 x g for 70 min. Pellet was resuspended into 100 mM potassium phosphate, 10 mM EDTA pH 6.6 using glass–teflon homogenizer. Low speed centrifugation was performed at 2500 rpm (JA 25.5 rotor, Beckman) for 30 min. to remove unbroken cells. The supernatants were centrifuged at 23,000 rpm, 30 min (JA 25.5 rotor). RSO vesicles were resuspended in 100 mM potassium phosphate buffer pH 7. All the centrifugations were carried out at 4°C.

Inside-out membrane vesicles (ISO) were prepared by degrading the nucleic acids using 0.5 mg/ml DNAse and RNAse and further passing the cell suspension through the French Pressure cell (Thermo Scientific) at 4000 psi. Unbroken cells and organelles were removed by low speed centrifugation at 10,000 x g, 15 min. at 4°C. ISO vesicles were sedimented by ultracentrifugation 200,000 x g, 45 min at 4°C. Crude ISO vesicles were resuspended in 100 mM potassium phosphate buffer pH 7.4 and further purified by sucrose density gradient centrifugation. The sucrose density step gradient was prepared with 0.77 M, 1.44 M and 2.02 M sucrose in 10 mM HEPES pH 7.4 (*130*). Crude ISO vesicles were added to the top of the gradient and overnight centrifugation was carried at 27,000 rpm (SW 28 rotor, Beckman) for 15 hrs. at 4°C. The upper band of proteins at the interface between 0.77 M and 1.44 M sucrose was collected by gradient collector. Preliminary studies showed that this band contained purified ISO membranes. The lower band between 1.44 M and 2.02 M contains cell wall fragment and other cellular debris (*130*). The upper band from step gradient containing ISO vesicles was diluted with 100 mM potassium phosphate buffer, pH 7.4 and centrifuged at 200,000 x g, 45 min at 4°C. ISO membrane vesicles were resuspended in 100 mM potassium phosphate pH 7.4. Phenylmethylsulfonyl

fluoride (PMSF), 0.5 mM, was added to all the steps to reduce proteolysis. Three independent right-side-out and inside-out membrane vesicle preparations were performed.

**Transport Assays**

Uptake of $^{14}$C-succinate by RSO and ISO membrane vesicles was performed by using a rapid filtration method. Transport buffer contained 10 mM NaCl, 90 mM choline chloride, 50 mM MOPS, pH 7. Transport buffer (40 µl) containing 40 µM $^{14}$C-succinate (specific activity of 44 mCi/mmol, PerkinElmer Life Sciences) was added to the bottom of a plastic tube (Falcon). A 10 µl drop of vesicles was added to the side of the tube and the reaction was initiated by vortexing the two together. The reaction was terminated after 10 sec. with addition of 1 ml ice-cold choline buffer (100 mM choline chloride, 50 mM MOPS pH 7), filtered immediately through Millipore filters (0.45 µm pore size, type HAWP) and washed with 4 ml of ice-cold choline buffer. The radioactivity retained by the filters was counted using Econo-Safe (Research products International Corp.) as scintillant on liquid scintillation counter (Packard Tri-Carb 2100 TR).

$Na^+$ activation of succinate uptake was determined by measuring the activation of succinate transport with increasing concentration of $Na^+$. For experiments to determine kinetic constants, 10 µl of vesicles were added to 40 µl of $Na^+$ buffer containing different concentrations of succinate. The final concentration of succinate was between 1 µM to 200 µM (1 to 400 µM for L436 RSO vesicles). Kinetic constants ($K_m$ and $V_{max}$) were determined by fitting the transport rates to the

Michaelis-Menten equation using nonlinear regression analysis (SigmaPlot 9, Systat Software Inc.).

For chemical labeling with MTSET, 40 µl of the vesicles were preincubated with 10 µl of 5 mM MTSET stock solution for 10 min. at room temperature. The MTSET labeling was followed by succinate transport assay in which 10 µl of pretreated vesicles were added to 40 µl of transport buffer containing $^{14}$C-succinate. Therefore, the final concentration of MTSET was 1 mM after dilution with the transport buffer. The final concentration of $Na^+$ and succinate was 5 mM and 10 mM respectively during the transport assay. MTSET was weighed out fresh for each experiment, kept on ice and diluted in buffer just before use. As a control, vesicles were preincubated with 10 µl of $Na^+$, choline or $Na^+$ with succinate buffers without MTSET. The transport reaction was stopped with 1 ml ice-cold choline buffer as described previously.

**Immunoblot Analysis**

RSO and ISO vesicles (25 µg) were diluted in gel loading buffer (150 mM Tris-HCl pH 7, 30% glycerol, 12% SDS, 6% β-mercaptoethanol, ~ 3% Coomassie blue R-250 (w/v)) and placed in a boiling water bath for 2 min. Vesicles were loaded and separated with 10 % Tricine SDS-PAGE, were transferred to nitrocellulose membrane for immunoblot analysis (*103*). Blots were incubated with 1:2000 dilutions of mouse monoclonal antibody reactive to the SdcS N-terminal $RGS(H)_4$ epitope tag (QIAGEN RGS-His antibody). Blots were incubated with the primary antibody for 2 hr. at room temperature with gentle shaking. The blots were then

incubated with 1:5000 dilution of horseradish peroxidase-conjugated anti-mouse immunoglobulin G antibody (Jackson ImmunoResearch Laboratories, Inc.) for 2 hr at room temperature, on rotary shaker (*29*). Supersignal West Pico chemiluminescent substrate kit (Pierce) was used to detect antibody binding. Images were captured with a Kodak Image Station 440CF and quantitated as described in chapter 2.

### Protein Determination

Protein contents of membrane vesicles were measured using the Bio-Rad protein assay based on the method by Bradford (*131*) with γ–globulin as a standard.

## RESULTS

### Assay of $Na^+$ Dependent Succinate Transport

Figure 4.1 indicates transport of succinate by right-side-out and inside-out membrane vesicles of *E. coli* BL21 cells harboring pQE-80L vector only, SdcS or the cysteineless mutant C457S. The transport was measured in the presence of 10 mM $Na^+$. Vesicles expressing SdcS and C457S showed rapid accumulation of succinate followed by a slow fall. The succinate uptake was linear until 15 sec. and therefore 10 sec. was used as an initial time point for further experiments. The peak of the overshoot was seen at 1 min. for both SdcS and C457S RSO and ISO. The uptake of succinate was due to the SdcS or C457S in the vesicles because very little succinate transport was detected in vesicles prepared from *E. coli* carrying the control plasmid, pQE-80L.

**Vesicle Orientation**

To verify the orientation of RSO and ISO membrane vesicles $Na^+$-coupled succinate uptake was measured in presence of methanethiosulfonate reagents. SdcS RSO and ISO membrane vesicles were preincubated with 1 mM [2-(trimethylammonium)ethyl]-methanethiosulfonate (MTSET), 1 mM (2-aminoethyl) methanethiosulfonate (MTSEA) or 1 mM (2-sulfonatoethyl) methanethiosulfonate (MTSES) for 10 min. No effect on succinate uptake was seen by SdcS RSO when treated with methanethiosulfonate reagents (Figure 4.2). SdcS ISO were completely inactive after preincubation with 1 mM MTSEA whereas preincubation with MTSET decreased the succinate uptake in SdcS ISO by ~ 85 % and preincubation with MTSES decreased the uptake by ~ 90 % (Figure 4.2). When cysteineless mutant, C457S RSO and ISO were preincubated with 1 mM MTSET reagent no decrease in succinate transport was seen indicating that SdcS contains a single cysteine at 457 that is accessible by cysteine specific MTSET reagent from inside the cell but not from outside (Figure 4.7).

**$Na^+$ Activation of Succinate Uptakes in RSO and ISO Membrane Vesicles**

Previous data from transport studies in whole cells indicate strong cation mediated inhibition of $Na^+$ dependent succinate uptake at higher $Na^+$ concentrations (*29*) whereas studies with proteoliposomes showed sigmoidal curve with two cooperative cation binding sites (*94*). Therefore, relationship between $Na^+$ concentration and SdcS, C457S RSO and ISO vesicles transport activity was examined. $Na^+$ activation of succinate uptake was measured in SdcS and C457S right-side-out and inside-out vesicles at 10 sec. with increasing $Na^+$ concentration.

SdcS and C457S, RSO and ISO membrane vesicles showed decreased succinate transport at higher $Na^+$ concentrations (Figure 4.3). In RSO membrane vesicles, peak for succinate transport was observed at 10 mM sodium for SdcS and 25 mM sodium for C457S. Further analysis of $Na^+$ dependent succinate transport in ISO vesicles showed peak for SdcS and C457S at ~ 10 mM $Na^+$ concentration. All subsequent experiments were done using 5 or 10 mM $Na^+$.

**Kinetics of Succinate Transport**

Succinate kinetic analysis was performed for SdcS and C457S in RSO and ISO membrane vesicles. The data were fitted to the Michaelis-Menten equation. Cysteineless mutant C457S showed similar succinate affinity ($K_m$) as well as maximum velocity ($V_{max}$) as that of wild-type SdcS. (Table 4.1). Kinetic constants of RSO and ISO vesicles were also compared. No significant difference in succinate affinity was seen between SdcS in RSO and ISO vesicles, similarly no difference was seen between C457S in RSO and ISO vesicles. When $V_{max}$ was compared, SdcS in RSO vesicles had a higher $V_{max}$ than in ISO vesicles. Similarly, C457S in RSO vesicles had a significantly higher $V_{max}$ than in ISO vesicles.

**Mutagenesis of SdcS**

Previous studies have shown that cysteine substitutions at residues Lys-84, Asp-373 and Met-493 from rbNaDC1 are accessible to methanethiosulfonate reagents (*70;72;74*). The rbNaDC1 mutant K84C is sensitive to MTSES in $Na^+$ buffer only and shows substrate protection. D373C is accessible to MTSET in $Na^+$ and choline

buffers and showed substrate protection in presence of 100 μM succinate. M493C is sensitive to inhibition by MTSET in presence of $Na^+$ buffer. The inhibition of M493C by MTSET was prevented by 1 mM succinate. These results suggest that K84C, D373C and M493C are not accessible from the outside in the absence of $Na^+$ (in presence of choline buffer). In the presence of $Na^+$ these residues become accessible due to conformation change that takes place in the transporter and the substrate protection was observed due to the steric hindrance of methanethiosulfonate reagents.

Sequence alignments of rbNaDC1 and SdcS showed that Lys-84, Asp-373 and Met-493 of rbNaDC1 correspond to Asn-108, Asp-329 and Leu-436 of SdcS (Figure 4.4). Therefore single cysteine-substituted mutants N108C, D329C and L436C were constructed in cysteineless mutant C457S. The accessibility of these substituted cysteines was tested from outside and inside the cell by using thiol specific MTSET labeling and rightside out and inside out vesicles.

**Protein Expression and Transport Activity of Cysteine-Substituted Mutants N108C, D329C and L436C**

The protein expression of SdcS and mutants in RSO and ISO membrane vesicles was determined by Western blotting (Figure 4.5). The succinate transport activity and protein expression of single cysteine mutants are compared in Figure 4.6. For right-side-out vesicles similar expression was seen for SdcS, cysteineless C457S and all the cysteine-substituted mutants. C457S RSO showed ~ 80 % succinate transport activity compared with the SdcS RSO. All the mutants showed ~ 45 to 60

% succinate activity as of C457S. C457S in ISO vesicles showed double the expression compared with SdcS in ISO vesicles. The succinate transport activity observed with C457S in ISO vesicles was much lower compared with RSO vesicles. This result correlates well with the kinetics data where $V_{max}$ of C457S ISO was significantly lower than RSO (Table 4.1). Mutant N108C ISO showed similar expression as that of C457S ISO whereas mutants D329C and L436C showed ~ 55 % of expression compared with the cysteineless mutant.

**Succinate Kinetics in Cysteine-Substituted Mutants**

The kinetics of succinate transport was measured in mutants N108C, D329C and L436C in RSO and ISO membrane vesicles. Cysteine-substituted mutants were compared with the parental C457S and also statistical analysis was done by comparing RSO with ISO membrane vesicles. As shown in Table 4.1, Michaelis constant of mutant L436C in RSO vesicles was four fold greater than that of the parental C457S in RSO vesicles. Other mutants showed similar succinate affinity compared with C457S. The maximum velocity ($V_{max}$) of L436C and D329C mutants in right-side-out vesicles were significantly lower than C457S. The cysteine-substituted inside-out vesicles showed similar $K_m$ and $V_{max}$ as that of cysteineless C457S. When right-side-out and inside-out vesicles were compared, L436C mutant in RSO showed significantly higher $K_m$ than L436C mutant in ISO vesicles. This indicates the lower affinity for the succinate in L436C RSO vesicles. Mutant N108C showed significant difference between its RSO and ISO $V_{max}$ values with similar protein expression.

**MTSET Sensitivity of Cysteine-Substituted Mutants**

To understand the accessibility of cysteine-substituted mutants from outside (in RSO vesicles) and inside (in ISO vesicles) chemical labeling with MTSET was carried out. To determine whether the substituted cysteines are accessible to MTSET in different conformational states of the transporter, $Na^+$, choline and $Na^+$ with 10 mM succinate buffers were used. Previous experiments suggest that SdcS follows an ordered binding mechanism where $Na^+$ binds first causes the conformational change in the transporter so that substrate can bind to substrate binding site in the transporter and translocation occurs (*29*). Therefore SdcS is likely to be in different conformational states in the presence and absence of $Na^+$ and substrate. Wild-type SdcS in RSO vesicles was not affected by 1 mM MTSET preincubation either in $Na^+$, choline or $Na^+$ + 10 mM succinate buffers (Figure 4.7A). SdcS in ISO vesicles showed ~ 80 % decrease in succinate activity when preincubated with 1 mM MTSET in $Na^+$, choline and $Na^+$ + 10 mM succinate buffers (Figure 4.7B). As expected, there was no change in succinate activity in vesicles expressing the cysteineless mutant, C457S, after preincubation with 1 mM MTSET. Mutant D329C MTSET in presence of $Na^+$ and $Na^+$ with succinate in RSO vesicles but not in ISO vesicles. Mutant L437C was not affected by MTSET in RSO or ISO vesicles, regardless of the incubation conditions. N108C in both RSO and ISO vesicles was inhibited by MTSET in the presence of $Na^+$ but not in choline. N108C in both RSO and ISO vesicles also showed substrate protection; there was decreased inhibition by MTSET in the presence of 10 mM succinate in $Na^+$ buffer.

**Effect of Temperature on MTSET inhibition**

As mentioned above, N108C showed substrate protection of MTSET inhibition. There are several explanations to account for substrate protection. It could be due to conformational change after substrate binding that occludes the substituted cysteine and makes it inaccessible to MTSET or substrate binding could physically prevent access of MTSET to the substituted cysteine. At cold temperatures large scale conformational changes of the transporter are slowed down but no effect of temperature would be seen if substrate binding prevents access of MTSET to a substituted cysteine (*132;133*). Therefore if substrate protection is due to a conformational change then we would predict a reduction in substrate protection at cold temperatures (on ice). However, there was no change in substrate protection at cold temperature in N108C in RSO (Figure 4.8) indicating that the substrate protection in N108C mutant is likely due to steric hindrance of MTSET labeling.

**Table 4.1** Succinate kinetics of wild-type SdcS, cysteineless C457S and cysteine-substituted mutants, N108C, D329C, L436C in right-side-out (RSO) and inside-out (ISO) inner membrane vesicles from E. coli[a]

| Protein | Vesicle | $K_m$ (μM) | $V_{max}$ (pmol/mg-min) | n |
|---|---|---|---|---|
| Parental | | | | |
| SdcS | RSO | 26.4 ± 1.2 | 6742 ± 1456 | 3 |
| | ISO | 36.0 ± 4.3 | 2050 ± 303* | 3 |
| C457S | RSO | 42.3 ± 8.0 | 5058 ± 509 | 3 |
| | ISO | 50.9 ± 7.5 | 1534 ± 118* | 3 |
| Cysteine-substituted mutants | | | | |
| N108C | RSO | 46.6 ± 11.6 | 8156 ± 1292 | 3 |
| | ISO | 38.2 ± 7.2 | 2759 ± 1369* | 3 |
| D329C | RSO | 44.5 ± 4.6 | 1069 ± 295[#] | 3 |
| | ISO | 48.1 ± 2.5 | 1522 ± 192 | 3 |
| L436C | RSO | 149.2 ± 23.0[#] | 3226 ± 362[#] | 4 |
| | ISO | 36.1 ± 6.0* | 2304 ± 921 | 4 |

[a]The kinetic values represent the mean ± standard error.
*Indicates significantly different from right-side-out membrane vesicles group ($p < 0.05$).
[#]Indicates significant difference compared with parental cysteineless C457S control group ($p < 0.05$).

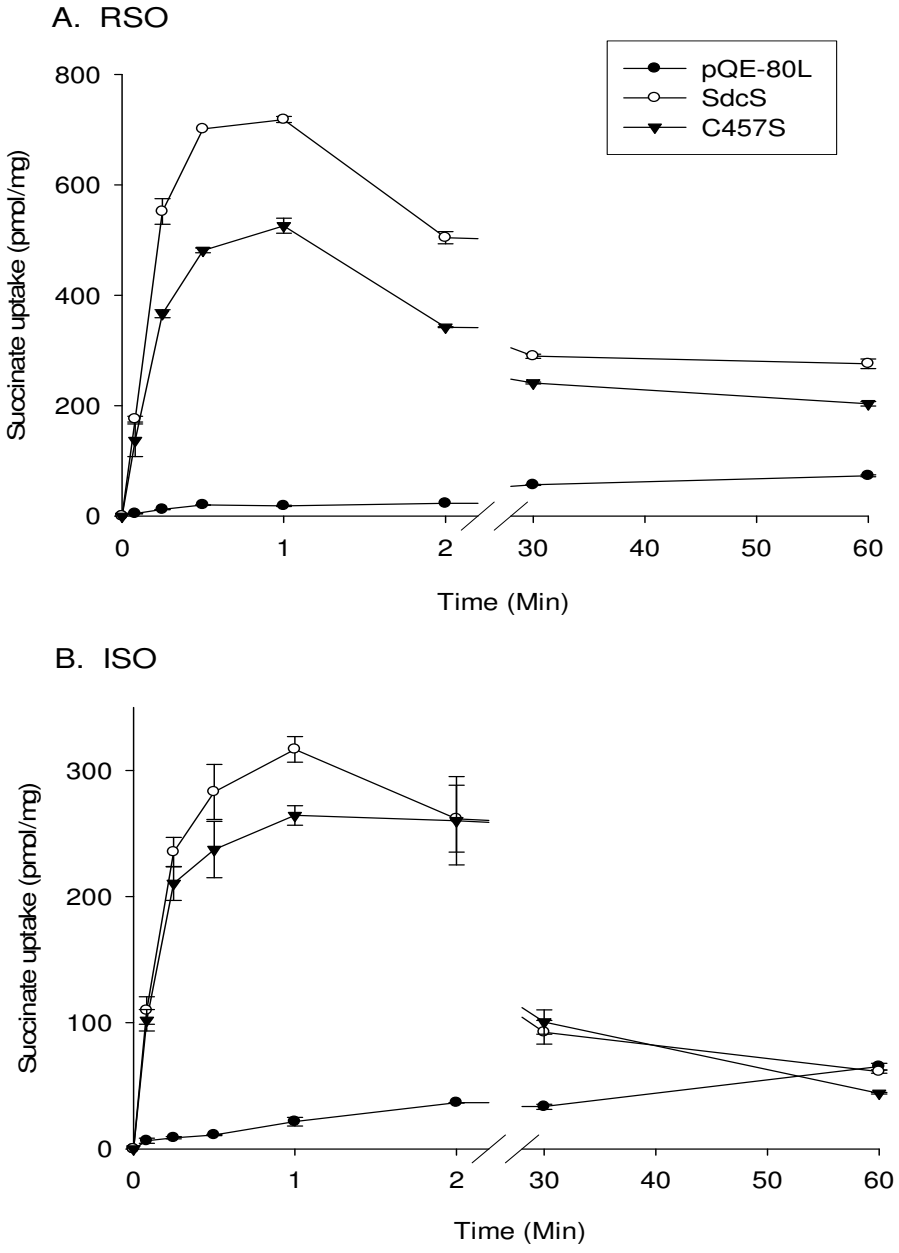


**Figure 4.1** Time course of succinate uptake by SdcS right-side-out and inside-out membrane vesicles. Uptake of 40 μM $^{14}$C-succinate was measured in the presence of transport buffer containing 10 mM $Na^+$ by (A) right-side-out (RSO) and (B) inside-out (ISO) membrane vesicles of E. coli (BL21 strain) housing either pQE-80L, SdcS or cysteineless mutant, C457S. Results are presented as mean ± range (n = 2 samples from same vesicle preparation).

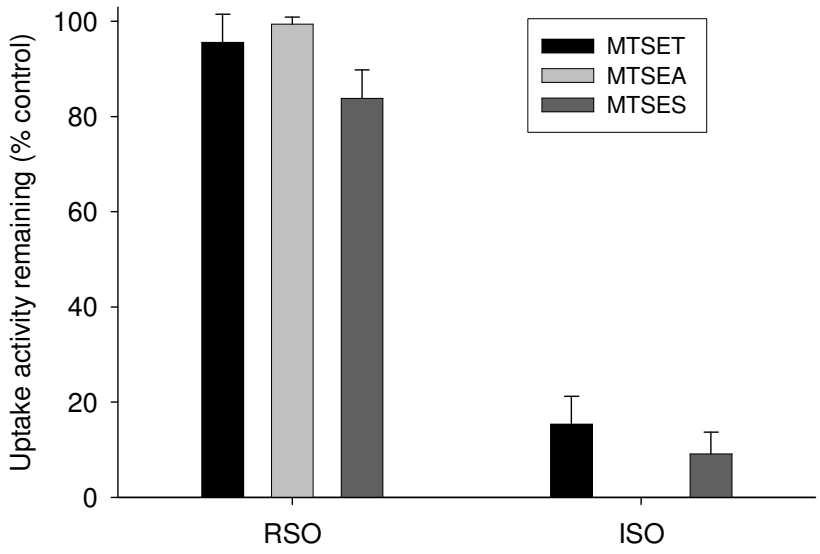


**Figure 4.2** Effect of methanethiosulfonate reagents on succinate uptake by SdcS in right-side-out (RSO) and inside-out (ISO) membrane vesicles. Vesicles were preincubated with 1 mM methanethiosulfonate reagents (MTSET, MTSEA and MTSES) in $Na^+$ containing buffer or with $Na^+$ buffer alone (control) for 10 min. Transport activity of 40 µM $^{14}C$-succinate was measured by right-side-out and inside-out vesicles with 10 sec. incubation in 10 mM $Na^+$ containing buffer. Uptake activities in vesicles preincubated with methanethiosulfonate reagents are expressed as a percentage of the uptakes in vesicles pretreated with $Na^+$ buffer alone. Bars represents mean ± range (n = 2).

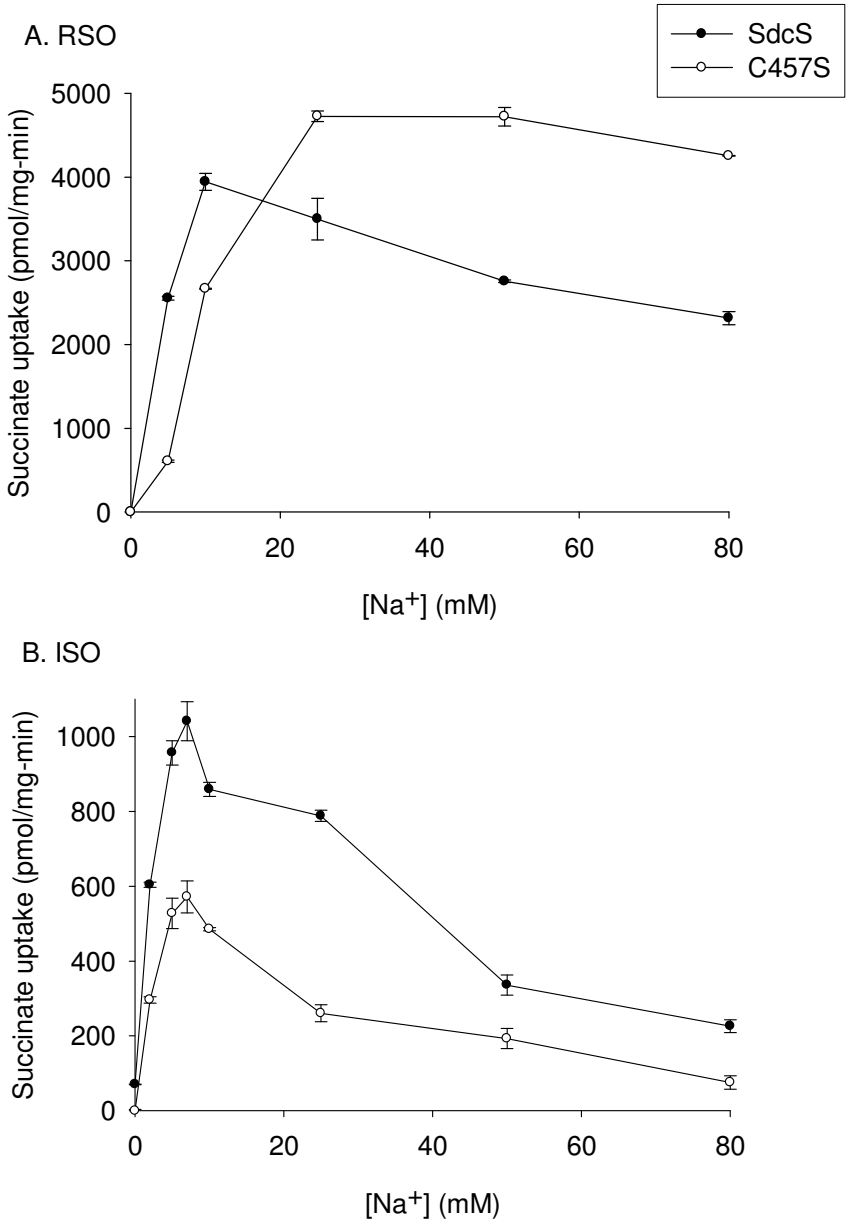


**Figure 4.3** $Na^+$-activation of succinate uptake. The transport of 40 µM $^{14}C$-succinate was measured by (A) right-side-out and (B) inside-out vesicles for 10 sec. in an assay buffer containing 0-80 mM $Na^+$ ($Na^+$ was replaced by choline). Results are shown as the mean ± range (n = 2 samples from same vesicle preparation).

| | 84 | 373 | 493 |
|---|---|---|---|
| rbNaDC1 | LEYL**K**DTNV | VMVS**D**GSAS | ILAS**M**AQAI |
| SdcS | SEYG**N**DIIF | SSVA**D**GTIA | ILAT**L**SVAV |
| | 108 | 329 | 436 |

**Figure 4.4** Sequence alignment of rabbit NaDC1 with SdcS. The sequence alignment was obtained by ClustalW2 (EMBL–EBI) with default parameters using Gonnet matrix. Amino acids of SdcS in bold letters indicate amino acids that were substituted with cysteines.

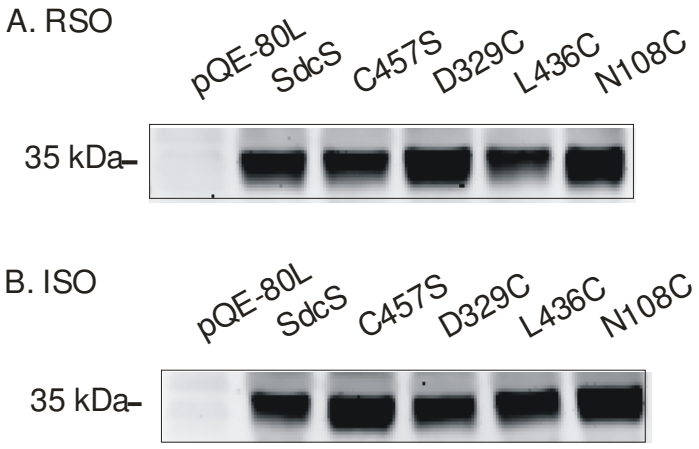


**Figure 4.5** Western blot of right-side-out (RSO, panel A) and inside-out membrane vesicles (ISO, panel B) expressing pQE-80L, SdcS, cysteineless C457S, N108C, D329C and L436C. Each lane contained 25 µg of protein. Protein was detected by using RGS-His antibody (Qiagen) a monoclonal antibody against the N-terminal histidine tag. The position of SdcS base on molecular mass standard is indicated in the first lane of each blot.

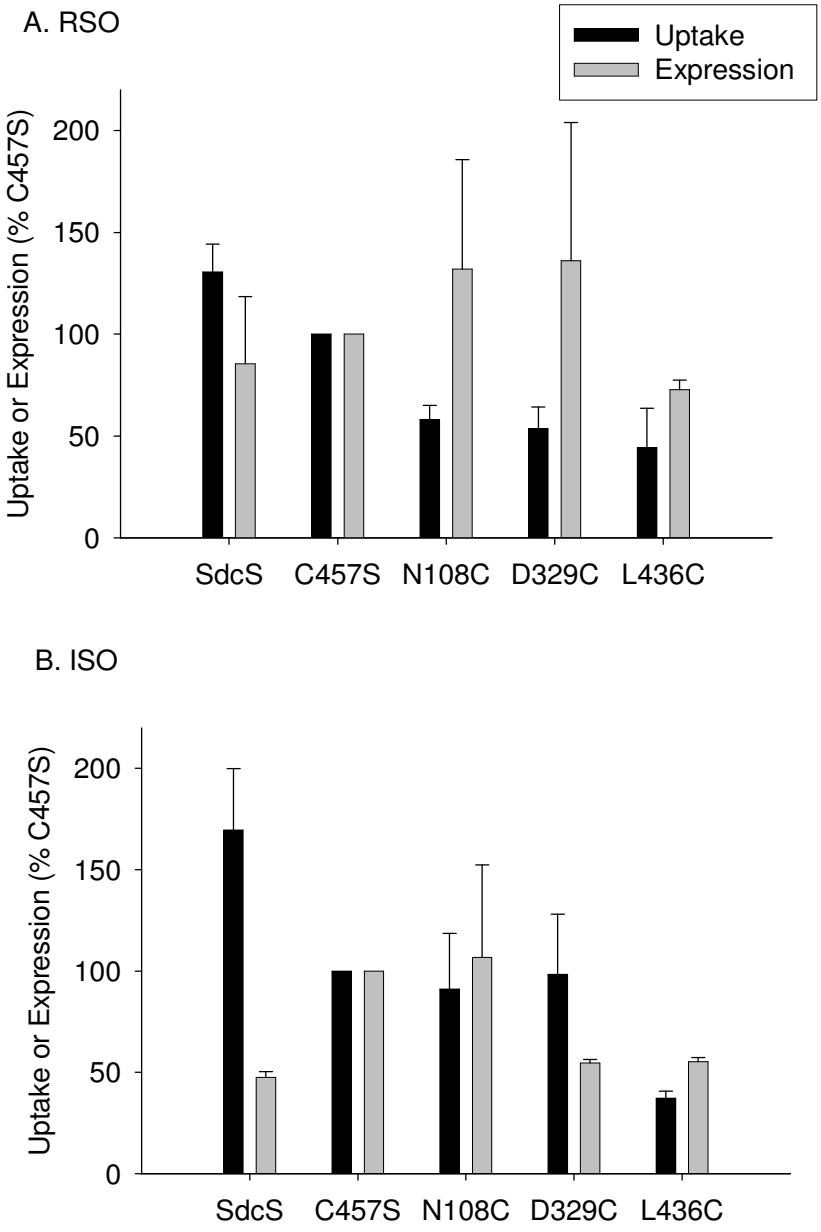


**Figure 4.6** Activity and expression of (A) right-side-out and (B) inside-out membrane vesicles. The activity and the protein expression of the mutant vesicles are shown as a percentage of cysteineless C457S. Transport activity of 40 µM $^{14}$C-succinate was measured for 10 sec. in assay buffer containing 10 mM $Na^+$. Transport results for the mutants are mean ± SEM (n = 3). Protein expression was determined by quantitating the intensities of SdcS vesicle protein bands from Western blots (such as in Figure 5) using Image 1D analysis software. Bars represents mean ± range (n = 2 separate blots).

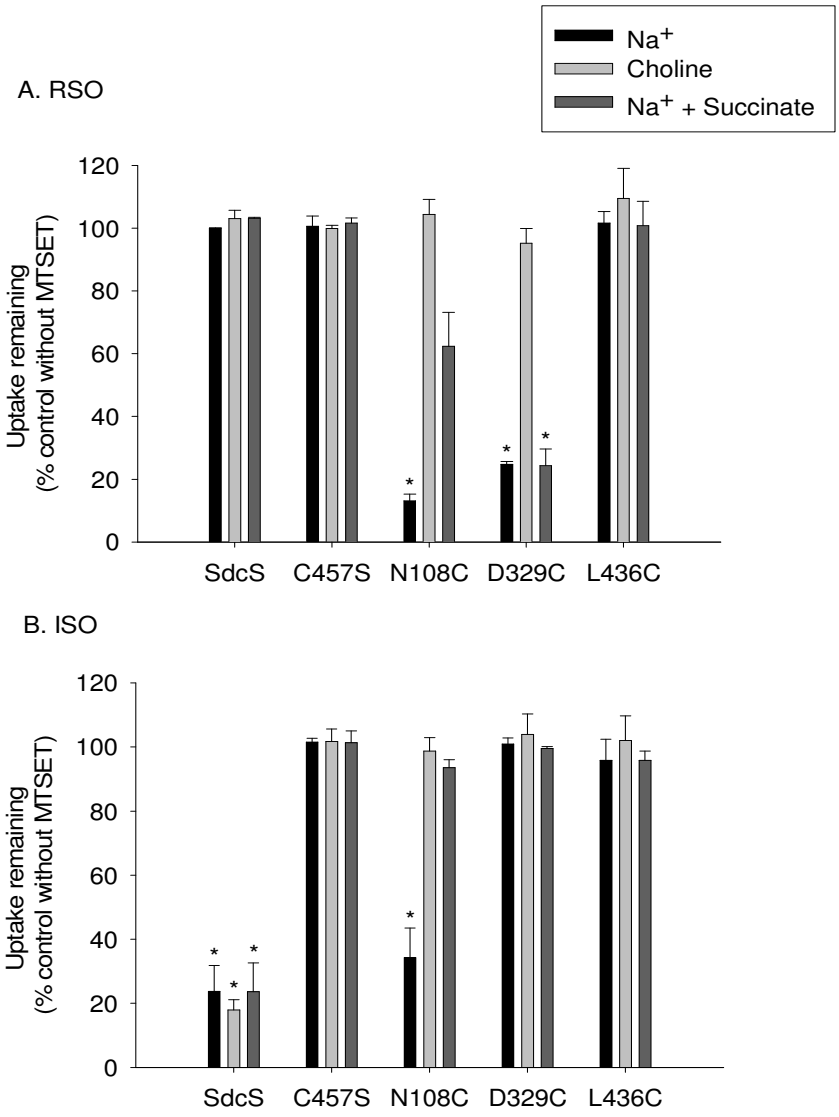


**Figure 4.7** Effect of MTSET on succinate transport by cysteine-substituted SdcS mutants. (A) Right-side-out and (B) inside-out vesicles of cysteine-substituted mutants were preincubated for 10 min. with $Na^+$, choline or $Na^+$ + 10 mM succinate buffers with 1 mM MTSET or without MTSET (control). At the end of preincubation time, transport activity of 40 µM $^{14}$C-succinate was measured for 10 sec. in assay buffer containing 10 mM $Na^+$. Uptake activities in vesicles preincubated with MTSET are shown as a percentage of the uptake control vesicles pretreated with the same buffer without MTSET. Bars represents mean ± SEM (n = 3 separate experiments). *, significant difference compared with control (without MTSET), $p < 0.05$.

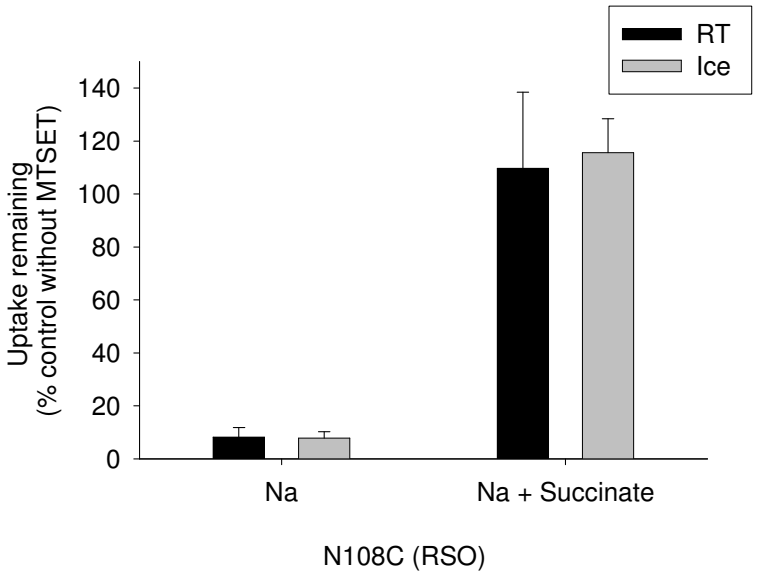


**Figure 4.8** Temperature dependence of MTSET labeling. N108C mutant in right-side-out membrane vesicles was preincubated in $Na^+$ buffer with or without 10 mM succinate and with or without 1 mM MTSET. The preincubations were done at room temperature (RT) or on ice for 10 min. After the preincubation, uptake of 40 μM $^{14}$C-succinate was measured as described previously. Data shown are mean ± range (n = 2 separate experiments).

## DISCUSSION

The aim of this study was to characterize SdcS, identify conformationally sensitive residues in SdcS and understand the mechanism of transport of succinate by $Na^+$/dicarboxylate cotransporters using SdcS as a model. In this study an attempt was made to identify and characterize residues in the transporter which are accessible from both the sides of the membrane. The major finding of this study was that residue Asn-108 is accessible from the outside as well as inside the cell in presence of $Na^+$ but not in absence of $Na^+$ thus suggesting conformational changes in the transporter depending on presence or absence of $Na^+$ or substrate.

To understand the transport mechanism of NaDC we used the bacterial homolog of NaDC, SdcS from *Staphylococcus aureus*. Bacterial homologs of eukaryotic transporters have been used previously to study structural and functional details of eukaryotic transporters. $Na^+/Cl^-$ dependent neurotransmitter transporters from *Aquifex aeolicus* have provided information about structure, substrate binding site as well as mechanism of transport by eukaryotic neurotransmitter transporters (*19;134*). TnaT from *Symbiobacterium thermophilum* have shown structural arrangement of the putative helices and had provided valuable structural information about neurotransmitter: sodium symporters (NSS) (*135*). Previous studies with astroglial glutamate transporter, GLT-1 and its homolog GltT from *Bacillus stearothermophilus* showed similar structural details. Both transporters contain a substrate sensitive reentrant loop (*136;137*) which played a crucial role in function of the glutamate transport. Crystal structure of glutamate transporter from *Pyrococcus horikoshii* played an important role in further understanding eukaryotic glutamate transporter structure (*17*). Previous studies have also used a gab permease (GabP)

which transports 4-aminobutyrate (GABA) across the *E. coli* plasma membrane as a model transporters to study its mammalian counterparts and have identified consensus amphipathic region within transmembrane helix 8 and the adjoining cytoplasmic loop (loop between TM8 and 9) which plays a significant role in the recognition and the translocation of ligands (*138*).

In this study, the E. coli expression system was used to functionally characterize SdcS from *Staphylococcus aureus* in right-side-out and inside-out membrane vesicles. For SdcS in RSO and ISO vesicles, succinate transport was time dependent with an overshoot observed at 1 min. Transport was also $Na^+$ dependent with an activation of transport by sodium at low $Na^+$ concentrations but an inhibition of succinate transport with increased $Na^+$ concentration. These results are consistent with the results from previous transport experiments conducted in whole cells (*29*). Our data show that SdcS in RSO vesicles has a $K_m$ for succinate of about 26 μM whereas the $K_m$ for succinate in ISO vesicles was 36 μM. Therefore the succinate affinity was similar for forward and reverse reactions. The affinity of SdcS for succinate was found to be comparable with the high affinity human $Na^+$/dicarboxylate cotransporter 3 ($K_m$ for succinate 20 μM). It was seen that the maximum velocity of succinate transport for RSO vesicles was four times higher than ISO vesicles after taking consideration of protein expression. The $Na^+$/succinate cotransporter from rabbit renal brush-border membranes which indicates that the transport system was asymmetric as the $V_{max}$ for the succinate influx was three times higher than that for efflux (*139*). The kinetic studies with rabbit renal brush-border membranes showed that the $K_m$ for influx and efflux were similar (*139*). The RSO and ISO vesicle preparations were pure as tested by MTSEA.

Our data suggest that residue Asn-108 is accessible from both sides of the membrane. Asn-108 from SdcS showed sensitivity to MTSET in the presence of $Na^+$ only and not in absence of $Na^+$. N108C also showed a substrate protection due to steric hindrance by MTSET binding. Position Asn-108 corresponds to Lys-84 of rbNaDC1. Previous studies have suggested that Lys-84 is sensitive by chemical labeling with methanethiosulfonate reagent in presence of $Na^+$ (*72*). Lys-84 is likely to be located within the substrate binding pocket of NaDC1 (*72*). The lysine at position 84 is highly conserved in the NaDC1 members as well as in $Na^+$/sulfate and $Na^+$/citrate transporters (*72*). Lysine is a positively charged amino acid whereas SdcS contains asparagine which is a hydrophilic amide containing residue, smaller than lysine. It was expected that cysteine replacement of amide containing asparagine 108 should have had functional effect on the transporter if this residue was directly in contact with the substrate, but no change in the substrate affinity was seen. Therefore, this study indicates that Asn-108 is not involved in direct binding with succinate but its accessibility changes due to conformational changes in the transporter.

Various mechanisms have been proposed in membrane transporters for transport of substrates across the membrane (*21*). Lactose permease (LacY) and glycerol-3-phosphate (GlpT) both secondary transporters from major facilitator superfamily follow an alternating access mechanism for transport of substrates (*12;15*). In this model the transporter contains a single substrate binding site which is alternately accessible from both sides of the membrane. After substrate is bound from one side, conformational changes take place so that the transporter is now accessible from another side of the membrane. One of the consequence of alternating

access model is accessibility of the amino acids, which resides in the permeation pathway of the transporter, from outside and inside of the cell. Therefore an important test to support this model would be to identify residues that are accessible from both sides of the membrane in different conformational states. A number of recent studies in transporters have shown residues that are accessible from both sides of the membranes (*137;140-142*). In this study although Asn-108 is accessible from outside and inside the cell, it is accessible in the same conformational state of the transporter that is in presence of $Na^+$, unless more than one conformational state exists in Na. One explanation for the accessibility of Asn-108 in both RSO and ISO vesicles is that it is in a re-entrant loop. The re-entrant loop or pore–loop structure was observed in GltT, glutamate transporter from *Bacillus stearothermophilus* where residues Ser-269, Ser-270 and Glu-271 were accessible from both sides of the membrane and were part of the reentrant loop which plays important role in substrate transport (*137*). Similarly in the $Na^+/Ca^+$ exchanger residues Asn-125 and Asp-825 were accessible from outside and inside and were also a part of a reentrant loop (*141*). Asn-108 could be exposed alternately to the inside and outside of the cell by tilting or twisting of TM3 (Figure 9B). The secondary structure model of SdcS based on rbNaDC1 model (*64*) predicted Asn-108 to be a part of transmembrane helical structure inside the membrane and not in the extracellular or intracellular loops (Figure 4.9). The exact location of Asn-108 can only be understood by knowing the three dimensional structure of SdcS at atomic resolution.

Cysteine-substitution at Leu-436 which corresponds to Met-493 of rbNaDC1 showed no sensitivity towards MTSET indicating that residue Leu-436 is either not accessible from either outside or inside the cell or the labeling with MTSET does not

have any effect on succinate transport. Only hydrophobic residues methionine or leucine was observed at that position when multiple alignment of SLC13 gene was carried out (*70*). Surprisingly right-side-out membrane vesicles of L436C showed four times higher $K_m$ than cysteineless SdcS right-side-out vesicles as well as than L436C inside-out vesicles, indicating lower affinity for succinate. The succinate transport activity and $V_{max}$ of mutant L436S right-side-out vesicles was greatly reduced. Therefore, it is likely that Leu-436 might be a crucial residue for transport in forward direction.

Mutant D329C showed accessibility to MTSET in the presence of $Na^+$ in RSO vesicles only. The aspartic acid residue is conserved in the SLC13 gene family. This residue was not accessible from inside nor showed differences in kinetic parameters. Secondary structure model place this resides in the extracellular side of the helix explaining its accessibility from the outside only (Figure 4.9).

Taken together, the present work represents the characterization of SdcS from outside as well as from inside the cell using bacterial expression system. The asymmetry in the transport and kinetic difference is due to transport velocity of the substrate rather than substrate affinity. This study indicates that residue Asn-108 is highly accessible from both sides of the membrane in presence of $Na^+$ and its accessibility decreases with the addition of substrate or replacement of $Na^+$ indicating that accessibility of Asn-108 changes with conformational state of the transporter. Our data also indicate the possibility that Asn-108 resides in a re-entrant loop. Residue Leu-436, although not conformationally sensitive, might be functionally important whereas sensitivity of mutant D329C to MTSET inhibition was in presence of $Na^+$ only. In conclusion, this study shows the common structural framework on

which SdcS and other SLC13 family transporters are based. This work further indicates that structural as well as functional knowledge acquired from bacterial transporter studies can be applied to their eukaryotic homologs.

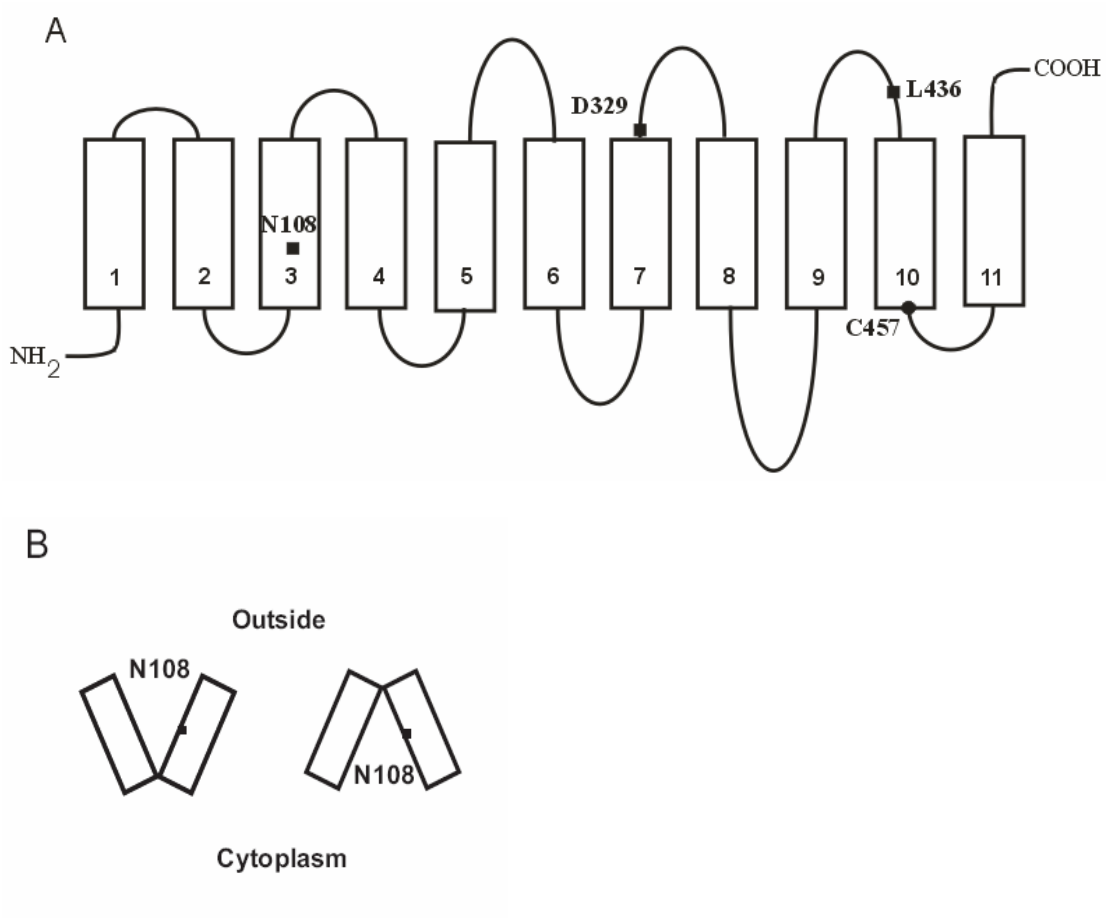


**Figure 4.9** (A) Secondary structure model of SdcS. The model was constructed by using rbNaDC1 model (*64*). The location of single cysteine mutated to construct cysteineless, C457S was shown in filled black circle and positions of three cysteine-substituted mutants in C457S namely N108C, D329C and L436C are shown in filled black squares. (B) Model showing potential exposure of Asn-108 to cytoplasmic or extracellular water filled cavity in different conformational states.

# CHAPTER 5: IDENTIFICATION OF DETERMINANTS OF CITRATE BINDING AND TRANSPORT IN THE BACTERIAL $Na^+$/DICARBOXYLATE SYMPORTER USING A RANDOM MUTAGENESIS APPROACH

## INTRODUCTION

Previous studies have used site-directed mutagenesis to identify structurally and functionally important amino acids in NaDC1 transporter (*69-73;75;115*). In this study a different approach was used to identify functionally important amino acids by randomly changing the wild-type DNA sequence of the transporter. This was achieved by using a random mutagenesis approach to design variants of transporter (*143*). The library of random mutants was selected for the desired function using a biochemical selection system. Random mutagenesis has been used extensively to develop vaccines (*144*), therapeutic proteins (*145*) and to elucidate structure-function relationships of various proteins such as aminoacyl-tRNA synthetase ribozymes (*146*), alkaline phosphatase (*147*), STRA6–a high affinity membrane receptor for plasma retinol binding protein (*148*), and fungal peroxidase (*149*). Therefore, random selection permits isolation of proteins with novel properties that would otherwise be difficult to obtain by conventional mutagenesis.

The $Na^+$/dicarboxylate cotransporter, NaDC1, is found on the apical membrane of the epithelial cells of the renal proximal tubule and in the small intestine (*34;35*). NaDC1 carries a broad range of divalent anion substrates including dicarboxylates, such as succinate and α-ketoglutarate, and protonated tricarboxylates, such as citrate$^{2-}$ (*35*). Recently a $Na^+$-coupled dicarboxylate transporter from

*Staphylococcus aureus*, $Na^+$/dicarboxylate symporter (SdcS) was cloned which is ~ 41 % identical to rabbit NaDC1 and was functionally expressed in *E. coli* (*29*). SdcS transports succinate, fumarate, and malate but not citrate or α-ketoglutarate (*94*). In this study the SdcS sequence was randomly changed with the purpose of producing a mutant SdcS that transports citrate. Therefore, this study was an attempt to identify residues involved in citrate binding and transport.

Genetic modifications or mutations are important tools to design variants of proteins or proteins with new properties (*143*). Structural diversity of protein can be created *in vitro* by introducing random mutations in the wild-type DNA sequence. To construct a citrate transporting SdcS mutant random mutagenesis was carried out and the SdcS random mutants transporting citrate were selected by using biochemical selection assay. Simmons citrate agar contains citrate as the sole carbon source (*150*). Bacteria that grow on this agar express citrate transporters that allow them to take up citrate from the medium. Wild-type *E. coli* does not grow on this medium. Therefore, citrate agar was used as a selection medium to identify mutants of SdcS that transport citrate. Although colonies were seen on the selection agar plates none of the mutants showed significant $^{14}$C-citrate transport activity. Though we do not know the precise reason for this growth, one of the possibilities is that these mutant transporters might be indirectly involved in activating endogenous citrate transporters in *E. coli* therefore growing on citrate selection plates. This study was discontinued at this point.

## MATERIALS AND METHODS

### Site-directed Mutagenesis

Site-directed mutagenesis of SdcS was performed in the same way as described in Chapter 2.

### Random Mutagenesis and Screening of Citrate Transporter

Random mutagenesis was performed by using GeneMorph® II Random Mutagenesis Kit (Stratagene). The general random mutagenesis approach is shown in Figure 5.1. The full-length SdcS was first amplified to introduce random mutations using error prone PCR with Mutazyme II DNA polymerase. These purified PCR products served as mega primers that annealed with the original donor plasmid (SdcS/pQE-80L) and extended by PCR reaction using a specialized high-fidelity enzyme mix. The denaturation temperature was 95°C whereas 60°C was used for annealing. The extension was carried out at 68°C. The restriction enzyme *Dpn*I was used to digest the unmutated donor plasmid DNA (wild-type SdcS/pQE-80L). The random mutants were transformed into DH5α ($F^-$ endA1 recA1 relA1 gyrA96 Φ80d*lac*ZΔM15 Δ(lacZYA-argF)U169, hsdR17($rK^-$ $mK^+$), $\lambda^-$), BL21 [$F^-$ ompT $hsdS_B(r_B^-$ $m_B^-)$ gal dcm] or XL10-Gold (endA1 recA1 relA1 Hte lac $Tet^R$ Amy $Cm^R$)]) strains of *E. coli*. Initially XL10-Gold strain was used for transformation of random mutants as XL10-Gold exhibits the Hte phenotype for high transformation efficiency and provides robust growth to produce larger colonies (*151*). None of the colonies of XL10-Gold with random mutants showed any citrate transport and therefore later *E. coli* strain DH5α was used for transformation of random mutants

In the random mutagenesis reaction, the mutation frequency can be controlled by adjusting the initial target DNA amounts in the amplification reaction. For the same PCR yield, targets amplified from low amounts of target DNA undergo more amplifications than high amounts of target DNA. The more amplification means more replications of target DNA causing more errors. Therefore, low mutation frequency was achieved (0-4.5 mutations/kb of DNA) by using 500-1000 ng of target SdcS. The medium mutation frequency (4.5-9 mutations/kb) was achieved by using 100-500 ng SdcS whereas high mutation frequency (9-16 mutations/kb) was achieved by using 0.1-100 ng of initial target SdcS. Error prone Mutazyme II DNA polymerase also exhibits less mutational bias than other error prone polymerases.

After the random mutagenesis reactions, transformed *E. coli* were plated on Simmons citrate agar (Simmons citrate agar, 50 µg/ml ampicillin, 100 µM IPTG, 12 µM thiamine pH 7). Plates were incubated for 48 hours at 30˚C. Bacteria were first plated on LB-ampicillin plates, without selection, and later approximately 1 x $10^6$ colonies were screened on the Simmons citrate selection agar. Colonies that grew on Simmons agar plate were then streaked on another Simmons citrate agar plate in a grid-format. Transport assays were then carried out to confirm citrate transport activity. To identify α-ketoglutarate transporting SdcS mutants 1 mM α-ketoglutarate was added to Simmons citrate agar and transport activity was checked with $^{14}$C-α-ketoglutarate transport assays.

**Whole cell Transport Assays**

Overnight cultures of mutants selected from Citrate agar plates were used to inoculate 50 ml Luria–Bertani broth containing 50 µg/ml ampicillin. Cells were grown with shaking 280 rpm at 37°C until optical density at 660 nm was 0.4–0.6 (approximately 2 hrs.). Protein synthesis was induced with addition of IPTG. 150 µM IPTG was used to induce SdcS/pQE-80L and the random mutants whereas for the positive control CitT/pSE380 (*152*)1 mM IPTG was used. The optimal concentration of IPTG was determined from previous studies. Cells were grown for an additional 2 to 3 hrs, harvested by centrifugation and washed twice and resuspended in assay buffer (Na buffer: 5 mM NaCl, 95 mM choline chloride, 50 mM MOPS pH 7 or Choline buffer: 100 mM choline chloride, 50 mM MOPS pH 7). The final optical density of the cells at 660 nm was at around 7. All the samples were at the same optical density. For the transport assay, 90 µl of cells were placed at the bottom of the polystyrene test tube (Falcon). 10 µl of 5 mM Na containing assay buffer with 10 µM $^{14}$C-succinate, $^{14}$C-citrate or $^{14}$C-α-ketoglutarate was placed on the side of the tube near the cells. The transport reaction was initiated by vortexing and stopped after 4 min. with addition of 1 ml ice cold choline buffer, filtered immediately through Millipore filters (0.45 µm pore size, type HAWP) and washed with 4 ml of ice-cold choline buffer. The radioactivity retained on the filter paper was measured by liquid scintillation counter (Packard Tri-Carb 2100 TR).

**Preparation of right-side-out vesicles and transport assays**

Preparation of right-side-out (RSO) vesicles and transport assay in RSO vesicles were performed in the same way as described in Chapter 4. For the transport

assay 40 µM of $^{14}$C-succinate, $^{14}$C-citrate and $^{14}$C-α-ketoglutarate was used. The $Na^+$ and choline buffers used were same as described in Chapter 4.

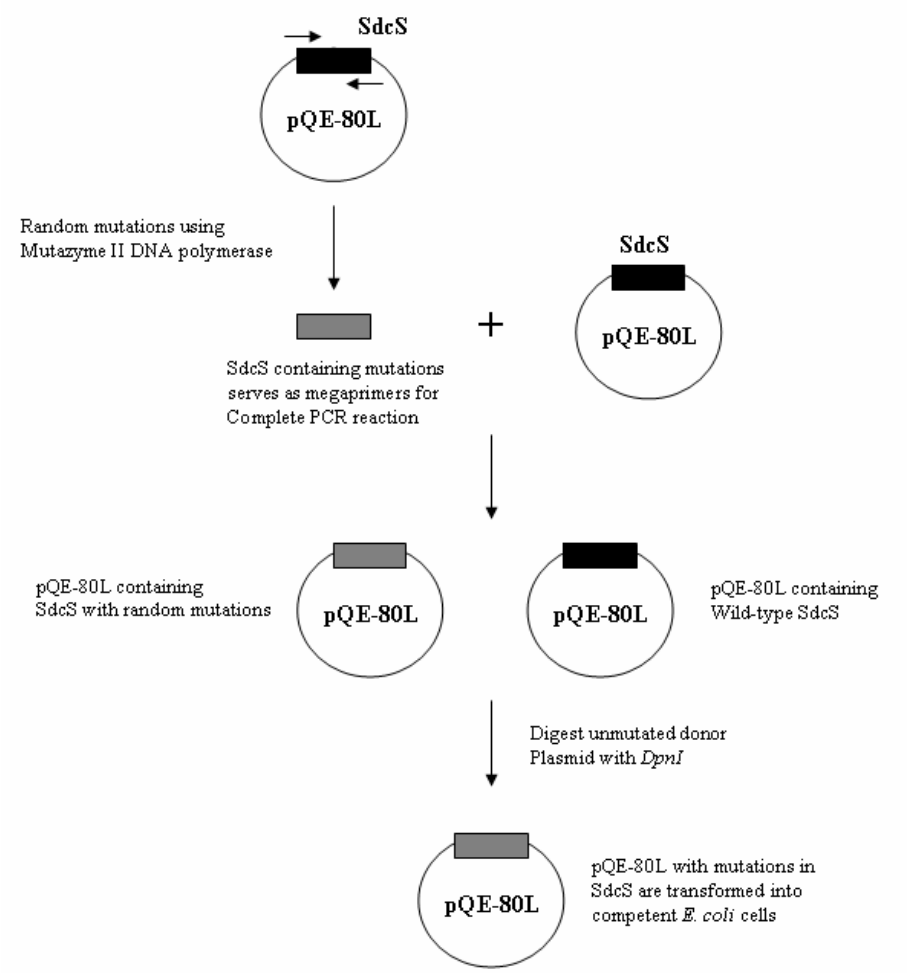


**Figure 5.1** The random mutagenesis approach using the GeneMorph II EZClone kit (Stratagene). This procedure was done in two steps. First, random mutations were introduced in the SdcS cDNA using the error-prone DNA polymerase, Mutazyme II DNA polymerase. The second step involved making the mutant DNA and vector in a megaprimer PCR reaction. DpnI was used to digest the unmutated SdcS (modified from www.stratagene.com)

## RESULTS

### Random Mutagenesis of SdcS to Identify Determinants of Citrate Binding

To identify residues that could be involved in citrate binding and transport in $Na^+$/dicarboxylate symporter (SdcS), random mutagenesis experiments were conducted. Wild-type SdcS transports succinate but not citrate. A citrate/succinate antiporter (CitT) which transports citrate was used as a positive control. Simmons citrate agar was used as a selection media, which contains citrate as the only source of carbon. *E. coli* transformed with wild-type SdcS did not transport citrate and would not grow on these plates whereas E. coli expressing CitT, which transports citrate, grew on the plates producing a change in the pH that changed the color of the agar from green to blue. Three different strains of *E. coli*, DH5α, BL21, and XL10-Gold containing wild-type SdcS were tested for their growth on Simmons citrate agar plates. None of the strains containing SdcS grew on the plates indicating the SdcS does not transport and utilize citrate.

SdcS was subjected to random mutagenesis producing a library of SdcS random mutants. 1 µg initial SdcS was subjected to random mutagenesis with error prone PCR reaction using Mutazyme II DNA polymerase. Another reaction was carried out using 100 ng initial target SdcS to achieve high mutation frequency. 1 µl of SdcS random mutants were transformed into 40 µl of electrocompetent XL10-Gold *E.coli* strain. After the transformation, 1 ml of SOC medium with XL10-Gold strain containing mutant SdcS was spread on the Simmons citrate agar plates (24 cm X 24 cm, 250 µl on each plate, 4 plates total). After 48 hours of incubation colonies that appeared on the initial plate were picked and streaked on Citrate agar plates with numbered grids. Whole cell preparations were made from the mutant colonies 2, 4

and 5 with low mutation frequency (L) and 1, 2 and 4 with high mutation frequency (H) and tested for $^{14}$C-citrate transport. None of the random mutants showed any citrate transport (Figure 5.2).

SdcS was again subjected to random mutagenesis producing a library of SdcS mutants. Initial SdcS amount used was 1 µg and 8 fold amplification was achieved with error prone PCR reaction using Mutazyme II DNA polymerase yielding low mutation frequency (0-4.5 mutations/kb). Another reaction to achieve high mutation frequency was carried out using 100 ng initial target SdcS. As previous transformation of random mutants into XL10-Gold was unable to determine citrate transporting mutants for this experiment a *E. coli* DH5α strain was used for transforming random mutants. After the transformation using electroporation, 1 ml of SOC medium with DH5α strain containing mutant SdcS was spread on the Simmons citrate agar plates (24 cm X 24 cm, 250 µl on each plate, 4 plates total). After 48 hours of incubation, 45 colonies were seen on the Simmons citrate agar plates. Colonies that appeared on the initial plate were picked and streaked on citrate agar plates with numbered grids. Whole cell preparations were made from the mutant colonies 1, 2, 3, 4 and 5 with low mutation frequency (L) and 1, 2 and 4 with high mutation frequency (H) and tested for $^{14}$C-citrate transport. None of the random mutants showed any citrate transport (Figure 5.3B). The control citT transport showed no succinate uptake but showed citrate uptake whereas the wild-type SdcS showed the succinate transport but no citrate transport. The original succinate transport activity was also lost in majority of the random mutants except in L3 and L4 (Figure 5.3A). Random mutant H1 showed reduced succinate transport activity but no citrate uptake.

**Random Mutagenesis of SdcS Mutants, SdcS-MASN and SdcS-LASS to Identify Determinants of Citrate binding**

Because none of the SdcS random mutants showed citrate transport, a directed evolution approach was used. Directed evolution requires various rounds of mutations to optimize a particular function, in this case citrate binding and transport. Previous studies with rbNaDC1 indicate that residue Ser-512 is a determinant of citrate and succinate transport (*76*). As discussed in Chapter 4, SdcS and rbNaDC1 have similar structural characteristics. Alignment of rbNaDC1 and SdcS amino acid sequences shows that residue Ala-455 of SdcS corresponds to Ser-512 of rbNaDC1. The single mutant A455S was constructed in SdcS and was designated as SdcS-MASN. This mutagenesis has added a single serine in SdcS which might promote the citrate transport. SdcS-MASN was used as a template for further random mutagenesis which will yield the library of SdcS random mutants possibly with increased citrate affinity. Using SdcS as a template another mutant was constructed and designated as SdcS-LASS. SdcS-LASS contain three mutations M453L, A455S and N456S which might promote the citrate transport (Figure 5.4). SdcS-LASS was also subjected to another round of random mutagenesis to yield mutant transporter with increased citrate affinity. Mutagenesis reactions with low, medium and high mutation frequency were made in SdcS-MASN and SdcS-LASS using DH5α as a host *E. coli* strain. DH5α was used as a host *E. coli* strain as no citrate transport was observed previously when random mutants were transformed into XL10-Gold. After the transformation using electroporation, 1 ml of SOC medium with DH5α strain containing mutant SdcS-MASN and SdcS-LASS was spread on the Simmons citrate agar plates (24 cm X 24

cm, 250 µl on each plate, 4 plates total) and screened for the random mutants transporting citrate. Whole cell preparations of random mutants were made and were tested for $^{14}$C-citrate transport. The parental transporters showed no succinate or citrate transport indicating that the parental transporters were inactive. No citrate transport was seen in any of the random mutants of SdcS-MASN or SdcS-LASS (Figure 5.5).

**Random Mutagenesis of SdcS to identify Determinants of Citrate and α-Ketoglutarate Binding**

Another experiment of SdcS random mutagenesis was conducted using 120 ng initial SdcS amount as a template to yield high mutation frequency. The 41-fold amplification was achieved. The wild-type SdcS does not transport any citrate as well as α-ketoglutarate. *E. coli* transformed with SdcS random mutants were plated on Simmons citrate agar supplemented with 1 mM α-ketoglutarate as selection medium. As before, a total of 1 ml of transformation solution was plated on 4 plates (24 cm X 24 cm, 250 µl on each plate). The α-ketoglutarate was chosen due to structural similarity between succinate and α-ketoglutarate and SdcS random mutants might have preference for binding and transport of α-ketoglutarate than citrate. Out of 95 colonies that were able to grow on the selection medium, 16 were tested in right-side-out (RSO) membrane vesicles for $^{14}$C-citrate and $^{14}$C-α-ketoglutarate transport (Figure 5.6). None of the groups except 13 and 17 showed citrate transport activity even though mutants grew on selection agar plates (Figure 5.6B). *E. coli* expressing mutants 16, 17, 18 and 19 showed α-ketoglutarate transport (Figure 5.6C).

Figure 5.7 indicates time course of succinate and α-ketoglutarate transport by right-side-out membrane vesicles of *E. coli* BL21 cells harboring vector pQE-80L, SdcS, SdcS random mutants 17 and 19. The transport was measured in the presence of 10 mM $Na^+$ buffer. Vesicles expressing SdcS showed rapid accumulation of succinate followed by a slow fall. The succinate uptake was linear until 1 min. No measurable α-ketoglutarate transport was detected for SdcS or mutants 17 and 19. To confirm that there was no uptake of α-ketoglutarate by SdcS random mutants, $^{14}C$- α-ketoglutarate uptake was also checked for mutants 16 and 17 in $Na^+$ versus choline containing buffers. No uptake was seen in presence of 10 mM $Na^+$ containing buffer compared with that in choline buffer indicating none of the mutants were able to transport α-ketoglutarate (Figure 5.8).

The DNA sequences of SdcS mutants 16 to 20 were analyzed. All five sequences contained premature termination codons in different locations, suggesting that truncated transporters were produced. At this point the project was discontinued.

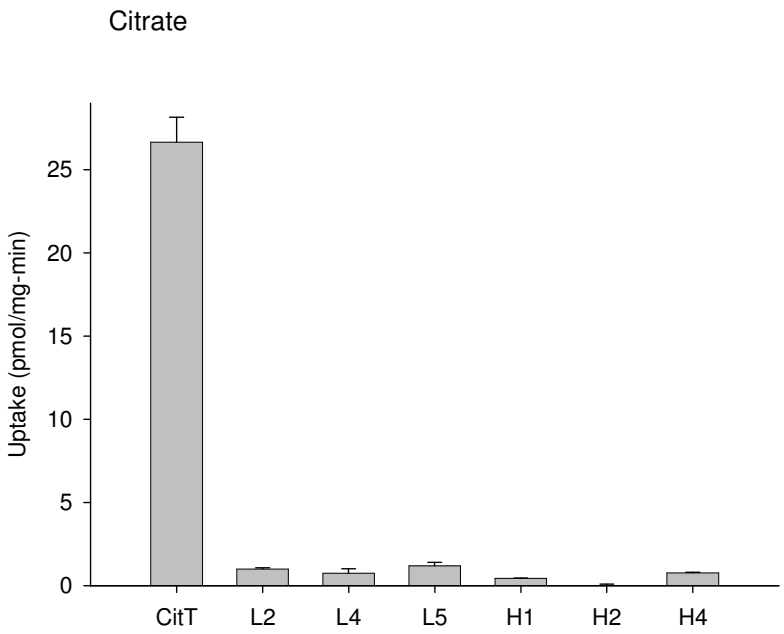


**Figure 5.2** Citrate transport activity of SdcS random mutants transformed into XL10-Gold strain of *E. coli.* Transport activity was estimated after 4 min. incubation of cells with 10 µM $^{14}$C-citrate with assay buffer containing 5 mM $Na^{+}$. Bars represents mean ± range (n = 2 whole cell samples from same preparation)

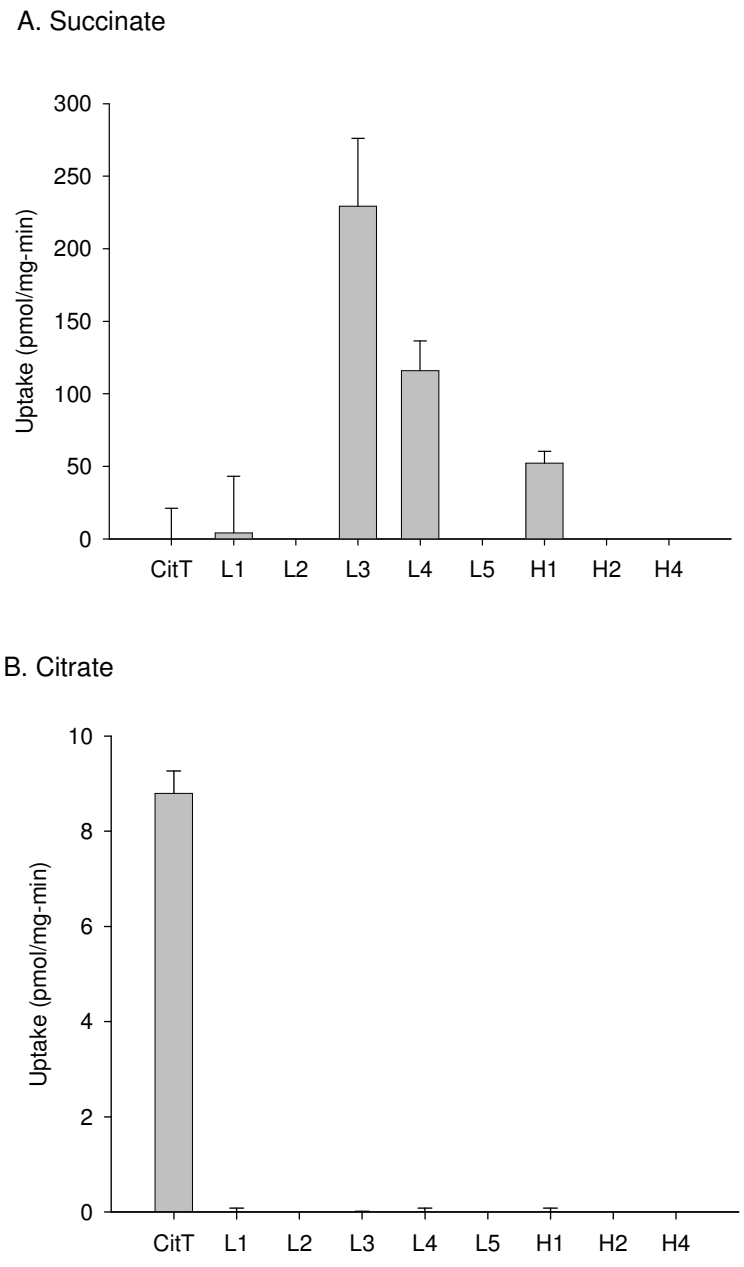


**Figure 5.3** Transport activity of SdcS random mutants transformed into DH5α strain of *E. coli*.Transport activity of SdcS random mutants. Transport activity was estimated after 4 min. incubation of cells with 10 µM (A) $^{14}$C-succinate or (B) $^{14}$C-citrate with assay buffer containing 5 mM $Na^+$. Bars represents mean ± range (n = 2).

```
                    510   513
rbNaDC1             L A S S

                    453   456
SdcS                M A A N

SdcS-MASN           M A S N

SdcS-LASS           L A S S
```

**Figure 5.4** Sequence alignment of rabbit NaDC1 with SdcS. The sequence alignment was obtained by ClustalW2 (EMBL–EBI). Amino acids of rbNaDC1 are shown with bold. The Amino acids of SdcS mutants in bold letter indicates the amino acids that were substituted.

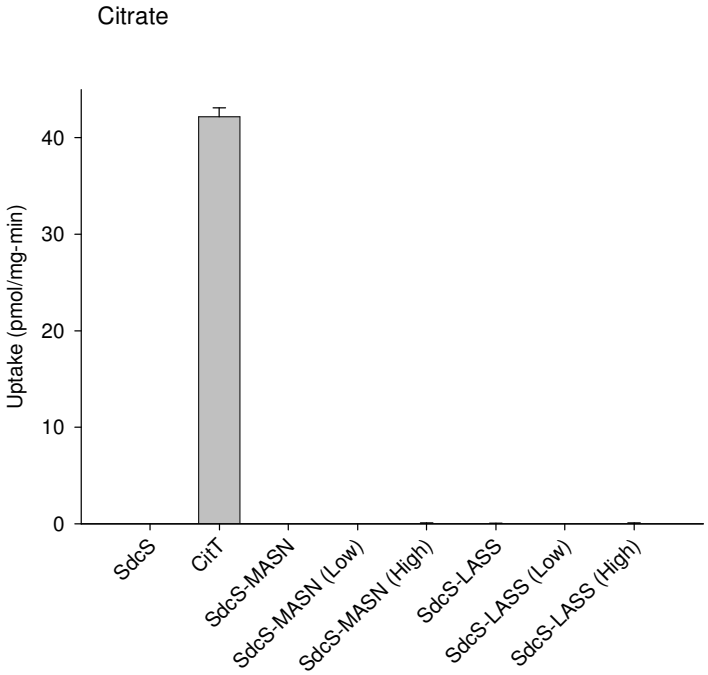


**Figure 5.5** Transport activity of SdcS random mutants. Transport activity of 10 µM $^{14}$C-citrate was measured after 4 min. incubation of cells with 5 mM $Na^+$ containing assay buffer. Bars represents mean ± range (n = 2 whole cell samples from same preparation).

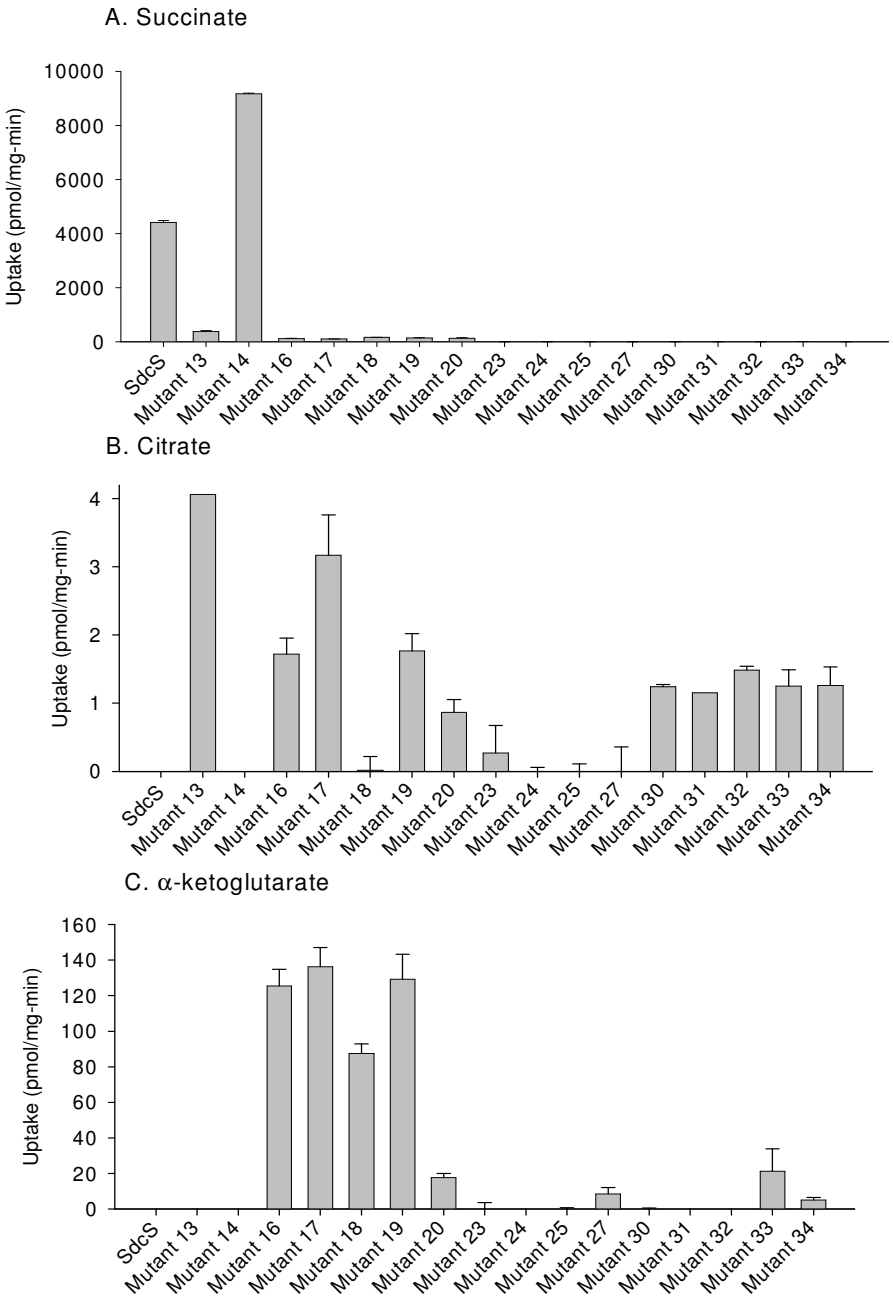


**Figure 5.6** Transport activity of SdcS and mutants (numbered 13-34) in right-side-out membrane vesicles of *E. coli* (BL21 strain). Transport activity of 40 μM (A) $^{14}$C-succinate, (B) $^{14}$C-citrate and (C) $^{14}$C-α-ketoglutarate was measured for 30 sec. in assay buffer containing 10 mM $Na^+$. Bars represents mean ± range (n = 2 RSO vesicle samples from same preparation)

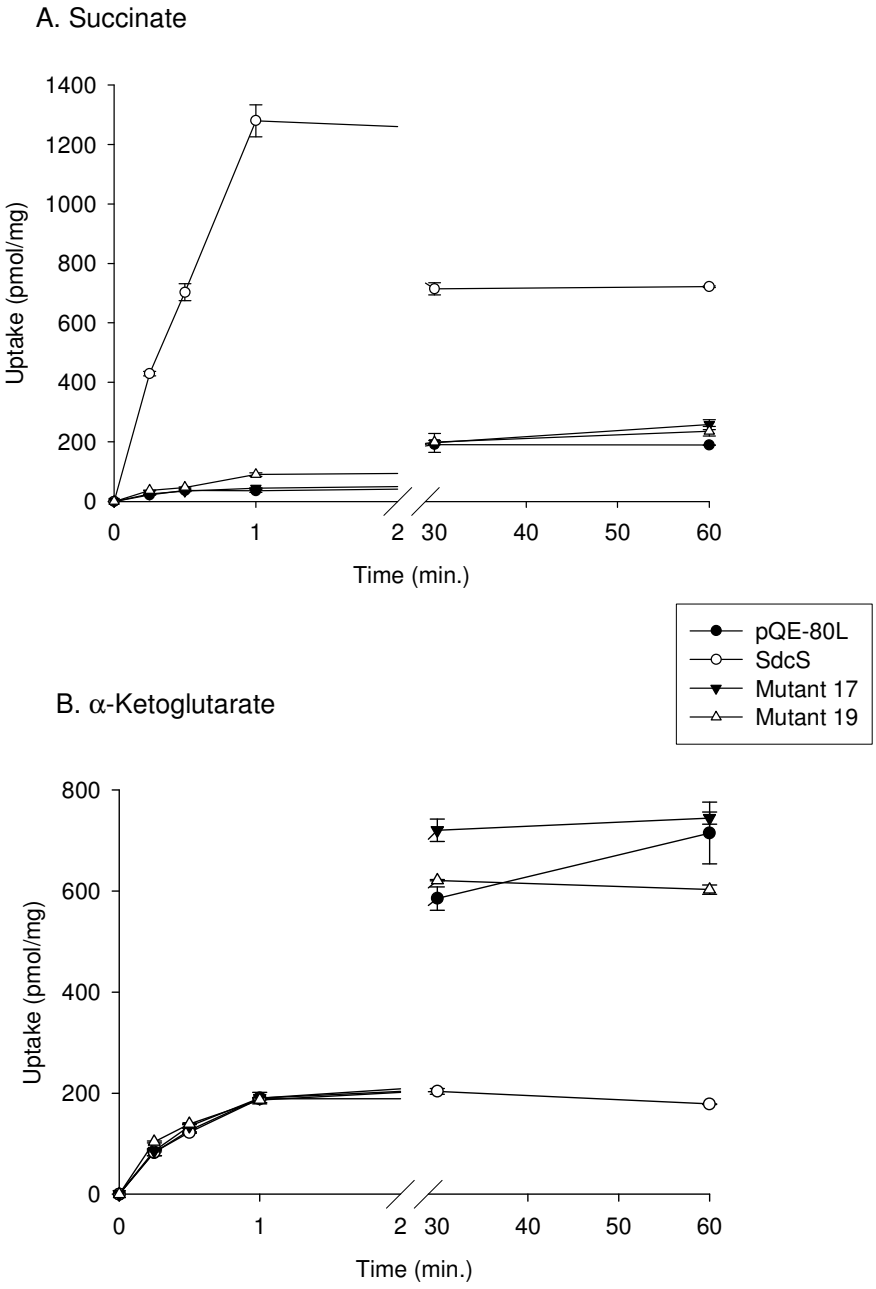


**Figure 5.7** Time course of succinate and α-ketoglutarate uptake by right-side-out membrane vesicles of *E. coli* (BL21 strain) housing pQE-80L, SdcS, SdcS random mutants 17 and 19. Uptake of 40 µM (A) $^{14}$C-succinate and (B) $^{14}$C- α-ketoglutarate was measured in the presence of transport buffer containing 10 mM $Na^+$. Results are presented as mean ± range (n = 2 independent experiments)

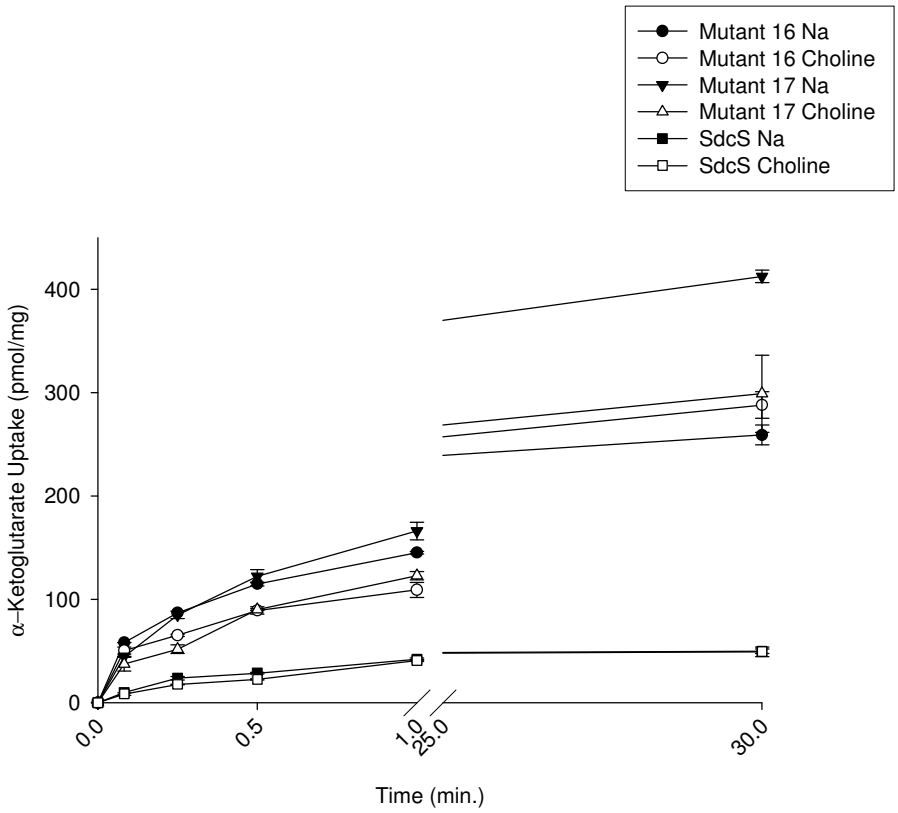


**Figure 5.8** Time course of α-ketoglutarate uptake by right-side-out membrane vesicles of *E. coli* (BL21 strain) housing SdcS, SdcS random mutants 17 and 19. Uptake of 40 μM $^{14}$C- α-ketoglutarate was measured in the presence of transport buffer containing 10 mM $Na^+$ or in absence of $Na^+$ containing buffer (buffer containing choline). Results are presented as mean ± range (n = 2 RSO vesicle samples from same preparation)

## DISCUSSION

In this study an attempt was made to identify amino acids that are important determinants of citrate binding in the SLC 13 family. The S*taphylococcus aureus* $Na^+$/dicarboxylate symporter (SdcS), which transports succinate but not citrate was subjected to random mutagenesis and selected on agar with citrate as the sole carbon source. The random mutants of SdcS were screened for their ability to transport citrate. Although the random mutant colonies grew on citrate selective Simmons citrate agar plates, none of the mutants showed radioactive citrate uptake. This indicates that the growth of the colonies on citrate agar was not because of citrate transport by the SdcS mutants and therefore we were unable to identify the amino acids involved in citrate transport.

Directed protein evolution is an important method to understand structure-function relationships of proteins. Conventional genetic or site-directed mutagenesis experiments have limitations with respect to frequency and diversity of the mutant proteins as it would be difficult to obtain interesting mutants that require more than one amino acid changes. On the other hand the random mutagenesis method can produce any possible amino acid change. There are various random mutagenesis methods available such as error prone PCR to achieve site-directed random mutagenesis, DNA shuffling, heavy metal and organic-solvent mediated PCR methods. The chemical random mutagenesis methods include deamination ($HNO_2$, $NaHSO_3$, $NH_2OH$ etc.), alkylation ($HNO_2$) or use of base-analog mutagens (5-bromouracil, 2-aminopurine). Other methods of achieving random mutagenesis are UV irradiation to randomly incorporate wrong nucleotides, using mutator strains (e.g. *E. coli* XL1 Red, stratagene) or applying environmental and physiological stress

(*143*). The random mutagenesis using GeneMorph® II Random Mutagenesis Kit has advantage as random mutations were only made in the target gene that is in the SdcS and the SdcS mutants were readily screened for citrate transport activity without a need of subcloning.

A recent study showed selective amino acid substitutions to convert creatine transporter to γ-aminobutyric acid transporter (*153*). As none of the SdcS random mutants showed any citrate transport a similar strategy was used in which a site-directed mutation at Ala-455 to serine was made in wild-type SdcS to construct SdcS-MASN and SdcS-LASS mutants. Previous studies with rabbit $Na^+$/dicarboxylate cotransporter 1, a homolog of SdcS indicates that amino acid corresponding to 455 in rbNaDC1, Ser-512 is a determinant of citrate and succinate transport. The random mutants of SdcS-MASN and SdcS-LASS grew on the citrate selection agar but no $^{14}$C-citrate transport was seen.

We later attempted to understand determinants of α-ketoglutarate transport using SdcS random mutants. Due to structural similarity between succinate and α-ketoglutarate it might be easier to convert from succinate transporter to α-ketoglutarate transporter than to transport citrate. The selection media to screen library mutants used was Simmons citrate agar with α-ketoglutarate. Therefore SdcS random mutants that were able to utilize citrate, α-ketoglutarate or both will grow on the selection agar. Some of the right-side-out vesicles of SdcS random mutants showed citrate as well as α-ketoglutarate transport but when DNA sequences of SdcS mutants were analyzed, in many of the mutants termination codon was introduced by random mutagenesis that produced truncated transporters. At the moment, there is no

explanation for the results. It is possible that the truncated transporters might be indirectly involved in regulating endogenous citrate transport.

It is known that *E. coli* can utilize $C_4$-dicarboxylates as a carbon and energy source under aerobic and anaerobic conditions (*154-156*). The *E. coli* contains an endogenous dicarboxylate transporter, DctA which catalyzes $H^+$/dicarboxylate cotransport and is expressed at low level under aerobic growth conditions (*157*). Another $C_4$-dicarboxylate carrier, DcuA has been suggested to catalyze the uptake of succinate or fumarate in aerobic conditions to some extent (*158*). Under anaerobic conditions $C_4$-dicarboxylate transport is affected by carriers DcuA, DcuB, DcuC and DcuD or citrate/succinate antiporter (CitT) (*159*). One of these transporters might be utilizing citrate as a carbon source and therefore the random SdcS mutants in *E. coli* grew on the Simmons citrate agar plates and due to these endogenous $C_4$-dicarboxylate transporters some citrate uptake was observed in the mutants. Although the complete regulation of these $C_4$-dicarboxylate transporters of *E. coli* is not known, previous studies indicate that cyclic AMP receptor protein (CRP), cyclic AMP and glucose regulate DctA (*157;160*). It was also observed that DctA expression is induced by succinate and citrate (*157*). Therefore availability of citrate might be inducing the DctA expression which is involved in citrate utilization and the growth of colonies was seen. It is surprising that some of the SdcS random mutants did grow on Simmons citrate agar selection medium but showed no citrate uptake. This might be because these truncated transporters might be indirectly involved in regulating endogenous citrate transport. To understand this complete understanding of regulation of $C_4$-dicarboxylate carriers and sensors of *E. coli* is required. Therefore the disadvantage of using the SdcS random mutants is that they might be

involved in interacting with other transporters and signaling proteins which might be further involved in regulatory mechanism. Another possibility is that the bacterial endogenous transporters might transport citrate for the survival of the bacteria on the Simmons citrate agar plates where citrate is an only source of carbon that bacterial cells have to utilize for their survival. After that the regulatory mechanism might turn the citrate transport off. This process might be by endogenous regulation mechanism not involving the mutant SdcS transporters. Previous studies have also identified α-ketoglutarate transporter from E. coli, *kgtP*, α-ketoglutarate permease (*161*) which might be involved in utilizing α-ketoglutarate from the selection agar plates and therefore responsible for growth of the random mutant colonies.

Therefore, a complete understanding of expression and regulation of these endogenous $C_4$-dicarboxylate transporters is necessary to troubleshoot the problems involved with generation of SdcS random mutants and to determine determinants of citrate binding and transport. In conclusion, although the random mutagenesis approach is useful in understanding functionally important regions of proteins, complete understanding of the experimental system especially the regulation of the transporters is lacking due to which it is difficult to predict the citrate binding region and to elucidate structure-function relationship in SdcS.

# CHAPTER 6: CONCLUSIONS AND FUTURE DIRECTIONS

To understand the function and complete mechanism of membrane transporters it is important to know detailed information about their structures. Out of 50,000 high resolution structures of proteins yet solved (www.rcsb,org/pdb) only 150 are of membrane proteins and about 20 of them are of membrane transporters (http://blanco.biomol.uci.edu). It is difficult to obtain high resolution structures of membrane proteins due to their amphipathic nature which makes it hard to purify the membrane protein out of its lipid bilayer. Another problem is with expressing eukaryotic membrane proteins in bacterial expression system. Despite this some high resolution structures of membrane transporters are available which provide a framework for understanding their function and mechanism. Availability of these structures will help us understand the mechanism of membrane transporter, the nature of the binding site that is how the transporter can selectively transport one substrate and not another. The structural studies will also enables us to understand the pathways through which substrate and ions pass in their movement from one side of the membrane to the binding site and then from the binding site to the other side of the membrane. Conformational changes in the transporter (close access from one side of the membrane and open access to the other) are required for translocation to occur only when the appropriate ligands are bound at the binding sites. To date the majority of the information about SLC 13 gene family transporters is about its physiological function and tissue distribution through cell culture and *in vivo* studies (*25;26*). In this dissertation, a combination of experimental methods along with computational modeling was utilized to understand the structural details of the Na/dicarboxylate cotransporters. This study underlined the importance of prolines in

TM 7 and 10 for structural stability of NaDC1. In this dissertation a membrane topology, the number of transmembrane segments and their orientation in the membrane, of rabbit NaDC1 was also determined. Based on cysteine accessibility method and homology modeling results a modified 11 TM model was proposed for rabbit NaDC1. This work also identified Asn-108 from $Na^+$/dicarboxylate symporter, a homolog of NaDC1 from *Staphylococcus aureus*, as a conformationally sensitive residue accessible from both sides of the membrane in the presence of $Na^+$. Thus new information was obtained about role of conserved proline residues in the structure and function of the $Na^+$/dicarboxylate cotransporter 1 (NaDC1), the topology of $Na^+$/dicarboxylate cotransporter 1 and the identification of conformationally sensitive amino acids in $Na^+$/dicarboxylate symporter (SdcS).

Previous chimera and site-directed mutagenesis studies showed that TM 7, 10 and 11 of rb NaDC1 contains portions of the citrate binding site (*66*). Therefore to understand the importance of prolines in TM 7 and 10 a site-directed mutagenesis approach was used. Prolines, which are imino acids, were particularly chosen because they lack an amino side chain and hence cannot take part in hydrogen bonding. Proline residues in a transmembrane helix typically introduce a kink in the helix. Proline residues play an important role in the function of other transporters or channels including gating mechanisms (*109*), assembly of transporters, inhibitor binding (*111*) as well as cell surface expression and targeting (*110;112*). Prolines at 327, 351 from TM 7 and 523, 524 from TM 10 were mutated to alanine and glycine. Alanine is a strong α-helix former and is less flexible whereas glycine is a strong helix breaker and is more flexible. If prolines in NaDC1 are responsible for kink formation and if kink is necessary for maintaining the stability of the transporter then

mutating proline to glycine will have less adverse effect compared with mutating to alanine. This study indicates that prolines in TM 7 are critical for cell surface expression and protein targeting. Proline 327 when mutated to glycine showed no expression as well as succinate transport activity. Proline 351 also plays an important role in cell surface regulation and protein trafficking. Prolines of TM 10, 523 and 524 may produce kinks in the helix as evident by increased cell surface expression and succinate transport when mutated to glycine than alanine. These prolines might be structurally important but did not have any functional role in the transporter. Understanding effects of proline kink will be further helpful in knowing the helix packing, structural stability of the protein, understanding the role of proline resides in a membrane helix as well as in later in predicting the structure of helix of a membrane protein with proline residues.

To understand the structure-function relationship of a membrane protein it is absolute to know the topology of the membrane protein. Topology information of NaDC1 is available from hydropathy analysis and some experimental data (*61;62*). In this study, the topology of rabbit NaDC1 was determined by using the reactivity of introduced cysteines towards methanethiosulfonate reagents. Our results support a model of 11 TM helices, with some differences compared to the initial 11 TM model proposed for rbNaDC1. Recently the topology of the human high affinity $Na^+$/dicarboxylate cotransporter 3 (hNaDC3) was determined using cysteine accessibility method as well as with confocal immunofluorescence microscopy with membrane biotinylation of epitope tagged N and C terminus (*63*). This study suggests that NaDC3 also contains 11 TM helices. Studies were also carried out in rbNaDC1 to check for the accessibility of introduced cysteines in presence and

absence of $Na^+$ and succinate. Mutants A39C, K84C, A133C, T252C, G356C, T482C and M493C were accessible to methanethiosulfonate reagents in both sodium and without sodium (in choline). Mutants A133C, T252C and T482C showed substrate protection. Later a homology model was constructed and the model matches well with the experimental results. This model is a common framework on which the SLC13 family transporters are based. Therefore this topology model will be helpful in further designing site-directed mutagenesis experiments as well as in further understanding structural details of SLC 13 family transporters using cross-linking experiments.

To determine conformationally important residues in the $Na^+$/dicarboxylate transporters that are accessible from both sides of the membrane, a bacterial homolog of NaDC1, $Na^+$/dicarboxylate symporter (SdcS) from *Staphylococcus aureus* was used (*29*). The eukaryotic transporter could not be used due to experimental difficulties in studying accessibility of the transporter from inside the cell. Using rbNaDC1 as a scaffold, cysteines were substituted in the SdcS sequence at positions that are accessible to cysteine specific methanethiosulfonate reagents. The right-side-out (RSO) and inside-out (ISO) vesicles of SdcS, cysteineless SdcS and the cysteine mutants were tested for their accessibility from outside the cell (using RSO) and from inside the cell (using ISO). Residue Asp-329 was accessible in presence of $Na^+$ from outside only and not from inside. Residue Leu-436 was not accessible in either orientation and is probably located in the transmembrane helix not in contact with the water phase. Residue Asn-108 was accessible from both outside and inside, but only in the presence of $Na^+$. Asn-108 was not accessible in the conformational state in the absence of $Na^+$ and showed substrate protection, likely due to steric hindrance due to

chemical labeling. Therefore residue Asn-108 is probably located in the transmembrane helix near the water-filled pore or in a reentrant loop accessible from both sides of the membrane. Identification of conformationally important residues in SdcS will be helpful in understanding the structure and permeation pathways not only in NaDC1 but also will provide an understanding of important residues in other SLC 13 gene family members and overall structure of transporters.

A major focus of this dissertation is to provide insight into structural details of the $Na^+$/dicarboxylate cotransporters. A fundamental aspect of the structure of polytopic membrane proteins is their membrane topology. The topology of NaDC1 is a starting point to understand the structure of NaDC1 and other members of SLC 13 gene family. There are difficulties in obtaining high resolution structures of membrane transport proteins. Since 1980s various mutagenesis and computational studies were carried out to understand topology and structure of lactose permease from *E. coli* (LacY) (*162-165*). In 2003, a crystal structure of LacY was solved at 3.5 Å (*12*). The biochemical studies to determine the structural aspects of LacY matches very well with the high resolution crystal structure. Therefore use of biochemical methods to determine the structural framework of membrane proteins proves to be an important tool. There are various relatively less complicated biochemical methods available to determine the topology of the membrane proteins which can be utilized to construct a structural model of the membrane proteins. The substituted cysteine accessibility method was successfully used in this study to determine topology of NaDC1. This topology model was further used to construct the homology model of NaDC1. Given the enormous number of membrane proteins it is not realistic to assume that the structures of all the encoded proteins will be solved using the

crystallographic approach. Therefore if a membrane topology of a protein is known along with the folding pattern of the amino acid sequence one can use *in silico* approach to predict the putative structure of the membrane proteins which will be useful in further understanding the function and mechanism.

This work also identifies accessibility of Asn-108 from outside and inside the cell. Asn-108 from $Na^+$/dicarboxylate symporter a bacterial homolog of $Na^+$/dicarboxylate cotransporter is accessible from both the sides of the membrane in presence of $Na^+$ buffer only. This residue is conformationally sensitive as Asn-108 is accessible only in presence of $Na^+$ and was not accessible in absence of $Na^+$ or in presence of $Na^+$ with the substrate, succinate. Identifying residues accessible from both sides of membrane will be important for understanding conformational states of the transporter under different substrate and cation conditions. Therefore this study not only provides structural details of transporter by identifying accessible residues but also is helpful in understanding the mechanism of membrane transport. In this study a bacterial homolog (SdcS) of eukaryotic transporters (NaDC1) have been used. Previously prokaryotic homologs have been used to understand the structure of its eukaryotic counterpart such as $Na^+/Cl^-$ dependent neurotransmitter transporters from *Aquifex aeolicus* have provided information about structure, substrate binding site as well as mechanism of transport by eukaryotic neurotransmitter transporters (*19;134*). This study provides evidence for similar structural details between prokaryotic and eukaryotic transporters by observing similar accessibility of amino acids and overall folding pattern of the transporter. It further confirms that the prokaryotic homologs can be used as a reference for understanding structure-function of eukaryotic transporters.

In this dissertation various biochemical and computational techniques were used to identify structural details of $Na^+$/dicarboxylate cotransporters. The information generated by these studies is useful in understanding the role of prolines not only in NaDC1 but in all the membrane proteins. An experimental topology model was constructed in this study which will be useful for further understanding the structure of SLC 13 family transporters. Identification of conformationally sensitive residue Asn-108 which is accessible from both sides of membrane is useful in providing insight into mechanisms of transport by SLC 13 family transporters. Therefore results of these studies will help us to understand detailed picture of structure and function of SLC 13 gene family transporters.

Previous experimental data and computational modeling suggest that TM 3, 7 and 10 might be forming the permeation pathway and may contain part of the substrate binding site. To confirm that these helices are indeed involved as a part of substrate binding site they should be in close proximity to each other. Determination of proximities of TM helices 3, 7 and 10 can be carried out by site-directed thiol cross-linking studies using MTS reagents of various lengths. Cross-linking studies have been previously carried out with lactose permease (LacY), serotonin (SERT), γ-aminobutyric acid transporter (GABA) (*166-168*). A pair of cysteine residues can be introduced in cysteineless SdcS, a bacterial homolog of NaDC1. The chemical cross-linking can be carried out by various MTS cross-linkers, from M2M (Cross-linking span of 5.2 Å) to M17M (cross-linking span of 24.7 Å). Mobility shift assay can be performed to determine disulfide cross-linking (*167*). Another method of analyzing the proximity of helices is using cysteine mutants and use of fluorescence and

luminescence energy transfer (FRET & LRET) to measure the distance between the probes on the two cysteines (*169*).

In 2005, a homolog of NaDC1 from S*taphylococcus aureus* was isolated, functionally reconstituted and characterized (*29;94*). This dissertation work also characterizes properties of SdcS in right-side-out and inside-out membrane vesicles and identifies conformationally sensitive residues in SdcS. It will be helpful to understand the topology of SdcS for further elucidating structural details. SdcS contains a single cysteine at 457 which was mutated to serine to obtain a cysteineless mutant, C457S, which shows similar transport properties as that of wild-type. Individual cysteines can be introduced in putative extracellular and intracellular loops and these cysteines can be labeled with sulfhydryl specific methanethiosulfonate reagents to determine the topology. Continued topological study, together with the ability to overexpress, purify, and reconstitute functional SdcS, will be helpful in conducting crystallization trials for understanding the SdcS and subsequently the NaDC transporter architecture.

This dissertation provides structural and functional information about $Na^+$/dicarboxylate cotransporters. The use of mutants and chimeric transporters and the combination of molecular and functional tools is useful in understanding the basic transporter structure, the putative substrate and cation binding sites as well as understanding the mechanism of transport. This work enables us to further study the transporter structure by using biophysical approaches and will be helpful in future development of targeted drugs for treatment and prevention of kidney stones.

# REFERENCES


1. Widdas, W. F. (1952) Inability of diffusion to account for placental glucose transfer in the sheep and consideration of the kinetics of a possible carrier transfer, *J. Physiol. 118*, 23-39.

2. LeFevre, P. G. (1961) Sugar transport in the red blood cell: structure-activity relationships in substrates and antagonists, *Pharmacol. Rev. 13*, 39-70.

3. Busch, W. and Saier, M. H., Jr. (2002) The transporter classification (TC) system, 2002, *Crit. Rev. Biochem. Mol. Biol. 37*, 287-337.

4. Busch, W. and Saier, M. H., Jr. (2004) The IUBMB-endorsed transporter classification system, *Mol. Biotechnol. 27*, 253-262.

5. Saier, M. H. (1999) Genome archeology leading to the characterization and classification of transport proteins, *Curr. Opin. Microbiol. 2*, 555-561.

6. Saier, M. H., Jr. (2000) A functional-phylogenetic classification system for transmembrane solute transporters, *Microbiology and Molecular Biology Reviews 64*, 354-411.

7. Saier, M. H., Jr. (2000) Families of transmembrane sugar transport proteins, *Mol. Microbiol. 35*, 699-710.

8. Hille, B. (1986) Ionic channels: molecular pores of excitable membranes, *Harvey Lect. 82*, 47-69.

9. Murakami, S., Nakashima, R., Yamashita, E., and Yamaguchi, A. (2002) Crystal structure of bacterial multidrug efflux transporter AcrB, *Nature 419*, 587-593.

10. Yu, E. W., Aires, J. R., and Nikaido, H. (2003) AcrB multidrug efflux pump of *Escherichia coli*: composite substrate-binding cavity of exceptional flexibility generates its extremely wide substrate specificity, *J. Bacteriol. 185*, 5657-5664.

11. Yu, E. W., McDermott, G., Zgurskaya, H. I., Nikaido, H., and Koshland, D. E., Jr. (2003) Structural basis of multiple drug-binding capacity of the AcrB multidrug efflux pump, *Science 300*, 976-980.

12. Abramson, J., Smirnova, I., Kasho, V., Verner, G., Kaback, H. R., and Iwata, S. (2003) Structure and mechanism of the lactose permease of *Escherichia coli*, *Science 301*, 610-615.

13. Huang, Y., Lemieux, M. J., Song, J., Auer, M., and Wang, D. N. (2003) Structure and mechanism of the glycerol-3-phosphate transporter from *Escherichia coli*, *Science 301*, 616-620.

14. Saier, M. H., Jr., Beatty, J. T., Goffeau, A., Harley, K. T., Heijne, W. H., Huang, S. C., Jack, D. L., Jahn, P. S., Lew, K., Liu, J., Pao, S. S., Paulsen, I. T., Tseng, T. T., and Virk, P. S. (1999) The major facilitator superfamily, *J. Mol. Microbiol. Biotechnol. 1*, 257-279.

15. Lemieux, M. J., Huang, Y., and Wang, D. N. (2004) The structural basis of substrate translocation by the *Escherichia coli* glycerol-3-phosphate transporter: a member of the major facilitator superfamily, *Curr. Opin. Struct. Biol. 14*, 405-412.

16. Khademi, S., O'Connell, J., III, Remis, J., Robles-Colmenares, Y., Miercke, L. J., and Stroud, R. M. (2004) Mechanism of ammonia transport by Amt/MEP/Rh: structure of AmtB at 1.35 A, *Science 305*, 1587-1594.

17. Yernool, D., Boudker, O., Jin, Y., and Gouaux, E. (2004) Structure of a glutamate transporter homologue from *Pyrococcus horikoshii*, *Nature 431*, 811-818.

18. Brocke, L., Bendahan, A., Grunewald, M., and Kanner, B. I. (2002) Proximity of two oppositely oriented reentrant loops in the glutamate transporter GLT-1 identified by paired cysteine mutagenesis, *J. Biol. Chem. 277*, 3985-3992.

19. Yamashita, A., Singh, S. K., Kawate, T., Jin, Y., and Gouaux, E. (2005) Crystal structure of a bacterial homologue of $Na^+/Cl^-$ dependent neurotransmitter transporters, *Nature 437*, 215-223.

20. Rudnick, G. (2006) Serotonin transporters--structure and function, *J. Membr. Biol. 213*, 101-110.

21. Sobczak, I. and Lolkema, J. S. (2005) Structural and mechanistic diversity of secondary transporters, *Curr. Opin. Microbiol. 8*, 161-167.

22. Zheng, L., Kostrewa, D., Berneche, S., Winkler, F. K., and Li, X. D. (2004) The mechanism of ammonia transport based on the crystal structure of AmtB of *Escherichia coli*, *Proc. Natl. Acad. Sci. U. S. A. 101*, 17090-17095.

23. Kanner, B. I. and Borre, L. (2002) The dual-function glutamate transporters: structure and molecular characterisation of the substrate-binding sites, *Biochim. Biophys. Acta 1555*, 92-95.

24. Kanner, B. I. (2006) Structure and function of sodium-coupled GABA and glutamate transporters, *J. Membr. Biol. 213*, 89-100.

25. Markovich, D. and Murer, H. (2004) The SLC13 gene family of sodium sulphate/carboxylate cotransporters, *Pflugers Arch. 447*, 594-602.

26. Pajor, A. M. (2006) Molecular properties of the SLC13 family of dicarboxylate and sulfate transporters, *Pflugers Arch. 451*, 597-605.

27. Fei, Y. J., Inoue, K., and Ganapathy, V. (2003) Structural and functional characteristics of two sodium-coupled dicarboxylate transporters (ceNaDC1 and ceNaDC2) from Caenorhabditis elegans and their relevance to life span, *J. Biol. Chem. 278*, 6136-6144.

28. Rogina, B., Reenan, R. A., Nilsen, S. P., and Helfand, S. L. (2000) Extended life-span conferred by cotransporter gene mutations in Drosophila, *Science 290*, 2137-2140.

29. Hall, J. A. and Pajor, A. M. (2005) Functional characterization of a $Na^+$-coupled dicarboxylate carrier protein from Staphylococcus aureus, *J. Bacteriol. 187*, 5189-5194.

30. Lee, A., Beck, L., and Markovich, D. (2000) The human renal sodium sulfate cotransporter (SLC13A1; hNaSi-1) cDNA and gene: organization, chromosomal localization, and functional characterization, *Genomics 70*, 354-363.

31. Markovich, D., Forgo, J., Stange, G., Biber, J., and Murer, H. (1993) Expression cloning of rat renal $Na^+/SO4^{2-}$ cotransport, *Proc. Natl. Acad. Sci. U. S. A. 90*, 8073-8077.

32. Beck, L. and Markovich, D. (2000) The mouse $Na^+$-sulfate cotransporter gene Nas1. Cloning, tissue distribution, gene structure, chromosomal assignment, and transcriptional regulation by vitamin D, *J. Biol. Chem. 275*, 11880-11890.

33. Nakada, T., Zandi-Nejad, K., Kurita, Y., Kudo, H., Broumand, V., Kwon, C. Y., Mercado, A., Mount, D. B., and Hirose, S. (2005) Roles of Slc13a1 and Slc26a1 sulfate transporters of eel kidney in sulfate homeostasis and

osmoregulation in freshwater, *Am. J. Physiol. Regul. Integr. Comp. Physiol. 289*, R575-R585.

34. Pajor, A. M. (1996) Molecular cloning and functional expression of a sodium-dicarboxylate cotransporter from human kidney, *Am. J. Physiol. 270*, F642-F648.

35. Pajor, A. M. (1995) Sequence and functional characterization of a renal $Na^+$/dicarboxylate cotransporter, *J. Biol. Chem. 270*, 5779-5785.

36. Sekine, T., Cha, S. H., Hosoyamada, M., Kanai, Y., Watanabe, N., Furuta, Y., Fukuda, K., Igarashi, T., and Endou, H. (1998) Cloning, functional characterization, and localization of a rat renal $Na^+$-dicarboxylate transporter, *Am. J. Physiol. 275*, F298-F305.

37. Pajor, A. M. and Sun, N. N. (2000) Molecular cloning, chromosomal organization, and functional characterization of a sodium-dicarboxylate cotransporter from mouse kidney, *Am. J. Physiol. Renal Physiol. 279*, F482-F490.

38. Aruga, S., Pajor, A. M., Nakamura, K., Liu, L., Moe, O. W., Preisig, P. A., and Alpern, R. J. (2004) OKP cells express the Na-dicarboxylate cotransporter NaDC-1, *Am. J. Physiol. Cell Physiol. 287*, C64-C72.

39. Bai, L. and Pajor, A. M. (1997) Expression cloning of NaDC-2, an intestinal $Na^+$- or $Li^+$-dependent dicarboxylate transporter, *Am. J. Physiol. 273*, G267-G274.

40. Wang, H., Fei, Y. J., Kekuda, R., Yang-Feng, T. L., Devoe, L. D., Leibach, F. H., Prasad, P. D., and Ganapathy, V. (2000) Structure, function, and genomic organization of human $Na^+$-dependent high-affinity dicarboxylate transporter, *Am. J. Physiol. Cell Physiol. 278*, C1019-C1030.

41. Kekuda, R., Wang, H., Huang, W., Pajor, A. M., Leibach, F. H., Devoe, L. D., Prasad, P. D., and Ganapathy, V. (1999) Primary structure and functional characteristics of a mammalian sodium-coupled high affinity dicarboxylate transporter, *J. Biol. Chem. 274*, 3422-3429.

42. Pajor, A. M., Gangula, R., and Yao, X. (2001) Cloning and functional characterization of a high-affinity $Na^+$/dicarboxylate cotransporter from mouse brain, *Am. J. Physiol. Cell Physiol. 280*, C1215-C1223.

43. Oshiro, N. and Pajor, A. M. (2005) Functional characterization of high-affinity $Na^+$/dicarboxylate cotransporter found in Xenopus laevis kidney and heart, *Am. J. Physiol. Cell Physiol. 289*, C1159-C1168.

44. Steffgen, J., Burckhardt, B. C., Langenberg, C., Kuhne, L., Muller, G. A., Burckhardt, G., and Wolff, N. A. (1999) Expression cloning and characterization of a novel sodium-dicarboxylate cotransporter from winter flounder kidney, *J. Biol. Chem. 274*, 20190-20196.

45. Girard, J. P., Baekkevold, E. S., Feliu, J., Brandtzaeg, P., and Amalric, F. (1999) Molecular cloning and functional analysis of SUT-1, a sulfate transporter from human high endothelial venules, *Proc. Natl. Acad. Sci. U. S. A. 96*, 12772-12777.

46. Markovich, D., Regeer, R. R., Kunzelmann, K., and Dawson, P. A. (2005) Functional characterization and genomic organization of the human $Na^+$-sulfate cotransporter hNaS2 gene (SLC13A4), *Biochem. Biophys. Res. Commun. 326*, 729-734.

47. Inoue, K., Zhuang, L., and Ganapathy, V. (2002) Human $Na^+$-coupled citrate transporter: primary structure, genomic organization, and transport function, *Biochem. Biophys. Res. Commun. 299*, 465-471.

48. Inoue, K., Zhuang, L., Maddox, D. M., Smith, S. B., and Ganapathy, V. (2002) Structure, function, and expression pattern of a novel sodium-coupled citrate transporter (NaCT) cloned from mammalian brain, *J. Biol. Chem. 277*, 39469-39476.

49. Inoue, K., Fei, Y. J., Zhuang, L., Gopal, E., Miyauchi, S., and Ganapathy, V. (2004) Functional features and genomic organization of mouse NaCT, a sodium-coupled transporter for tricarboxylic acid cycle intermediates, *Biochem. J. 378*, 949-957.

50. Mann, S. S., Hart, T. C., Pettenati, M. J., von Kap-herr, C., and Holmes, R. P. (1999) Assignment of the sodium-dependent dicarboxylate transporter gene (SLC13A2 alias NaDC-1) to human chromosome region 17p11.1-q11.1 by radiation hybrid mapping and fluorescence in situ hybridization, *Cytogenet. Cell Genet. 34*, 89-90.

51. Yao, X. and Pajor, A. M. (2000) The transport properties of the human renal $Na^+$- dicarboxylate cotransporter under voltage-clamp conditions, *Am. J. Physiol. Renal Physiol. 279*, F54-F64.

52. Wright, E. M., Wright, S. H., Hirayama, B. A., and Kippen, I. (1982) Interactions between lithium and renal transport of Krebs cycle intermediates, *Proc. Natl. Acad. Sci. U. S. A. 79*, 7514-7517.

53. Pajor, A. M., Hirayama, B. A., and Loo, D. D. F. (1998) Sodium and lithium interactions with the $Na^+$/dicarboxylate cotransporter, *J. Biol. Chem. 273*, 18923-18929.

54. Pajor, A. M. (2000) Molecular properties of sodium/dicarboxylate cotransporters, *J. Membr. Biol. 175*, 1-8.

55. Pajor, A. M. and Sun, N. (1996) Functional differences between rabbit and human $Na^+$-dicarboxylate cotransporters, NaDC-1 and hNaDC-1, *Am. J. Physiol. 271*, F1093-F1099.

56. Pajor, A. M. (1994) Expression cloning of a renal sodium/dicarboxylate cotransporter, *J. Amer. Soc. Nephrol. 5*, 296.

57. Pajor, A. M. (1999) Sodium-coupled transporters for Krebs cycle intermediates, *Annu. Rev. Physiol. 61*, 663-682.

58. Wright, E. M. (1985) Transport of carboxylic acids by renal membrane vesicles, *Ann. Rev. Physiol. 47*, 127-141.

59. Parent, L., Supplisson, S., Loo, D. D. F., and Wright, E. M. (1992) Electrogenic properties of the cloned $Na^+$/glucose cotransporter: I. Voltage-clamp studies, *J. Membrane Biol. 125*, 49-62.

60. Eskandari, S., Loo, D. D., Dai, G., Levy, O., Wright, E. M., and Carrasco, N. (1997) Thyroid $Na^+/I^-$ symporter. Mechanism, stoichiometry, and specificity, *J. Biol. Chem. 272*, 27230-27238.

61. Pajor, A. M. and Sun, N. (1996) Characterization of the rabbit renal $Na^+$-dicarboxylate cotransporter using antifusion protein antibodies, *Am. J. Physiol. 271*, C1808-C1816.

62. Zhang, F. F. and Pajor, A. M. (2001) Topology of the $Na^+$/dicarboxylate cotransporter: the N-terminus and hydrophilic loop 4 are located intracellularly, *Biochim. Biophys. Acta 1511*, 80-89.

63. Bai, X. Y., Chen, X., Sun, A. Q., Feng, Z., Hou, K., and Fu, B. (2007) Membrane topology structure of human high-affinity, sodium-dependent dicarboxylate transporter, *FASEB J. 21*, 2409-2417.

64. Rao, J. K. M. and Argos, P. (1986) A conformational preference parameter to predict helices in integral membrane proteins, *Biochim. Biophys. Acta 869*, 197-214.

65. Pajor, A. M., Sun, N., Bai, L., Markovich, D., and Sule, P. (1998) The substrate recognition domain in the $Na^+$/dicarboxylate and $Na^+$/sulfate cotransporters is located in the carboxy-terminal portion of the protein, *Biochim. Biophys. Acta 1370*, 98-106.

66. Kahn, E. S. and Pajor, A. M. (1999) Determinants of substrate and cation affinities in the $Na^+$/dicarboxylate cotransporter, *Biochemistry 38*, 6151-6156.

67. Oshiro, N., King, S. C., and Pajor, A. M. (2006) Transmembrane helices 3 and 4 are involved in substrate recognition by the $Na^+$/dicarboxylate cotransporter, NaDC1, *Biochemistry 45*, 2302-2310.

68. Oshiro, N. and Pajor, A. M. (2006) Ala-504 is a determinant of substrate binding affinity in the mouse $Na^+$/dicarboxylate cotransporter, *Biochim. Biophys. Acta 1758*, 781-788.

69. Pajor, A. M. (2001) Conformationally-sensitivity residues in transmembrane domain 9 of the $Na^+$/dicarboxylate cotransporter, *J. Biol. Chem. 276*, 29961-29968.

70. Pajor, A. M. and Randolph, K. M. (2005) Conformationally sensitive residues in extracellular loop 5 of the $Na^+$/dicarboxylate co-transporter, *J. Biol. Chem. 280*, 18728-18735.

71. Pajor, A. M., Kahn, E. S., and Gangula, R. (2000) Role of cationic amino acids in the sodium/dicarboxylate co-transporter NaDC-1, *Biochem. J. 350*, 677-683.

72. Weerachayaphorn, J. and Pajor, A. M. (2007) Sodium-dependent extracellular accessibility of Lys-84 in the sodium/dicarboxylate cotransporter, *J. Biol. Chem. 282*, 20213-20220.

73. Griffith, D. A. and Pajor, A. M. (1999) Acidic residues involved in cation and substrate interactions in the $Na^+$/dicarboxylate cotransporter, NaDC-1, *Biochemistry 38*, 7524-7531.

74. Yao, X. and Pajor, A. M. (2002) Arginine-349 and aspartate-373 of the $Na^+$/dicarboxylate cotransporter are conformationally sensitive residues, *Biochemistry 41*, 1083-1090.

75. Pajor, A. M., Sun, N., and Valmonte, H. G. (1998) Mutational analysis of histidines in the $Na^+$/dicarboxylate cotransporter, NaDC1, *Biochem. J. 331*, 257-264.

76. Weerachayaphorn, J. and Pajor, A. M. (2008) Threonine-509 is a determinant of apparent affinity for both substrate and cations in the human $Na^+$/dicarboxylate cotransporter, *Biochemistry 47*, 1087-1093.

77. Hamm, L. L. (1990) Renal handling of citrate, *Kidney International 38*, 728-735.

78. Murer, H. and Burckhardt, G. (1983) Membrane transport of anions across epithelia of mammalian small intestine and kidney proximal tubule, *Rev. Physiol. Biochem. Pharmacol. 96*, 1-51.

79. Murer, H., Manganel, M., and Roch-Ramel, F. (1992) Tubular transport of monocarboxylates, Krebs cycle intermediates, and inorganic sulfate, in *Handbook of Physiology-Renal Physiology* (Windhager, E. E., Ed.) pp 2165-2188, Am. Physiol. Soc., New York, NY.

80. Nieth, H. and Schollmeyer, P. (1966) Substrate-utilization of the human kidney, *Nature 209*, 1244-1245.

81. Ho, H. T., Ko, B. C., Cheung, A. K., Lam, A. K., Tam, S., Chung, S. K., and Chung, S. S. (2007) Generation and characterization of sodium-dicarboxylate cotransporter deficient mice, *Kidney Int. 72*, 63-71.

82. Anzai, N., Kanai, Y., and Endou, H. (2006) Organic anion transporter family: current knowledge, *J. Pharmacol. Sci. 100*, 411-426.

83. Anzai, N., Jutabha, P., Kanai, Y., and Endou, H. (2005) Integrated physiology of proximal tubular organic anion transport, *Curr. Opin. Nephrol. Hypertens. 14*, 472-479.

84. Wright, S. H. and Dantzler, W. H. (2004) Molecular and cellular physiology of renal organic cation and anion transport, *Physiol. Rev. 84*, 987-1049.

85. Ekaratanawong, S., Anzai, N., Jutabha, P., Miyazaki, H., Noshiro, R., Takeda, M., Kanai, Y., Sophasan, S., and Endou, H. (2004) Human organic anion transporter 4 is a renal apical organic anion/dicarboxylate exchanger in the proximal tubules, *J. Pharmacol. Sci. 94*, 297-304.

86. Pritchard, J. B., Sweet, D. H., Miller, D. S., and Walden, R. (1999) Mechanism of organic anion transport across the apical membrane of choroid plexus, *J. Biol. Chem. 274*, 33382-33387.

87. Sweet, D. H., Chan, L. M., Walden, R., Yang, X. P., Miller, D. S., and Pritchard, J. B. (2003) Organic anion transporter 3 (Slc22a8) is a dicarboxylate exchanger indirectly coupled to the $Na^+$ gradient, *Am. J. Physiol. Renal Physiol. 284*, F763-F769.

88. Sekine, T., Cha, S. H., and Endou, H. (2000) The multispecific organic anion transporter (OAT) family, *Pflugers Arch. 440*, 337-350.

89. Pak, C. Y. (1991) Etiology and treatment of urolithiasis, *Am. J. Kidney Dis. 18*, 624-637.

90. Aruga, S., Moe, O. W., Preisig, P. A., Pajor, A. M., and Alpern, R. J. (1999) Genomic organization and tissue specific expression of the human NaDC-1 gene, *Amer. Soc. Nephrol. 10*, 50A.

91. He, W., Miao, F. J., Lin, D. C., Schwandner, R. T., Wang, Z., Gao, J., Chen, J. L., Tian, H., and Ling, L. (2004) Citric acid cycle intermediates as ligands for orphan G-protein-coupled receptors, *Nature 429*, 188-193.

92. Inoue, K., Fei, Y. J., Huang, W., Zhuang, L., Chen, Z., and Ganapathy, V. (2002) Functional identity of Drosophila melanogaster Indy as a cation-independent, electroneutral transporter for tricarboxylic acid-cycle intermediates, *Biochem. J. 367*, 313-319.

93. Lakowski, B. and Hekimi, S. (1998) The genetics of caloric restriction in Caenorhabditis elegans, *Proc. Natl. Acad. Sci. U. S. A. 95*, 13091-13096.

94. Hall, J. A. and Pajor, A. M. (2007) Functional reconstitution of SdcS, a $Na^+$-coupled dicarboxylate carrier protein from *Staphylococcus aureus*, *J. Bacteriol. 189*, 880-885.

95. Woolfson, D. N. and Williams, D. H. (1990) The influence of proline residues on alpha-helical structure, *FEBS Lett. 277*, 185-188.

96. Shelden, M. C., Loughlin, P., Tierney, M. L., and Howitt, S. M. (2001) Proline residues in two tightly coupled helices of the sulphate transporter, SHST1, are important for sulphate transport, *Biochem. J. 356*, 589-594.

97. Lu, H., Marti, T., and Booth, P. J. (2001) Proline residues in transmembrane alpha helices affect the folding of bacteriorhodopsin, *J. Mol. Biol. 308*, 437-446.

98. Sansom, M. S. (1992) Proline residues in transmembrane helices of channel and transport proteins: a molecular modelling study, *Protein Eng. 5*, 53-60.

99. Brandl, C. J. and Deber, C. M. (1986) Hypothesis about the function of membrane-buried proline residues in transport proteins, *Proc. Natl. Acad. Sci. U. S. A. 83*, 917-921.

100. Sansom, M. S. and Weinstein, H. (2000) Hinges, swivels and switches: the role of prolines in signalling via transmembrane alpha-helices, *Trends Pharmacol. Sci. 21*, 445-451.

101. King, S. C. (2004) The "Transport Specificity Ratio": a structure-function tool to search the protein fold for loci that control transition state stability in membrane transport catalysis, *BMC. Biochem. 5*, 16.

102. King, S. C. and Brown-Istvan, L. (2003) Use of the transport specificity ratio and cysteine-scanning mutagenesis to detect multiple substrate specificity determinants in the consensus amphipathic region of the Escherichia coli GABA (gamma-aminobutyric acid) transporter encoded by gabP, *Biochem. J. 376*, 633-644.

103. Li, H. and Pajor, A. M. (2003) Mutagenesis of the N-glycosylation site of hNaSi-1 reduces transport activity, *Am. J. Physiol. Cell Physiol. 285*, C1188-C1196.

104. Tamarappoo, B. K. and Verkman, A. S. (1998) Defective aquaporin-2 trafficking in nephrogenic diabetes insipidus and correction by chemical chaperones, *J. Clin. Invest 101*, 2257-2267.

105. Barlow, D. J. and Thornton, J. M. (1988) Helix geometry in proteins, *J. Mol. Biol. 201*, 601-619.

106. Cordes, F. S., Bright, J. N., and Sansom, M. S. (2002) Proline-induced distortions of transmembrane helices, *J. Mol. Biol. 323*, 951-960.

107. Richardson, J. S. and Richardson, D. C. (1988) Amino acid preferences for specific locations at the ends of alpha helices, *Science 240*, 1648-1652.

108. Sankararamakrishnan, R. and Vishveshwara, S. (1990) Conformational studies on peptides with proline in the right-handed alpha-helical region, *Biopolymers 30*, 287-298.

109. Labro, A. J., Raes, A. L., Bellens, I., Ottschytsch, N., and Snyders, D. J. (2003) Gating of shaker-type channels requires the flexibility of S6 caused by prolines, *J. Biol. Chem. 278*, 50724-50731.

110. Lin, Z., Itokawa, M., and Uhl, G. R. (2000) Dopamine transporter proline mutations influence dopamine uptake, cocaine analog recognition, and expression, *FASEB J. 14*, 715-728.

111. Paczkowski, F. A. and Bryan-Lluka, L. J. (2004) Role of proline residues in the expression and function of the human noradrenaline transporter, *J. Neurochem. 88*, 203-211.

112. Slepkov, E. R., Chow, S., Lemieux, M. J., and Fliegel, L. (2004) Proline residues in transmembrane segment IV are critical for activity, expression and targeting of the $Na^+/H^+$ exchanger isoform 1, *Biochem. J. 379*, 31-38.

113. Sato, S., Ward, C. L., Krouse, M. E., Wine, J. J., and Kopito, R. R. (1996) Glycerol reverses the misfolding phenotype of the most common cystic fibrosis mutation, *J. Biol. Chem. 271*, 635-638.

114. de Jong, J. C., Willems, P. H., Goossens, M., Vandewalle, A., van den Heuvel, L. P., Knoers, N. V., and Bindels, R. J. (2004) Effects of chemical chaperones on partially retarded NaCl cotransporter mutants associated with Gitelman's syndrome in a mouse cortical collecting duct cell line, *Nephrol. Dial. Transplant. 19*, 1069-1076.

115. Joshi, A. D. and Pajor, A. M. (2006) Role of conserved prolines in the structure and function of the $Na^+$/dicarboxylate cotransporter 1, NaDC1, *Biochemistry 45*, 4231-4239.

116. Pajor, A. M., Krajewski, S. J., Sun, N., and Gangula, R. (1999) Cysteine residues in the $Na^+$/dicarboxylate cotransporter, NaDC-1., *Biochem. J. 344*, 205-209.

117. Avidin-Biotin Products: A Technical Handbook (2005) Literature Number # Pierce 1601227.

118. Ginalski, K., Elofsson, A., Fischer, D., and Rychlewski, L. (2003) 3D-Jury: a simple approach to improve protein structure predictions, *Bioinformatics 19*, 1015-1018.

119. Soman, K. V. and Braun, W. (2001) Determining the three-dimensional fold of a protein from approximate constraints: a simulation study, *Cell Biochem. Biophys. 34*, 283-304.

120. Schaumann, T., Braun, W., and Wutrich, K. (1990) The program FANTOM for energy refinement of polypeptides and proteins using Newton-Raphson minimizer in torsion angle space, *Biopolymers 29*, 679-694.

121. Holmgren, M., Liu, Y., Xu, Y., and Yellen, G. (1996) On the use of thiol-modifying agents to determine channel topology, *Neuropharmacology 35*, 797-804.

122. Sato, Y., Zhang, Y. W., ndroutsellis-Theotokis, A., and Rudnick, G. (2004) Analysis of transmembrane domain 2 of rat serotonin transporter by cysteine scanning mutagenesis, *J. Biol. Chem. 279*, 22926-22933.

123. Bowie, J. U., Luthy, R., and Eisenberg, D. (1991) A method to identify protein sequences that fold into a known three-dimensional structure, *Science 253*, 164-170.

124. Jones, D. T., Taylor, W. R., and Thornton, J. M. (1992) A new approach to protein fold recognition, *Nature 358*, 86-89.

125. Ginalski, K. and Rychlewski, L. (2003) Protein structure prediction of CASP5 comparative modeling and fold recognition targets using consensus alignment approach and 3D assessment, *Proteins 53 Suppl 6*, 410-417.

126. Sujatha, M. S. and Balaji, P. V. (2006) Fold-recognition and comparative modeling of human alpha2,3-sialyltransferases reveal their sequence and structural similarities to CstII from *Campylobacter jejuni*, *BMC. Struct. Biol. 6*, 9.

127. Mirza, O., Guan, L., Verner, G., Iwata, S., and Kaback, H. R. (2006) Structural evidence for induced fit and a mechanism for sugar/$H^+$ symport in LacY, *EMBO J. 25*, 1177-1183.

128. Kaback, H. R., Dunten, R., Frillingos, S., Venkatesan, P., Kwaw, I., Zhang, W., and Ermolova, N. (2007) Site-directed alkylation and the alternating access model for LacY, *Proc. Natl. Acad. Sci. U. S. A. 104*, 491-494.

129. Kaback, H. R. (1971) Bacterial membranes, *Methods Enzymol. 22*, 99-120.

130. Schnaitman, C. A. (1970) Protein composition of the cell wall and cytoplasmic membrane of Escherichia coli, *J. Bacteriol. 104*, 890-901.

131. Bradford, M. M. (1976) A rapid and sensitive method for the quantitation of microgram quantities of protein utilizing the principle of protein-dye binding, *Anal. Biochem. 72*, 248-254.

132. Parent, L., Supplisson, S., Loo, D. D., and Wright, E. M. (1992) Electrogenic properties of the cloned $Na^+$/glucose cotransporter: II. A transport model under nonrapid equilibrium conditions, *J. Membr. Biol. 125*, 63-79.

133. Wadiche, J. I. and Kavanaugh, M. P. (1998) Macroscopic and microscopic properties of a cloned glutamate transporter/chloride channel, *J. Neurosci. 18*, 7650-7661.

134. Beuming, T., Shi, L., Javitch, J. A., and Weinstein, H. (2006) A comprehensive structure-based alignment of prokaryotic and eukaryotic neurotransmitter/$Na^+$ symporters (NSS) aids in the use of the LeuT structure to probe NSS structure and function, *Mol. Pharmacol. 70*, 1630-1642.

135. Androutsellis-Theotokis, A., Goldberg, N. R., Ueda, K., Beppu, T., Beckman, M. L., Das, S., Javitch, J. A., and Rudnick, G. (2003) Characterization of a functional bacterial homologue of sodium-dependent neurotransmitter transporters, *J. Biol. Chem. 278*, 12703-12709.

136. Grunewald, M. and Kanner, B. I. (2000) The accessibility of a novel reentrant loop of the glutamate transporter GLT-1 is restricted by its substrate, *J. Biol. Chem. 275*, 9684-9689.

137. Slotboom, D. J., Sobczak, I., Konings, W. N., and Lolkema, J. S. (1999) A conserved serine-rich stretch in the glutamate transporter family forms a substrate-sensitive reentrant loop, *Proc. Natl. Acad. Sci. U. S. A. 96*, 14282-14287.

138. Hu, L. A. and King, S. C. (1998) Functional sensitivity of polar surfaces on transmembrane helix 8 and cytoplasmic loop 8-9 of the Escherichia coli GABA (4-aminobutyrate) transporter encoded by gabP: mutagenic analysis of a consensus amphipathic region found in transporters from bacteria to mammals, *Biochem. J. 330 (Pt 2)*, 771-776.

139. Hirayama, B. and Wright, E. M. (1984) Asymmetry of the $Na^+$-succinate cotransporter in rabbit renal brush-border membranes, *Biochim. Biophys. Acta 775*, 17-21.

140. Grunewald, M., Menaker, D., and Kanner, B. I. (2002) Cysteine-scanning mutagenesis reveals a conformationally sensitive reentrant pore-loop in the glutamate transporter GLT-1, *J. Biol. Chem. 277*, 26074-26080.

141. Iwamoto, T., Uehara, A., Imanaga, I., and Shigekawa, M. (2000) The $Na^+/Ca^{2+}$ exchanger NCX1 has oppositely oriented reentrant loop domains that contain conserved aspartic acids whose mutation alters its apparent $Ca^{2+}$ affinity, *J. Biol. Chem. 275*, 38571-38580.

142. Nicoll, D. A., Ottolia, M., and Philipson, K. D. (2002) Toward a topological model of the NCX1 exchanger, *Ann. N. Y. Acad. Sci. 976*, 11-18.

143. Wong, T. S., Zhurina, D., and Schwaneberg, U. (2006) The diversity challenge in directed protein evolution, *Comb. Chem. High Throughput. Screen. 9*, 271-288.

144. Locher, C. P., Soong, N. W., Whalen, R. G., and Punnonen, J. (2004) Development of novel vaccines using DNA shuffling and screening strategies, *Curr. Opin. Mol. Ther. 6*, 34-39.

145. Kurtzman, A. L., Govindarajan, S., Vahle, K., Jones, J. T., Heinrichs, V., and Patten, P. A. (2001) Advances in directed protein evolution by recursive genetic recombination: applications to therapeutic proteins, *Curr. Opin. Biotechnol. 12*, 361-370.

146. Lee, N., Bessho, Y., Wei, K., Szostak, J. W., and Suga, H. (2000) Ribozyme-catalyzed tRNA aminoacylation, *Nat. Struct. Biol. 7*, 28-33.

147. Koutsioulis, D., Wang, E., Tzanodaskalaki, M., Nikiforaki, D., Deli, A., Feller, G., Heikinheimo, P., and Bouriotis, V. (2008) Directed evolution on the cold adapted properties of TAB5 alkaline phosphatase, *Protein Eng. Des. Sel. 21*, 319-327.

148. Kawaguchi, R., Yu, J., Wiita, P., Honda, J., and Sun, H. (2008) An essential ligand binding domain in the membrane receptor for retinol binding protein revealed by large-scale mutagenesis and a human polymorphism, *J. Biol. Chem. 283*, 15160-15168.

149. Cherry, J. R., Lamsa, M. H., Schneider, P., Vind, J., Svendsen, A., Jones, A., and Pedersen, A. H. (1999) Directed evolution of a fungal peroxidase, *Nat. Biotechnol. 17*, 379-384.

150. Simmons, J. S. (1926) A culture medium for differentiating organisms of typhoid-colon aerogenes groups and for isolating of certain fungi, *J. Infect. Dis. 39*, 209-241.

151. Greener, A., Callahan, M., and Jerpseth, B. (1997) An efficient random mutagenesis technique using an *E. coli* mutator strain, *Mol. Biotechnol. 7*, 189-195.

152. Li, H. and Pajor, A. M. (2002) Functional characterization of CitM, the $Mg^{2+}$-citrate transporter, *J. Membr. Biol. 185*, 9-16.

153. Dodd, J. R. and Christie, D. L. (2007) Selective amino acid substitutions convert the creatine transporter to a gamma-aminobutyric acid transporter, *J. Biol. Chem. 282*, 15528-15533.

154. Engel, P., Kramer, R., and Unden, G. (1992) Anaerobic fumarate transport in *Escherichia coli* by an fnr-dependent dicarboxylate uptake system which is different from the aerobic dicarboxylate uptake system, *J. Bacteriol. 174*, 5533-5539.

155. Six, S., Andrews, S. C., Unden, G., and Guest, J. R. (1994) *Escherichia coli* possesses two homologous anaerobic $C_4$-dicarboxylate membrane transporters (DcuA and DcuB) distinct from the aerobic dicarboxylate transport system (Dct), *J. Bacteriol. 176*, 6470-6478.

156. Zientz, E., Six, S., and Unden, G. (1996) Identification of a third secondary carrier (DcuC) for anaerobic $C_4$-dicarboxylate transport in *Escherichia coli*: roles of the three Dcu carriers in uptake and exchange, *J. Bacteriol. 178*, 7241-7247.

157. Davies, S. J., Golby, P., Omrani, D., Broad, S. A., Harrington, V. L., Guest, J. R., Kelly, D. J., and Andrews, S. C. (1999) Inactivation and regulation of the aerobic $C_4$-dicarboxylate transport (dctA) gene of *Escherichia coli*, *J. Bacteriol. 181*, 5624-5635.

158. Golby, P., Kelly, D. J., Guest, J. R., and Andrews, S. C. (1998) Transcriptional regulation and organization of the dcuA and dcuB genes, encoding homologous anaerobic $C_4$-dicarboxylate transporters in *Escherichia coli*, *J. Bacteriol. 180*, 6586-6596.

159. Janausch, I. G., Zientz, E., Tran, Q. H., Kroger, A., and Unden, G. (2002) $C_4$-dicarboxylate carriers and sensors in bacteria, *Biochim. Biophys. Acta 1553*, 39-56.

160. Kay, W. W. and Kornberg, H. L. (1971) The uptake of $C_4$-dicarboxylic acids by *Escherichia coli*, *Eur. J. Biochem. 18*, 274-281.

161. Seol, W. and Shatkin, A. J. (1991) Escherichia coli kgtP encodes an alpha-ketoglutarate transporter, *Proc. Natl. Acad. Sci. U. S. A. 88*, 3802-3806.

162. Kaback, H. R., Sahin-Toth, M., and Weinglass, A. B. (2001) The kamikaze approach to membrane transport, *Nat. Rev. Mol. Cell Biol. 2*, 610-620.

163. Kaback, H. R. (1983) The lac carrier protein in Escherichia coli, *J. Membr. Biol. 76*, 95-112.

164. Kaback, H. R. (1990) *Lac* permease of *Escherichia coli*: on the path of the proton, *Phil. Trans. R. Soc. Lond. B 326*, 425-436.

165. Seok, Y. J., Sun, J., Kaback, H. R., and Peterkofsky, A. (1997) Topology of allosteric regulation of lactose permease, *Proc. Natl. Acad. Sci. U. S. A. 94*, 13515-13519.

166. Kniazeff, J., Loland, C. J., Goldberg, N., Quick, M., Das, S., Sitte, H. H., Javitch, J. A., and Gether, U. (2005) Intramolecular cross-linking in a bacterial homolog of mammalian SLC6 neurotransmitter transporters suggests an evolutionary conserved role of transmembrane segments 7 and 8, *Neuropharmacology 49*, 715-723.

167. Wolin, C. D. and Kaback, H. R. (2000) Thiol cross-linking of transmembrane domains IV and V in the lactose permease of *Escherichia coli*, *Biochemistry 39*, 6130-6135.

168. Zomot, E., Zhou, Y., and Kanner, B. I. (2005) Proximity of transmembrane domains 1 and 3 of the gamma-aminobutyric acid transporter GAT-1 inferred from paired cysteine mutagenesis, *J. Biol. Chem. 280*, 25512-25516.

169. Selvin, P. R. (2002) Principles and biophysical applications of lanthanide-based probes, *Annu. Rev. Biophys. Biomol. Struct. 31*, 275-302.

# VITA

Aditya Joshi was born to Dilip and Sunanda Joshi in Mumbai, India on March 2nd, 1980. After graduating from University of Mumbai, India in April 2000 with a Bachelor's degree in Microbiology, Aditya further attended the University of Mumbai for his Master's degree in Biophysics. In 2003, Aditya matriculated in the Cellular Physiology and Molecular Biophysics graduate program at University of Texas Medical Branch. During his graduate training at UTMB, Aditya was awarded the Mason Guest Scholar Award for Graduate Students in Cellular Physiology and Molecular Biophysics in 2006 and American Physiological Society (Cell and Molecular Physiology Section) Student award in 2005.

Aditya can be contacted through his parents at 2-Sneh, 31 Prashant Co. Op. Society, Paud Rd., Pune 411 038, India.

## Education

Bachelor of Science (Microbiology), April 2000, University of Mumbai, Mumbai, India
Master of Science (Biophysics), April 2002, University of Mumbai, Mumbai, India

## Publications

Joshi, A.D. and Pajor, A.M., Role of conserved prolines in the structure and function of the $Na^+$/dicarboxylate cotransporter 1, NaDC1. *Biochemistry*, 45 (13) 4231 – 4239, 2006.

Joshi, A.D., Negi, S.S., Braun, W., Pajor, A.M., A membrane topology model of $Na^+$/dicarboxylate cotransporter 1 (Manuscript in preparation).

Joshi, A.D. and Pajor A.M., Identification of conformationally sensitive amino acids in $Na^+$/dicarboxylate symporter, SdcS, from *Staphylococcus aureus* (Manuscript in preparation).

## Abstracts

Joshi A.D. and Pajor A.M. Topology model of $Na^+$/dicarboxylate cotransporter 1. *FASEB Journal*, 21 (5) A530, Experimental Biology 2005 and 37th International Congress of Physiological Sciences, Washington DC 2007.

Joshi A.D., Negi, S.S., Braun, W. and Pajor A.M. Conserved proline residues in transmembrane helices 7 and 10 of $Na^+$/dicarboxylate cotransporter 1 affect succinate transport. *FASEB Journal*, 19 (5) A1168, Experimental Biology 2005 and 35th International Congress of Physiological Sciences, San Diego April 2005.